EPITHERMAL GOLD MINERALIZATION OF THE SAN NICOLAS VEIN, EL CUBO MINE, GUANAJUATO, MEXICO: TRACE ELEMENT DISTRIBUTION FLUID INCLUSION MICROTHERMOMETRY AND GAS CHEMISTRY

by

Reyna L. Abeyta

Department of Earth and Environmental Sciences
New Mexico Institute of Mining and Technology
Socorro, New Mexico

THESIS
Submitted as partial fulfillment of the
Requirements for the Degree of

Masters of Science in Geology

December, 2003

This thesis is accepted on behalf of the
Faculty of the Institute by the following committee:

David A. Noman
Advisor

William X. Chavez Jr.

Andrew Campbell

6-20-03
Date

I release this document to the New Mexico Institute of Mining and Technology.

Jaya L Atwyte
Student's Signature

6-20-03
Date

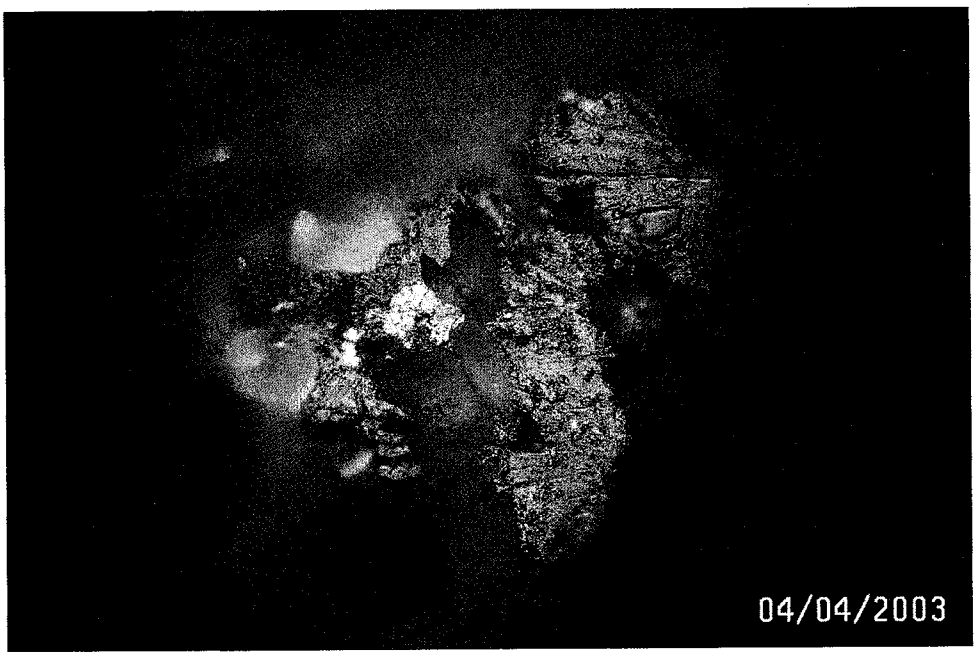

Electrum (brightest) intergrown with chalcopyrite, silver sulfides and bladed calcite from the San Nicolas vein (Sn-6).

ABSTRACT

The bonanza-gold San Nicolas vein is located in the Guanajuato, Mexico silver mining district. With an average grade of 6.8 g/ton Au and 141 g/ton Ag, this vein is unique because it has gold/silver ratios five times greater than most other veins in the district. This research uses paragenetic relationships, trace element geochemistry, fluid inclusion microthermometry, and fluid inclusion gas analyses to study the San Nicolas vein and determine the cause of its anomalously high gold concentrations.

The San Nicolas vein developed in three paragenetic stages: an early vein opening event involving wallrock silicification and brecciation (Stage I), an ore mineralization stage associated with brecciation, amorphous silica and bladed calcite (Stage II), and the collapse of the hydrothermal system as evidenced by the presence of amethyst and blocky calcite (Stage III).

Gold occurs as electrum intergrown with polybasite, aguilarite, chalcopyrite, bladed calcite and amorphous silica and is associated with brecciation. Zones of alteration in the wallrock of the San Nicolas vein consist of a lowermost propylitic zone of green wallrock and abundant pyrite, a middle zone of grey, white and yellow clay, and an uppermost zone of reddish-orange clay. Two XRD analyses reveal that the clays in the middle and uppermost zones are respectively illite and smectite.

Trace element geochemistry shows that Au, Ag, Cu, Pb, Zn, As, and Sb are concentrated in the northeast and in the southwest ends of the San Nicolas vein. Gold concentrations correlate well with Ag and moderately with Cu, Pb, Zn and Sb.

Fluid inclusion homogenization temperatures Th and salinities range from 172-282 °C and 0-2.95 wt % NaCl eq. Bladed calcite associated with ore mineralization was deposited from ~225 °C fluids containing 0.5 wt % NaCl eq. Late stage amethyst crystallized from ~238 °C fluids containing 0.8 wt % NaCl eq., and blocky calcite crystallized from ~221 °C fluids with 1 wt % NaCl eq. The coexistence of both liquid-dominated and vapor-dominated fluid inclusions in the San Nicolas vein, along with the occurrence of bladed calcite and electrum intergrowths, indicates that ore mineralization occurred from boiling fluids. Salinity and Th analyses show both boiling and mixing trends when plotted together which suggests both processes were operating during San Nicolas Mineralization.

Fluid inclusion gas analyses indicate that San Nicolas fluids were dominantly meteoric in origin with possibly a minor input of magmatic fluids. Hydrogen sulfide concentrations were sufficient to transport Au complexed with HS^- and deposit the San Nicolas ores. Most gas analyses show a boiling trend when plotted on a CO_2/N_2 vs. total gas discrimination diagrams.

Intergrown gold, bladed calcite and amorphous silica associated with breccia fragments indicate that gold mineralization occurred in response to catastrophic depressurization and extreme boiling. Homogenization temperatures indicate fluids and wallrock temperatures are 220-238 °C. Amorphous silica can only be precipitated if temperatures decreased to 180 °C or if about 40% water was removed by boiling. Bladed

calcite is deposited in response to CO_2 loss caused by boiling. The most reasonable explanation for the presence of Au in association with minerals deposited in an extreme boiling environment is that Au was deposited as a result of this environment as well.

Intense boiling coupled with sufficient H_2S to transport >10 ppm Au were crucial to creating the bonanza-Au San Nicolas vein. This mechanism of ore mineralization was absent or not preserved during the development of other vein systems in this mining district such as the Veta Madre and La Luz system.

ACKNOWLEDGEMENTS

I would like to dedicate this thesis to my mom and dad. Thank you for all your love and ceaseless support throughout the years. I love you. I would also like to thank you, my dearest Scott, for sharing your positive energy and wisdom with me. I am going to miss you dearly.

Much thanks to my advisor Dave Norman and my committee members Andy Campbell, Bill Chavez and honorary committee member Virgil Lueth.

Gracias a mis amigos a la mina El Cubo!! Pienso mucho de uds. ☺

Many thanks to the Compania Mineral del Cubo for funding this project and providing me with a dream vacation in Guanajuato.

TABLE OF CONTENTS

LIST OF TABLES

LIST OF FIGURES

1.0 INTRODUCTION

The Guanajuato mining district is located 475 kilometers northwest of Mexico City in central Mexico **(Fig. 1)**. Guanajuato is best known for its' abundant veins and stockwork silver mineralization. Mining commenced at Guanajuato in the mid 1500's and continues to today. Most of the mineralized veins in the Guanajuato district are northwest striking structures. The San Nicolas vein, which was discovered in 1983, is a northeast-striking vein. This vein is unique in the district because it is perpendicular to the major vein systems in the district and it has significantly higher gold concentrations than other Guanajuato district veins. Gold to silver ratios are (1/20) where Au/Ag ratios of (1/100) are common elsewhere in the district. Also, San Nicolas gold mineralization is located both stratigraphically and topographically above the silver-rich veins. The uniqueness of the San Nicolas vein to the Guanajuato district, proposes the question: Why is there higher gold grades in the San Nicolas vein than in other veins in the Guanajuato district?

This study uses vein paragenesis, trace element geochemistry, fluid inclusion microthermometry, fluid inclusion gas analyses, qualitative microprobe analyses and XRD clay analysis and to determine why San Nicolas Au grades are higher than elsewhere in the district and to characterize the vein mineralization. Understanding the genesis of the San Nicolas vein, will help in future exploration for gold rich veins of this type in the Guanajuato district, and elsewhere.

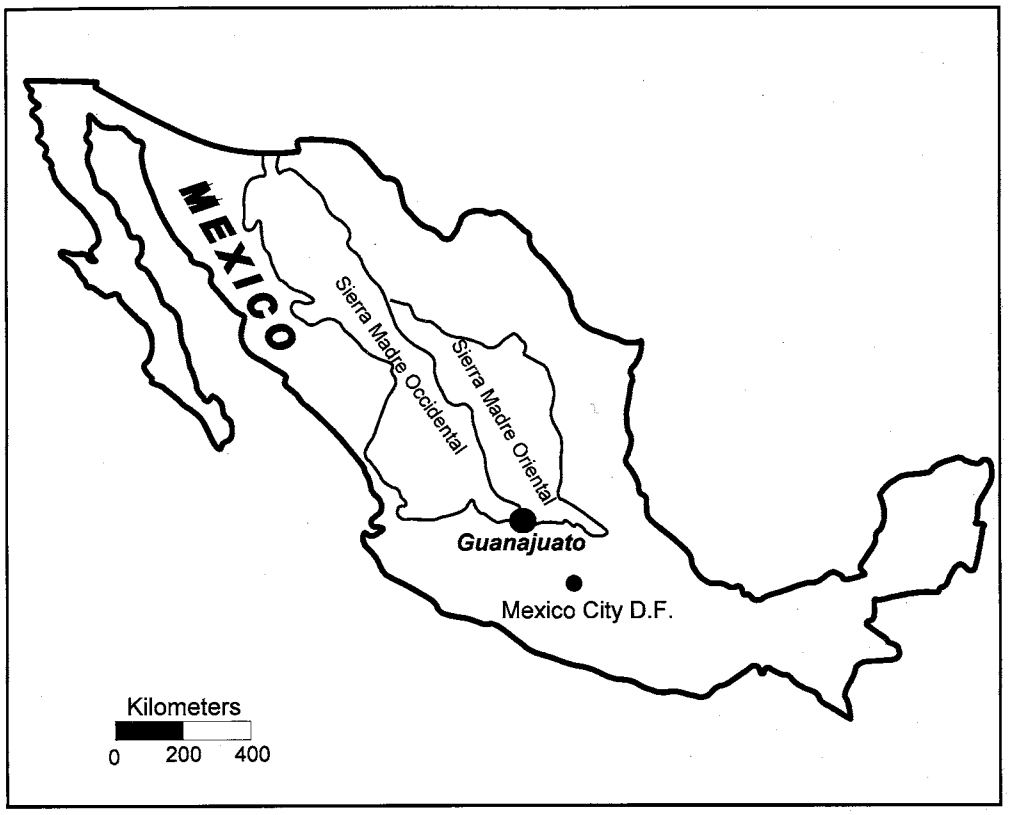

Figure 1. Map of Mexico showing the location of the Guanajuato district.

2.0 GUANAJUATO DISTRICT BACKGROUND GEOLOGY AND HISTORY

2.1 Geography

The Guanajuato Mining district is centrally located in Mexico **(Fig 1)**. It lies within mountainous terrain about 2,000 meters above sea level. Ore deposits of this region are found within the Sierra de Guanajuato mountain range which is a 100 km long and 20 km wide anticlinal structure with a northwest trend that parallels the Zacatecas, Fresnillo, Velardena and Santa Eulalia Ag-Pb-Zn district.

2.2 Mining History

Ore was discovered in the Guanajuato northwest region in 1548 when Spanish packers found an ore-bearing vein. It wasn't until 1550, however, that outcroping mineralization was found that would eventually be named the Veta Madre. The Veta Madre discovery resulted in a local population explosion and Guanajuato was founded (Wandke and Martinez, 1928). The Spaniards continued to explore and mine the area until 1810 when exploration and mining slowed down. In 1868 the Valenciana mine was reopened by English capital and continued until 1888. In the 20th century American mining companies invested in reworking old mine dumps and tailings but only a small amount of exploration was done at this time. In 1968 the Compañía Fresnillo discovered a new ore shoot along the Veta Madre (Querol and Navarro, 1990). After this time, numerous companies began exploring and developing mines throughout the district making it one of the richest silver producers in the country.

2.3 Regional Geology

The Guanajuato mining district is located in the Mesa Central physiographic province on the southern margin of the Eocene-Oligocene Sierra Madre Occidental volcanic province. The Sierra Madre Occidental province is bound to the east by the Sierra Madre Oriental and to the south by the Trans-Mexican volcanic axis. Subduction-related overthrusting of Mesozoic basic and ultrabasic rocks onto Cretaceous volcanic and sedimentary sequences occurred between the Cretaceous and the Mesozoic time periods (Martinez et al., 1991). This sequence was later intruded by a Tertiary granitoid batholith. Deposition and preservation of the Guanajuato Conglomerate occurred after this time and was subsequently covered by a series of Oligocene caldera related volcanic rocks including: ignimbrites, megabreccias and rhyolitic and andesitic domes. These volcanic sequences were then crosscut by northwest-trending silver-rich fissure vein systems that now comprises the district **(Fig. 2)** (Randall, et al., 1994).

2.4 Stratigraphy

The stratigraphic record of the Guanajuato district shows a long history of volcanism and tectonism **(Fig. 3)**. The Jurassic Esperanza Slate is comprised of a sequence of shale limestone and basic lava flows and is overlain by the Cretaceous La Luz Andesite, which is a weakly metamorphosed sequence of clastic sedimentary rocks, massive tholeiitic lavas and pillow lavas. Both formations are intruded by basaltic dikes and plagiogranites (Cavila and Martinez, 1987; Randall, 1982). This sequence was overthrust by the Cerro Pelon Tonalite oceanic crustal complex (Sedlock et al., 1983). This is overlain by the Eocene continental Guanajuato Conglomerate that is covered by

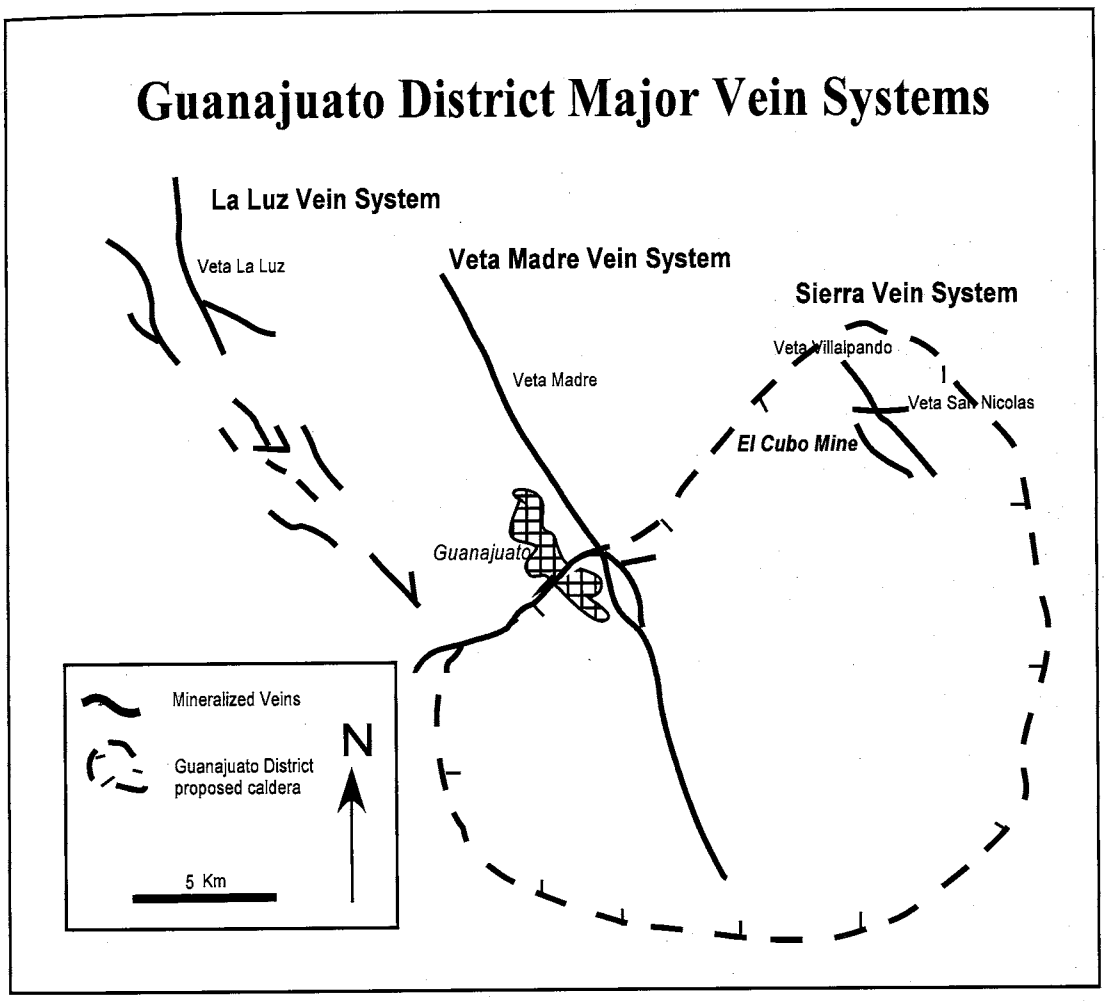

Figure 2. Location of major northwest-striking vein systems and caldera structure of the Guanajuato mining district.

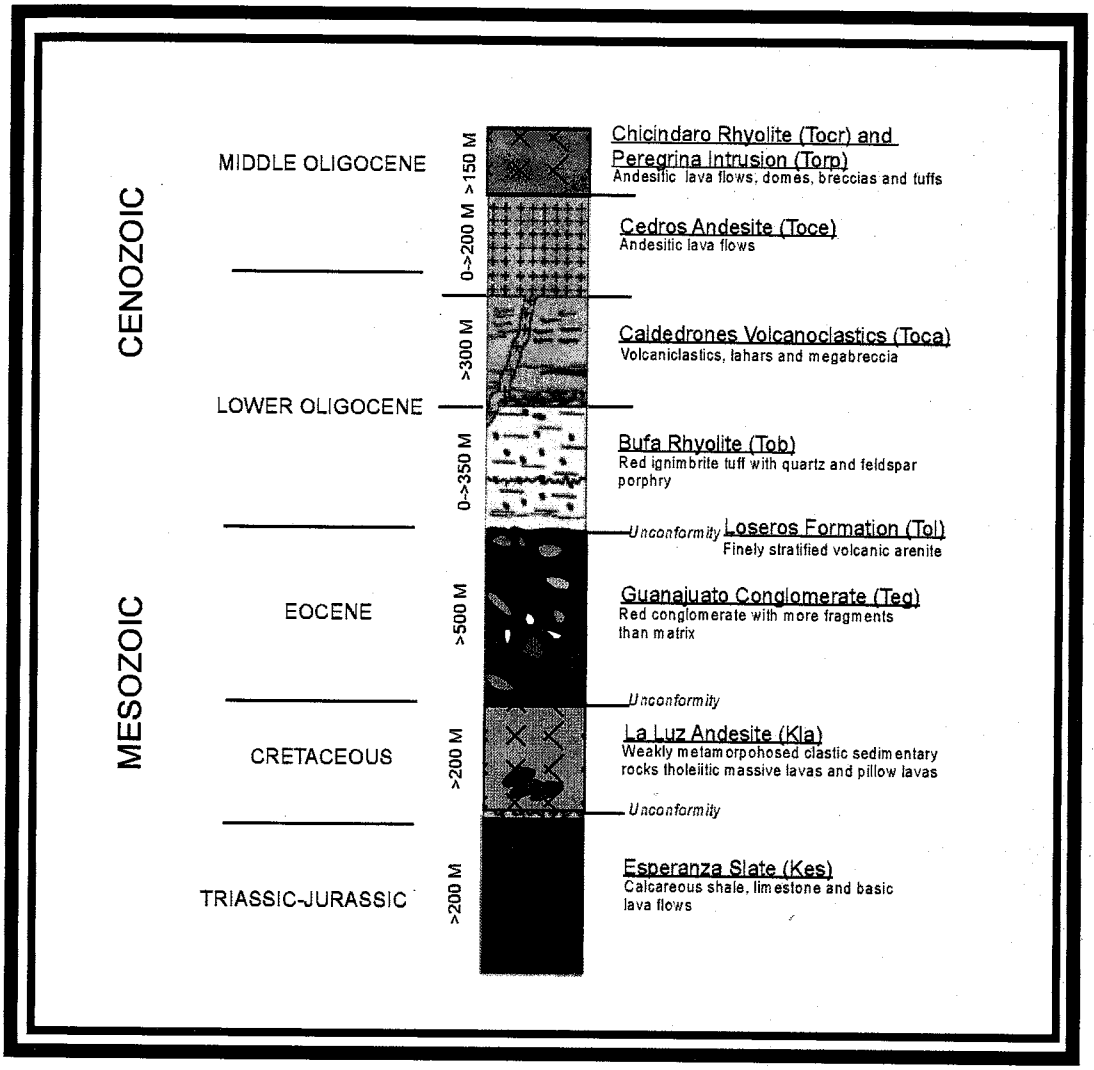

Figure 3. Guanajuato District stratigraphic column.
(Modified from CIA MINERAL DEL CUBO SA DE C.V.,1999: Randall, Saldana and Clark, 1994).

intermediate-felsic volcanic rocks in order: Loseros Formation (green volcanic arenite), Bufa rhyolite tuff (ignimbrite), Caldedrones (volcaniclastics, lahars and megabreccias), Cedros Andesite (andesitic lava flows), and Peregrina intrusive (domes and lava flows interbedded with volcanic breccias and tuffs (Saldana, 1990; Martinez, 1991). Quarternary sands, gravels, the Cubilete basalt and alluvium top the sequence (Randall et al., 1994).

2.5 Structure and Vein Systems

The Guanajuato district is located in a Laramide, northwest-trending anticlinal structure (Saldaña, 1990). This anticlinal structure is locally crosscut by Eocene normal faulting (Martínez, 1987). Normal faults form perpendicular northwest and northeast fault sets (Aranda et al., 1989). Most of the silver mineralization is located in veins within these northwest-trending fault sets. North-south trending faults crosscut the Ag-bearing faults in many locations. Intersections of east-west trending fault sets and northeast trending veins have elevated gold grades (Randall, et al., 1994).

Northwest-trending mineralized veins in the district are divided into three major vein systems: the La Luz, the Veta Madre and the Sierra **(Fig. 2)**. The El Cubo mine and the San Nicolas vein are located in the easternmost Sierra vein system **(Fig. 2)**

2.6 Caldera

Epithermal mineralization postdates caldera formation. This caldera structure, **(Fig. 4)** was originally proposed by Randall (1987). He suggested that the caldera is up to 16 km in diameter and that Oligocene intermediate and felsic volcanic units found in the area are all related to caldera formation due to their proximity to the proposed caldera

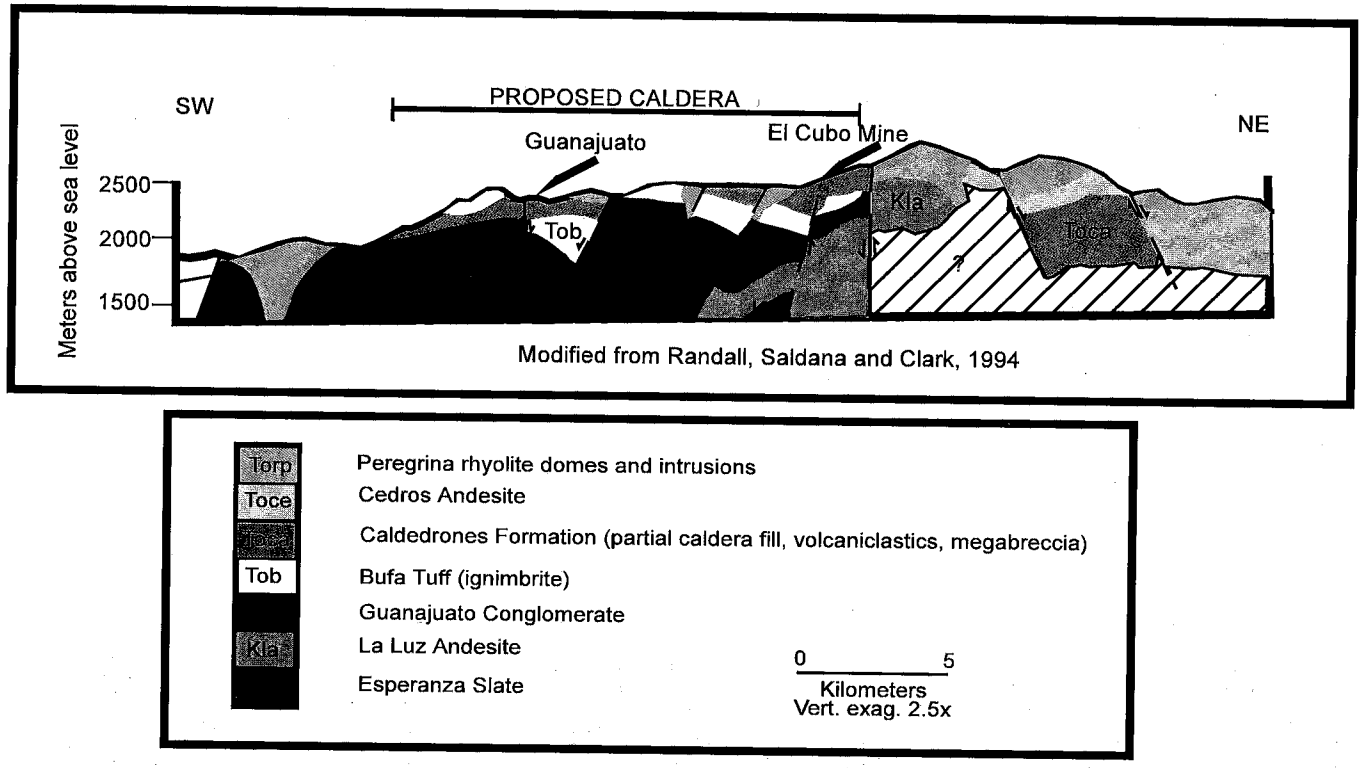

Figure 4. Cross-section of geology in and around the proposed Guanajuato caldera margins (Randall, Saldana and Clark, 1994).

margins. Work conducted by Davis, personal comm., (2002) reaffirms this idea and adds to it by suggesting that this caldera is hinged to the east because the caldera floor and the caldera wall are located topographically higher. This partial collapse is thought to have occurred due to an asymmetrical magma chamber (Davis, personal comm., 2002). He also suggests that many of the northeast-trending faults in the eastern part of the district may have formed during collapse when the northeastern portion of the caldera wall was formed.

2.7 Mineralization

Ore shoots within the Guanajuato district have been subdivided into three categories based on elevation. The "Upper" ore is located above 2,100-meter level; the " Lower" ore occurs between 1,700 and 2,200 meter level and the "Deep" ore occurs below the 1,700-meter level (Gross, 1975). The San Nicolas vein is located within the "Upper" ore horizon. These horizons are generally separated by barren zones. The upper and lower ore assemblages are distinguished by acanthite, pyrite, calcite, adularia, sericite, and quartz (Gross, 1975). Deep ore assemblages have chalcopyrite, galena, sphalerite, acanthite along with quartz and adularia (Gross, 1975).

Potassium/argon (K/Ar) dates of hydrothermal adularia from several silver-rich northwest-trending vein systems, indicate mineralization occurred between 31 and 26 Ma. (Randall, et al., 1994). Age dating has not been performed on any veins of the El Cubo mine.

2.8 Metal Sources

Randall, (1987, 1989) suggested that the source of gold may be the La Luz formation. He stated that gold is generally found where the La Luz formation is the thickest **(Fig. 4)**. Much of the gold in the district is found at the El Cubo mine where the La Luz formation is found to be very thick (350 meters) and of basaltic composition (Randall, 1987, 1989). In other areas where the La Luz formation is thin, gold is not present (Randall, 1987, 1989).

2.9 Wallrock Alteration

A detailed study of wallrock alteration by Buchanan (1980) along 16 miles of the Veta Madre describes alteration that is typical to most of the veins in the district. District-wide vein alteration is strongest at the vein selvage and progressing into a zone of potassic alteration followed by strong to weak propylitic alteration. Superimposed on this vein alteration assemblage is croscutting fracture-controlled phyllic and argillic alteration. Argillic and phyllic alteration zones are believed to be genetically related to one another and are commonly associated with ore.

2.10 Temperature and Salinity of Fluids

Several fluid inclusion studies are reported on Guanajuato from the Veta Madre. Gross (1975) reports homogenization temperatures Th range from 260-320 ° C in vein minerals from elevations of 1,700 meters to 2400 meters. Mango and others (1991) report Th ranges 230-305 °C in lower ore quartz, calcite and sphalerite with an average Th of 268 °C and average salinitiy of 1.18 wt % NaCl eq. These fluid inclusion studies disclose no evidence for fluid boiling in the lower Veta Madre mineralization. Girnius

(1993) reports Th values between 220°- 235° C for San Nicolas minerals that have no evidence of fluid boiling. He reports an average Th of 245° for two samples that exhibit boiling and salinities <1 wt % NaCl eq.

2.11 Source of Fluids

There are limited stable isotope analyses on sulfur, lead, carbon and oxygen from the Veta Madre. Gross (1975) reports sulfur isotopic values ($\delta^{34}S$ -3.4 to -19.5 per mil) from vein sulfide minerals, which are similar to sulfur isotopic composition in the Mesozoic sedimentary rock sulfides ($\delta^{34}S$ -12.6 to -16.6 per mil). Mango and others (1991) measured oxygen, carbon and lead isotopes. They concluded that carbon ($\delta^{13}C_{PDB}$ values -12.2 to -9.2 per mil) were derived from an organic-rich rock similar to the Esperanza Formation. They interpreted oxygen isotope values ($\delta^{18}O_{SMOW}$= 9.7 to 18.3 per mil) to be the result of either equilibration of meteoric water, with isotopically heavy country rocks, or mixing of fluids from different sources. Mango and others (1991) conclude that lead isotopic ratios closely resemble values measured in Oligocene volcanic rocks and their intrusive counterparts.

2.12 El Cubo Mine

The Mexican company, Compania Mineral Del Cubo owns and operates the El Cubo Mine. This mine is one of the largest gold and silver producers located on the Sierra de Guanajauto vein system **(Fig. 2).** Yearly production is about 1,050,000 oz. of Ag and 51,750 oz. of Au at an average grade of 140 g/ton Ag and 6.9 g/ton Au respectively (Martinez, personal comm., 2000). The San Nicolas vein was discovered in 1983. This bonanza vein had local grades of 100g/ton Au and gold/silver ratios of (1/20). An

estimation of total San Nicolas vein production to date is ~500,000 oz. Prior production at the El Cubo mine was predominately from the northwest-striking, silver-rich Villalpando Vein. Other smaller, but important producing veins in the El Cubo mine are the Los Panchos, Villalpando del Alto, 750 vein, Soledad, San Juan de Dios, San Francisco, Reina Isabel, La Loca and La Immaculada. **(Fig. 5).**

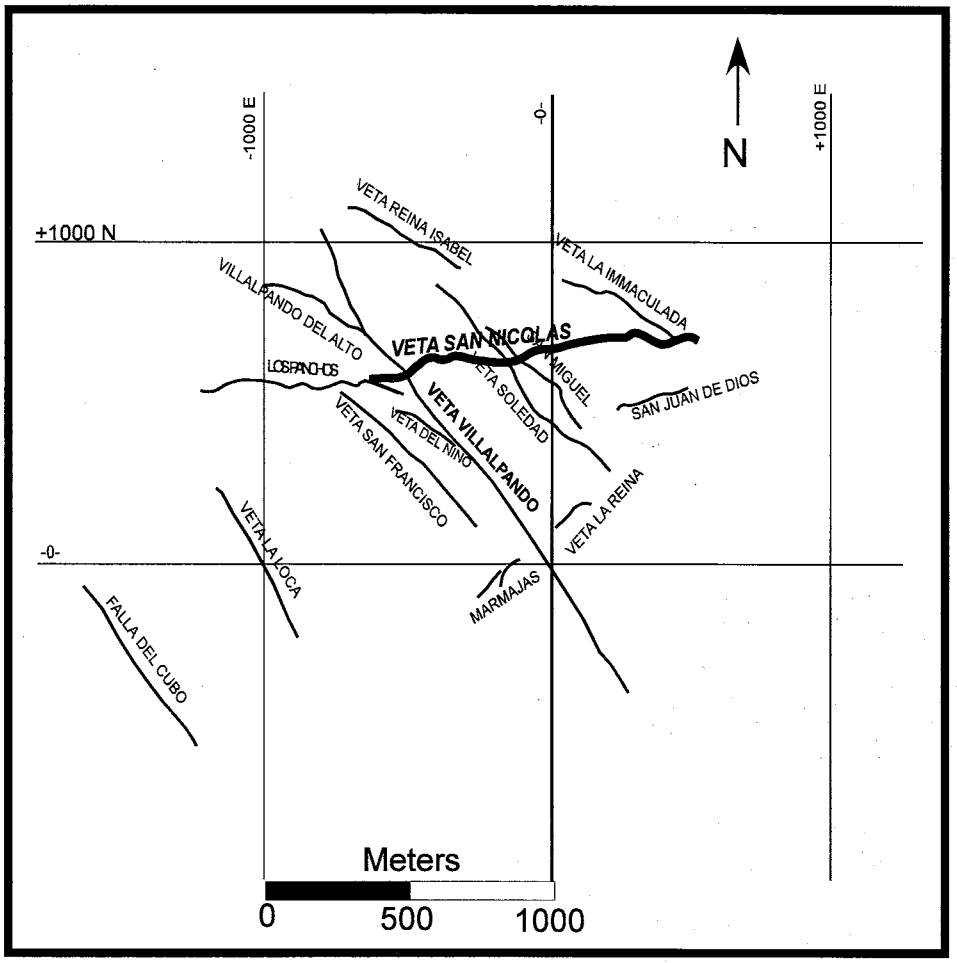

Figure 5. Principal veins of the El Cubo Mine.
(Modified from CIA MINERAL DEL CUBO SA DE C.V., 1999)

3. METHODS OF INVESTIGATION

Samples were collected between June and August 2000 at the El Cubo mine in Guanajuato, Mexico. Ninety underground samples were collected from the San Nicolas, Villalpando, Los Panchos and San Juan de Dios veins **(Appendix 1)**. At each of the 90 sample locations, two samples of vein material were collected for paragenesis and geochemical studies and one sample of host rock was taken for clay mineral analysis. Samples were collected along the length of the veins on most underground levels to obtain a widespread distribution. The initial goal of this thesis was to perform whole rock geochemistry, clay analyses, fluid inclusion microthermometry and gas analyses on all samples. Due to time constraints, the primary focus of this study was narrowed to the San Nicolas vein. Geochemical analyses, however, were performed on all samples from all veins **(Appendix 2)**. **Table 1** is a summary of analyses performed on each vein, **Table 2** indicates analyses performed on individual samples from the San Nicolas vein. San Nicolas vein sample locations are shown in **(Fig. 6).**

3.1 Petrography

Petrographic descriptions on thick sections and hand samples with clearly defined mineral banding from both the San Nicolas and Villalpando veins were used to determine vein paragenesis.. Qualitative backscatter images of samples Sn-6 and Sn-11were created by Electron Microprobe Analysis (EMPA) at the New Mexico Bureau of Mines and Mineral Resources (NMBMMR), microprobe lab, Socorro, New Mexico, to aid in the

Table 1. Number and type of analyses performed on each El Cubo vein.

	Whole Rock Geochemistry	Fluid Inclusion Microthermometry	Fluid Inclusion Gas	(XRD) Clay Analyses	Microprobe	Paragenesis
San Nicolas	42 samples	23 samples	17	2 samples	2 samples	10 samples
Villalpando	19 samples					1 sample
Los Panchos	11 samples					
San Juan de Dios	14 samples					

Table 2. Analyses performed on each San Nicolas vein samples.

	Sample #	Geochemistry	Fluid Inclusion	Gas Analyses
1	Sn-1	X	X	X
2	Sn-2	X	X	X
3	Sn-3	X	X	X
4	Sn-4	X	X	X
5	Sn-5	X	X	X
6	Sn-6	X	X	X
7	Sn-7	X		
8	Sn-8	X	X	X
9	Sn-9	X	X	
10	Sn-10	X	X	X
11	Sn-11	X		
12	Sn-12	X		
13	Sn-13	X	X	X
14	Sn-14	X	X	X
15	Sn-15	X	X	X
16	Sn-16	X		
17	Sn-17	X		
18	Sn-18	X		
19	Sn-19	X	X	X
20	Sn-20	X		
21	Sn-21	X		
22	Sn-22	X	X	X
23	Sn-23	X	X	
24	Sn-49	X	X	X
25	Sn-50	X		
26	Sn-58	X	X	
27	Sn-59	X		
28	Sn-60	X	X	X
29	Sn-61	X	X	
30	Sn-66	X	X	X
31	Sn-69	X	X	X
32	Sn-73	X		
33	Sn-74	X	X	
34	Sn-76	X		
35	Sn-77	X		
36	Sn-78	X		
37	Sn-79	X		
38	Sn-80	X		
39	Sn-81	X		
40	Sn-82	X	X	
41	Sn-200	X		
42	Sn-299	X		

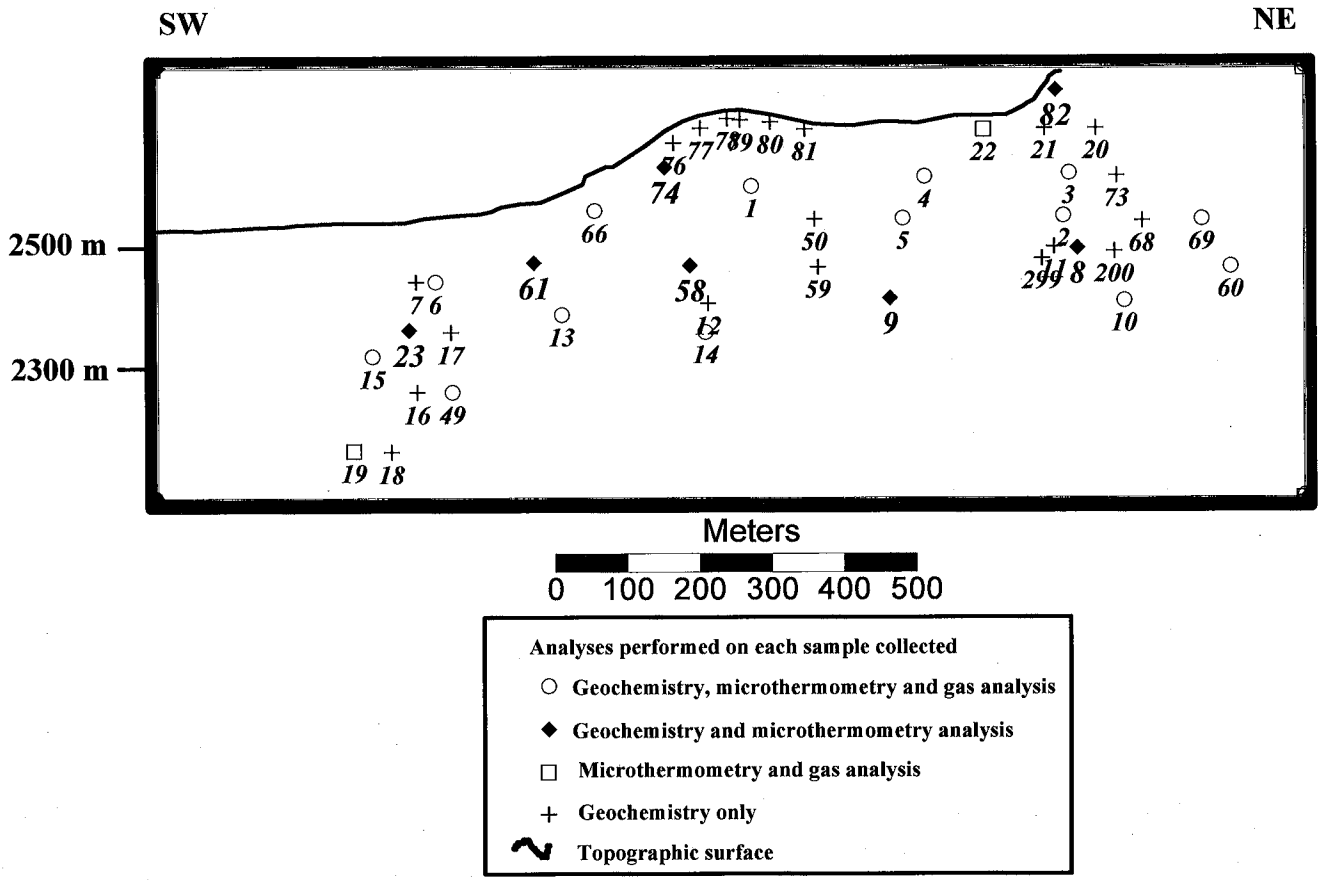

Figure 6. Sample location map along longitudinal section of the San Nicolas vein.

identification of sulfides. Two samples of clay (Sn-74) and (Sn-3) from a clay-rich horizons in the San Nicolas vein were analyzed by X-Ray Diffraction (XRD) also at the NMBMMR to determine clay mineralogy.

3.2 Trace element geochemical analyses

A thirty element geochemical analysis to determine trace element metal distributions was performed on 82 samples from the San Nicolas, Villalpando, Los Panchos and San Juan de Dios veins. Geochemical Inductively Coupled Plasma (ICP) analyses were made on whole rock samples by Bondar Clegg Geochemical Company in Toronto Canada. Inductively Coupled Plasma (ICP) digestion using a HCL:HNO_3 ratio of (3:1) was performed on 32 elements (Ag, Cu, Pb, Zn, Mo, Ni, Co, Cd, Bi, As, Sb, Fe, Mn, Te, Ba, Cr, V, Sn, W, La, Al, Mg, Ca, Na, K, Sr, Y, Ga, Li, Nb, Sc and Ta). Gold was analyzed by Fire Assay-Atomic Absorption (AA) and Gravimetric methods. The maximum values for gold obtained by this method are 10000 ppb (10 ppm or 10g/ton). Element distribution plots or "image maps" by the Kriging statistical method were created by the "Golden Software Surfer 7" program. Image maps helped visually understand the distribution of elements at each sample location along the length of the San Nicolas vein.

3.3 Fluid inclusion microthermometry

Fluid inclusion heating and freezing measurements were conducted on 186 fluid inclusions from 23 San Nicolas vein samples. Microthermometry measurements were performed at New Mexico Tech on a Linkham THMSG 600 heating and freezing stage. Final melting temperatures of ice Tm and final vapor bubble homogenization temperatures Th were obtained to understand the temperature and salinity conditions of mineralizing

fluids. A H_2O calibration was made before each measurement session to reduce analytical error. The precision of temperature measurements is ± 0.2 °C. The temperature rate was slowed to 0.2 °C/min as melting and homogenization temperatures in order to reduce error resulting from thermal gradients.

3.4 Fluid inclusion gas analysis

Gas analyses were performed at New Mexico Tech by crushing samples and measuring the released gas in single and dual Quadrupole Mass Spectrometers. In February 2002 a single Pfeiffer Mass Spectrometer analyses of volatile species H_2O, CO_2, CH_4, H_2S, H_2, N_2 and Ar and was performed on 7 quartz and calcite samples from the San Nicolas vein. In June of 2002 a dual Balzers and Pfeiffer Mass Spectrometer analyses of and H_2O, CO_2, CH_4, H_2S, H_2, N_2 and Ar and organics were performed on 9 samples of quartz and calcite from the San Nicolas vein. Under normal circumstances samples are analyzed by dual Mass Spectrometers Balzers and Pfeiffer. Due to technical problems in February 2002, samples were run only on the Pfeiffer Mass Spectrometer. The data were plotted on template discrimination diagrams using the "Igpet99" program and as Image Maps in Surfer 7.

4. RESULTS

4.1 Vein Geology

The San Nicolas vein has a general strike of N70-75E and fills an original tension fault. Vein splays along the length of the vein have varying strikes. The longitudinal section center of the vein constitutes a change in strike from N73W to N72E. This area also represents a decrease in vein width from almost two meters in the northeast and in the southwest to almost half a meter in the longitudinal section center. The vein is composed of alternating bands of quartz and sulfides near the vein margin grading to massive quartz and calcite in the middle vein. Locally, several generations of barren amethyst and calcite veins and veinlets crosscut the primary vein feature. The large Au-rich and Ag-rich veins Soledad, San Miguel, Villalpando, Villalpando del Alto and Contra veins crosscut the San Nicolas vein **(Fig. 7).** The intersection of the Villalpando, Villalpando del Alto and Contra veins enrich the San Nicolas vein in gold. Massive calcite veining up to two meters wide is found at the deepest levels of the vein particularly in the southwestern part below 2300 meters.

High grade ore zones occur in the northeastern and southwestern sections of the San Nicolas vein, where most of the mining occurs. Some of the highest grade ore occurs in the southwest section where the Villalpando vein crosscuts the San Nicolas **(Fig. 7)** The San Nicolas vein transects the Guanajuato Conglomerate, Bufa Rhyolite, Caldedrones

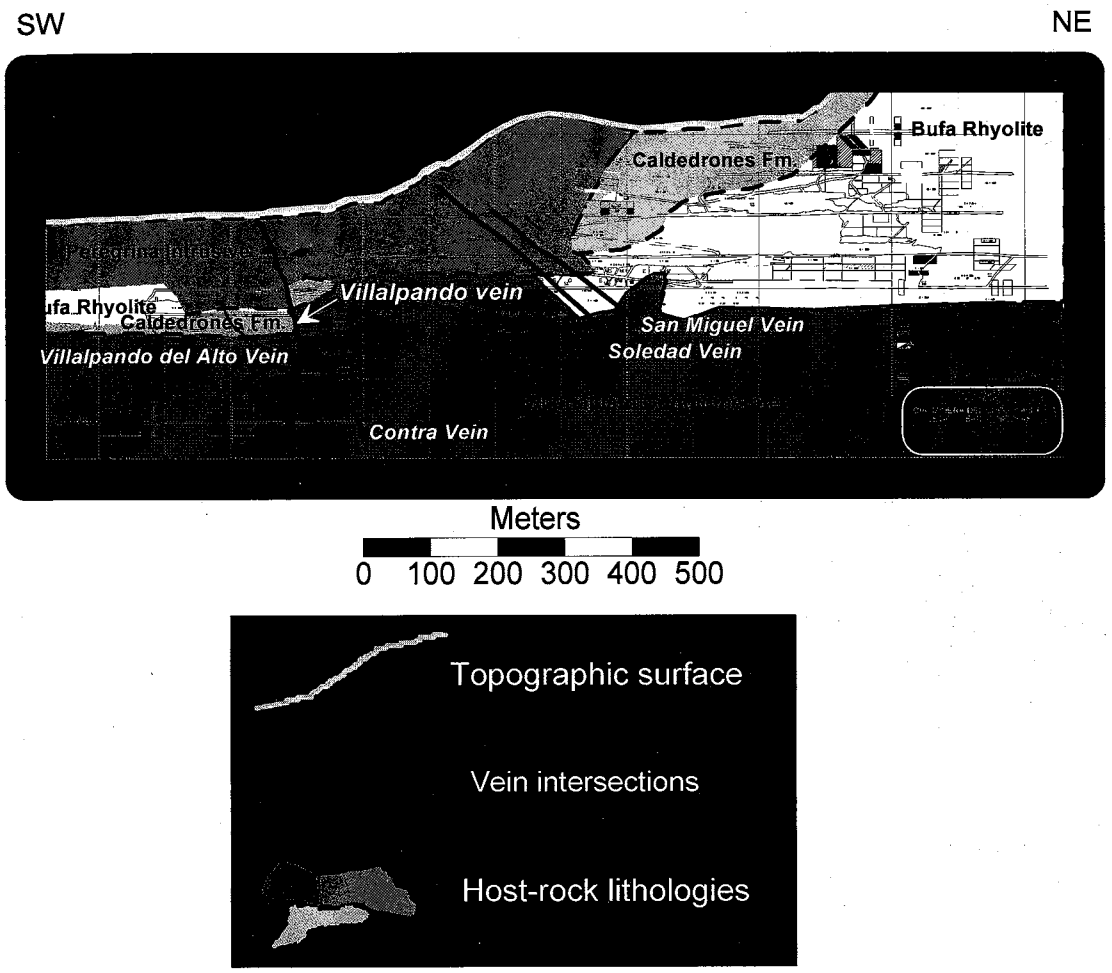

Figure 7. Longitudinal section of San Nicolas vein showing topographic surface, intersecting veins and host-rock lithologies (no vertical exageration).

Formation and the Peregrina Intrusive **(Fig. 7)** Mineralization is not associated with any one rock type.

4.2 Mineralogy and Petrology

Mineralization occurs in the San Nicolas vein as crustiform bands. Fine-grained sulfide minerals along with electrum occur in dark bands intergrown with fine-grained mosaic quartz and bladed calcite. Gangue minerals include quartz, chalcedony, amorphous silica, amethyst, bladed and blocky calcite. Amorphous silica (mosaic quartz) is discerned from chalcedony by its fine-grained <20 μm interpenetrating jigsaw, granular texture (Guoyi, Morrison, Jaireth, 1995). Chalcedony generally retains its characteristic botryoidal, flamboyant and feathery textures (Guoyi, Morrison, Jaireth, 1995). Quartz is subhedral, clear and has crystals >20 μm. Pyrite is the most abundant sulfide mineral. It is found early in the paragenesis in association with chlorite and calcite as propylitic alteration within the wallrock lithologies. Euhedral pyrite is associated with chalcopyrite, aguilarite (Ag_4SeS), polybasite $(Ag,Cu)_{16}Sb_2S_{11}$, and electrum (Au,Ag) which is considered the mineralizing stage **(Figs. 8 and 9)** The silver sulfides aguilarite and polybasite are fine-grained (<50 μm) and occur in stringers and as wispy intergrowths with chalcopyrite and electrum **(Figs. 10 and 11)**. Electrum grains are sub-rounded, very bright in reflected light and tend to have the straw-yellow color of pyrite **(Fig. 11)** Electrum was discerned from pyrite by microscope because it is very bright in reflected light, soft and scratches easily, unpitted and is associated with silver sulfides and chalcopyrite.

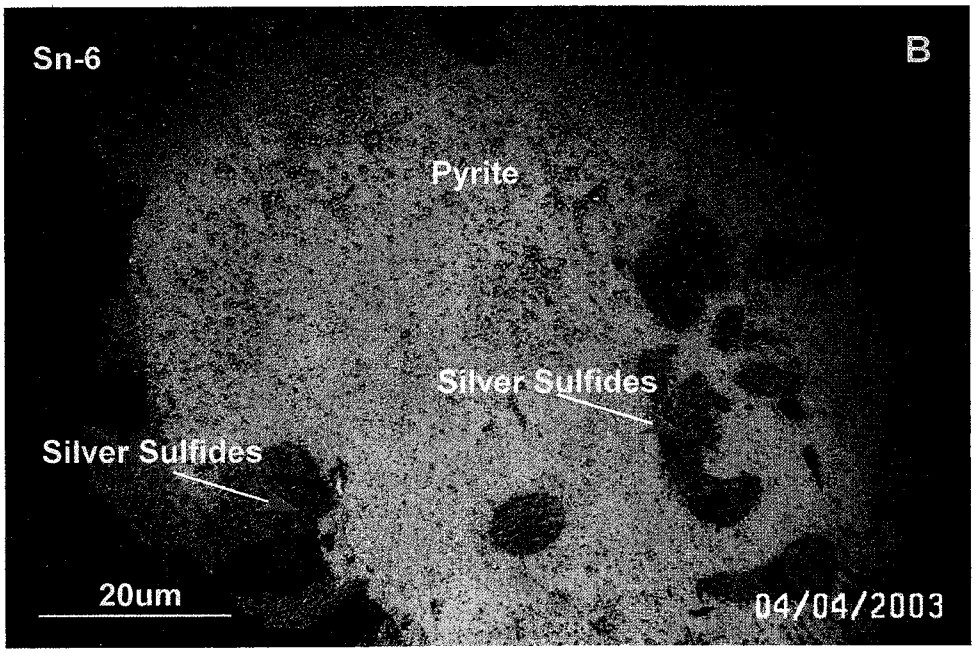

Figure 8. Reflected light petrogrpahic photo showing: A. Scratched silver sulfide surface (Sn-6; Stage 2 ore; X:-1124, Y:-330) B. Silver sulfides within the pyrite crystal and on grain boundaries (Sn-6; Stage 2 ore; X:-1124,Y:-330).

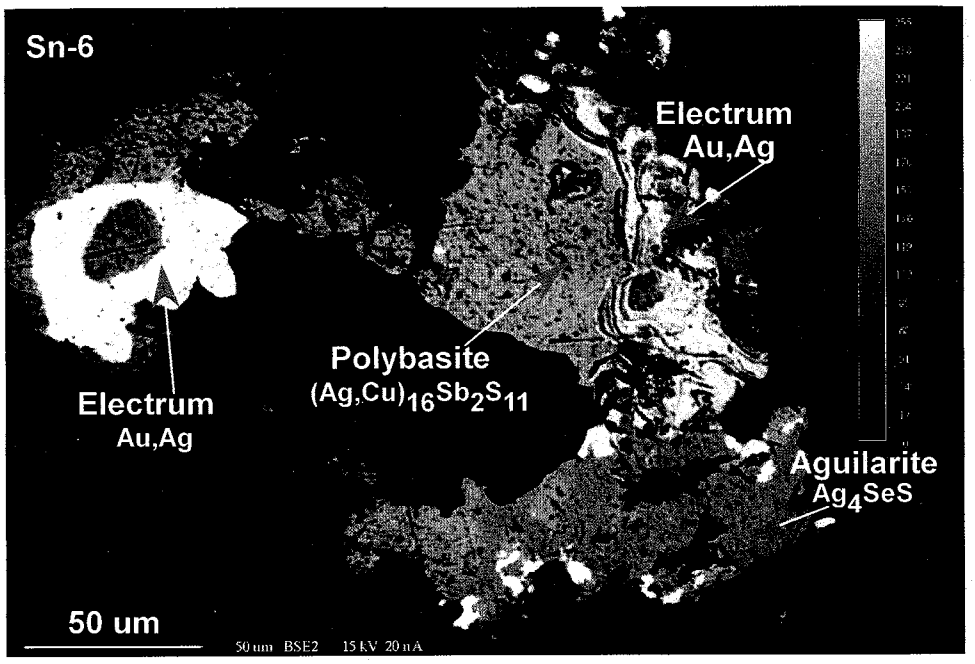

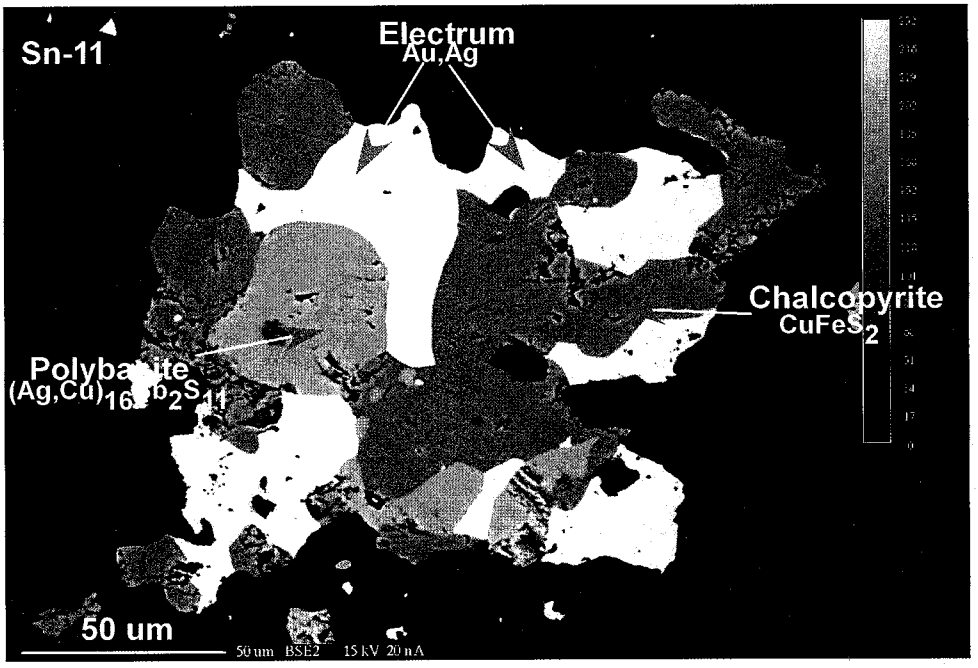

Figure 9. Backscatter electron image (15 kV, 20 nA) of (Sn-6; Stage 2 ore; X:-1124, Y: -330) and (Sn-11; Stage 2 ore; X: -272, Y: -281) showing electrum, polybasite, aguilarite and chalcopyrite.

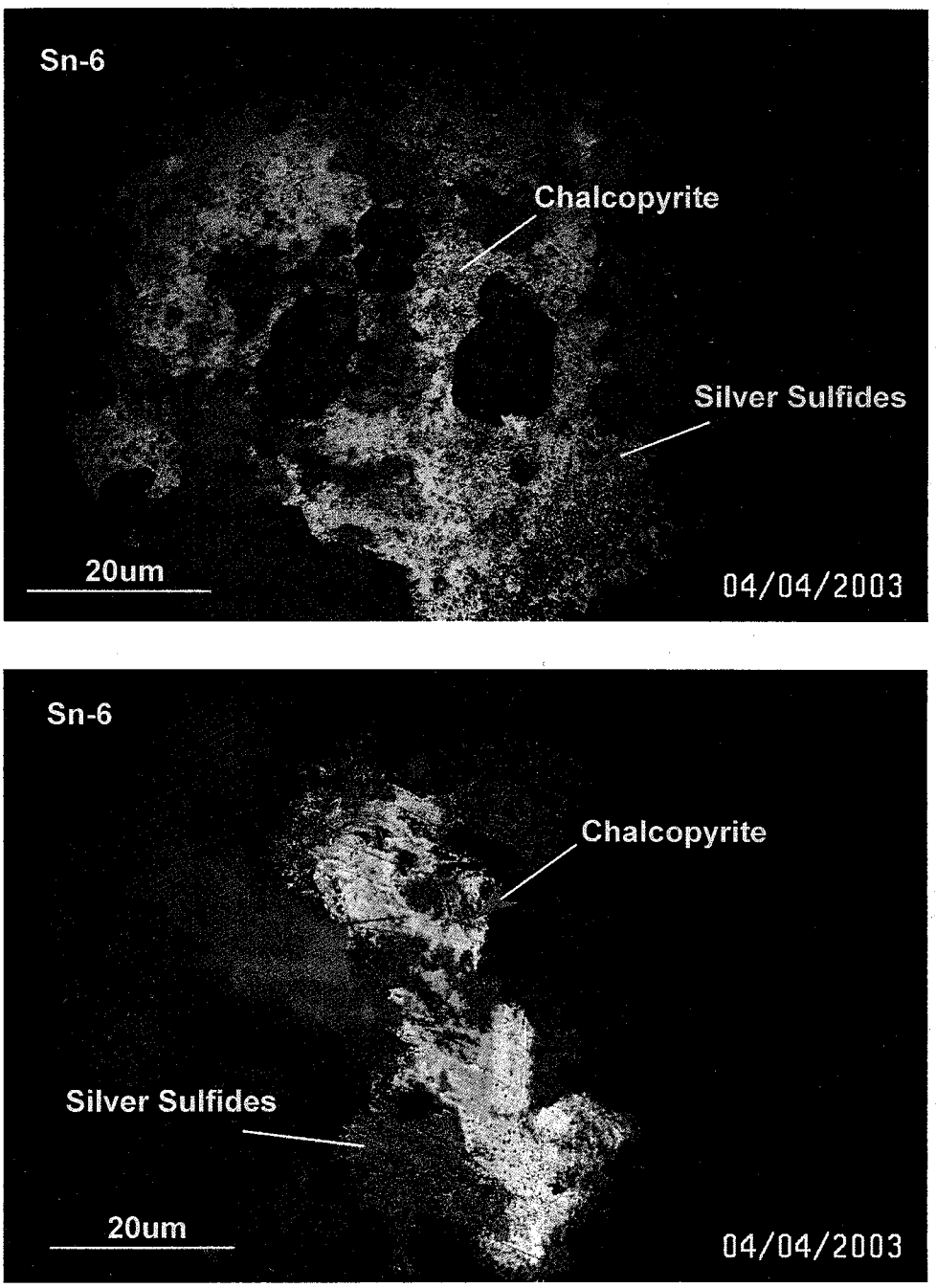

Figure 10. Reflected light petrographic photos showing intergrowth of chalcopyrite and silver sulfides (Sn-6; Stage 2 ore; X:-1124, Y: -330).

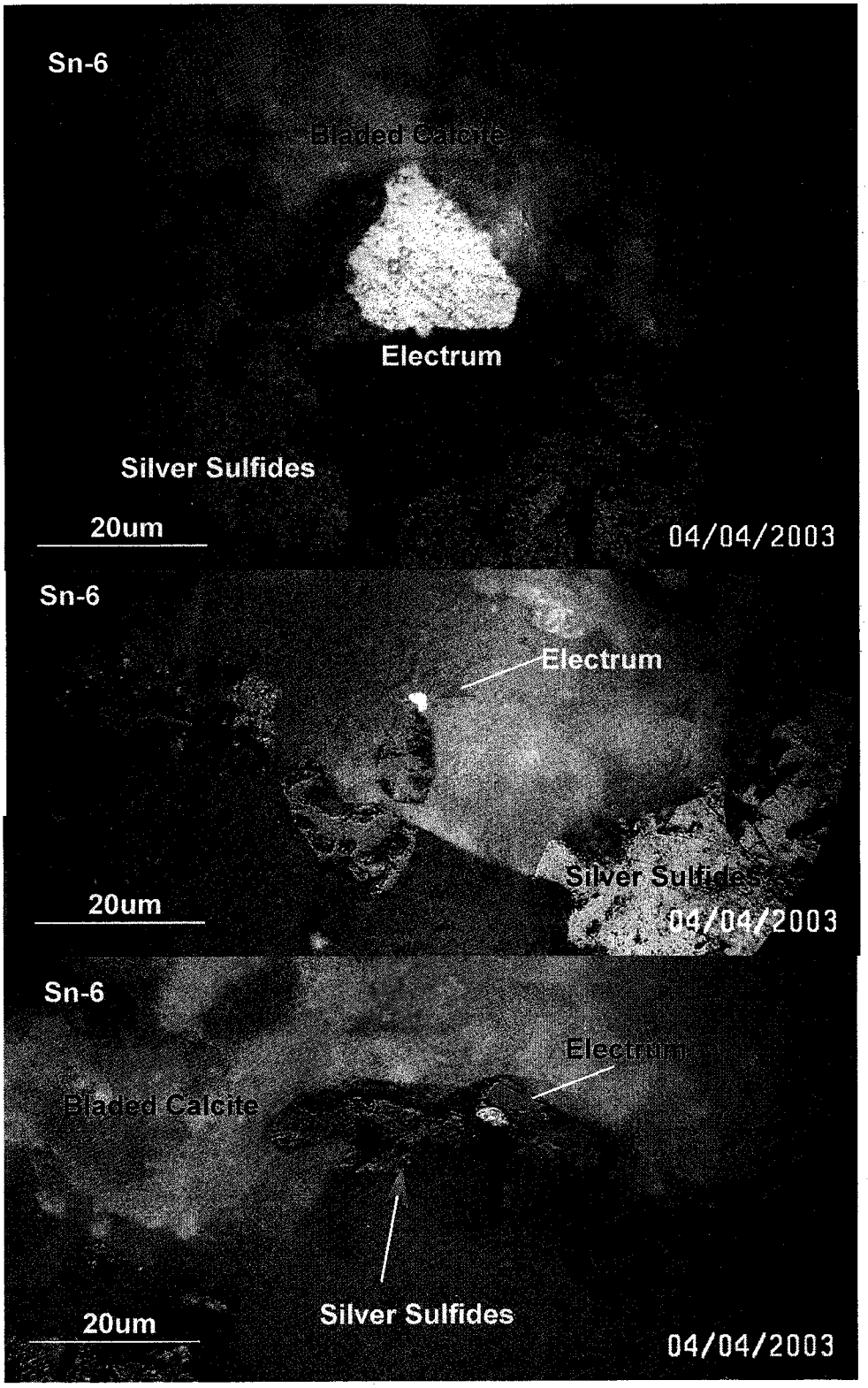

Figure 11. Reflected light petrographic photos showing intergrowth of electrum and silver sulfides (Sn-6; Stage 2 ore; X:-1124, Y: -330).

4.3 Vein Paragenesis

Observations made on hand samples and polished thick sections from the San Nicolas and Villalpando vein were used to determine paragenesis **(Fig. 12)**. The hand samples and thick sections that most completely define the entire vein paragenesis are shown in **(Fig. 13 -15)**. Not all stages can be seen everywhere in the veins, and Stage II is repetitive locally.

Stage I

The first stage of the San Nicolas vein paragenesis begins with the initial vein opening event that is less commonly accompanied by wallrock brecciation**(Fig. 15A).** Pyrite is the only sulfide present in this stage and occupies from 1-10% of the wallrock. Propylitic alteration is best developed in the Guanajuato Conglomerate and Caldedrones formations. Fractured wallrock is cemented by fine-grained quartz. Quartz veinlets commonly crosscut cementation but are terminated by banding from Stage II banded mineralization.

Stage II

Stage II is the most economically important stage of the San Nicolas vein because it is the sulfide-bearing or ore stage. Stage II commences with a preore event which consists of a bands of mosaic quartz crystallizing from amorphous silica and chalcedony grading to quartz and blocky calcite. Etching of euhedral quartz grains is visible in areas that contain blocky calcite **(Fig. 16)**. A dark band containing sulfides, mosaic quartz and infrequently bladed calcite forms a sharp boundary with the milky white band **(Fig. 17A and B).** In hand sample, this band is milky white and can either massive (2-3 cm) or finely banded (~1 mm). Brecciated fragments of wallrock and vein material are commonly found within milky white quartz and sulfides **(Figs. 14 and 15A)** This band is abundant in vapor-rich fluid inclusions and therefore is not translucent in some patches. The milky white quartz and sulfide band are commonly repetitive. The mosaic quartz-sulfide- bladed calcite band is followed by chalcedony that has partially recrystallized to quartz **(Fig. 17A).**

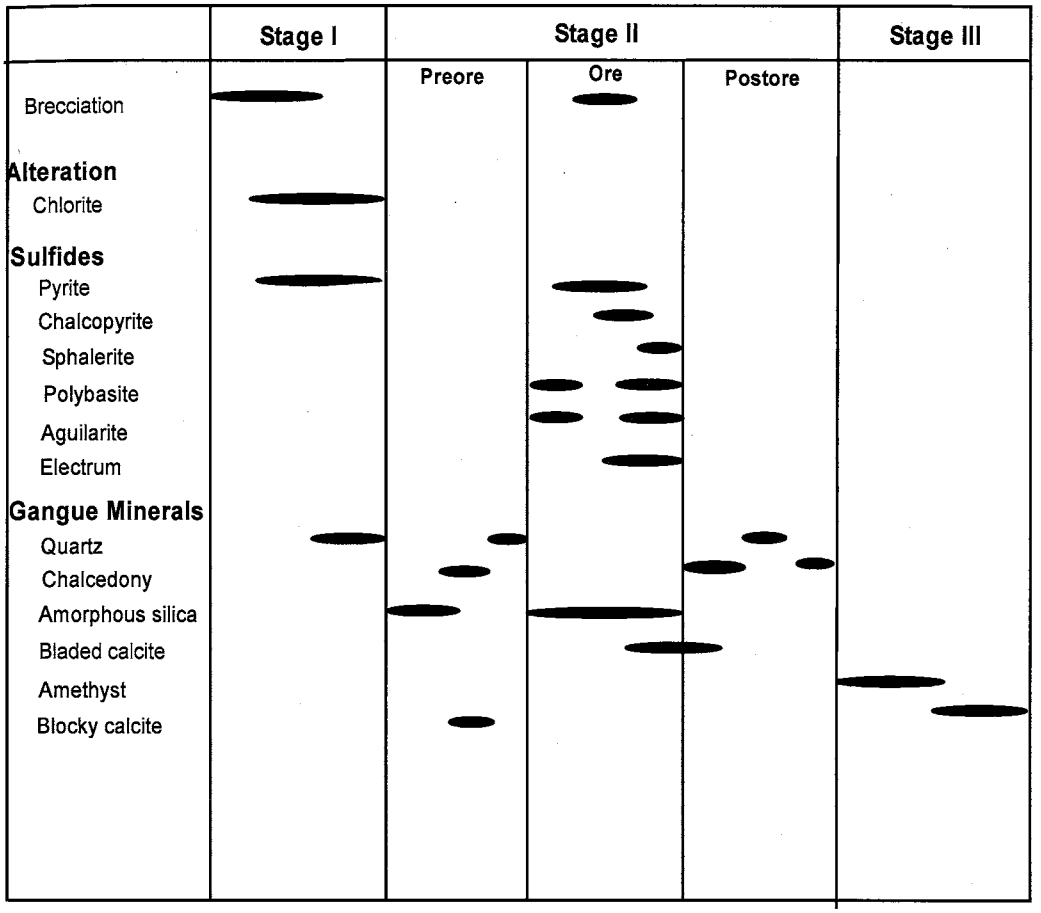

Figure 12. Paragenetic sequence of the San Nicolas and Villalpando veins showing mineral relationships.

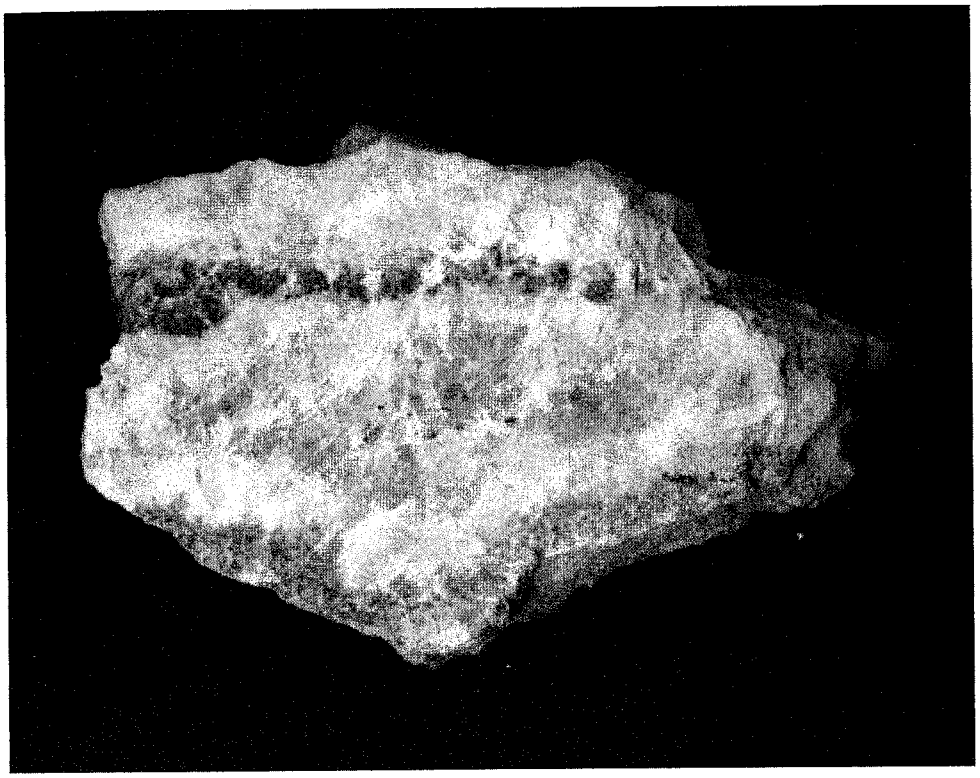

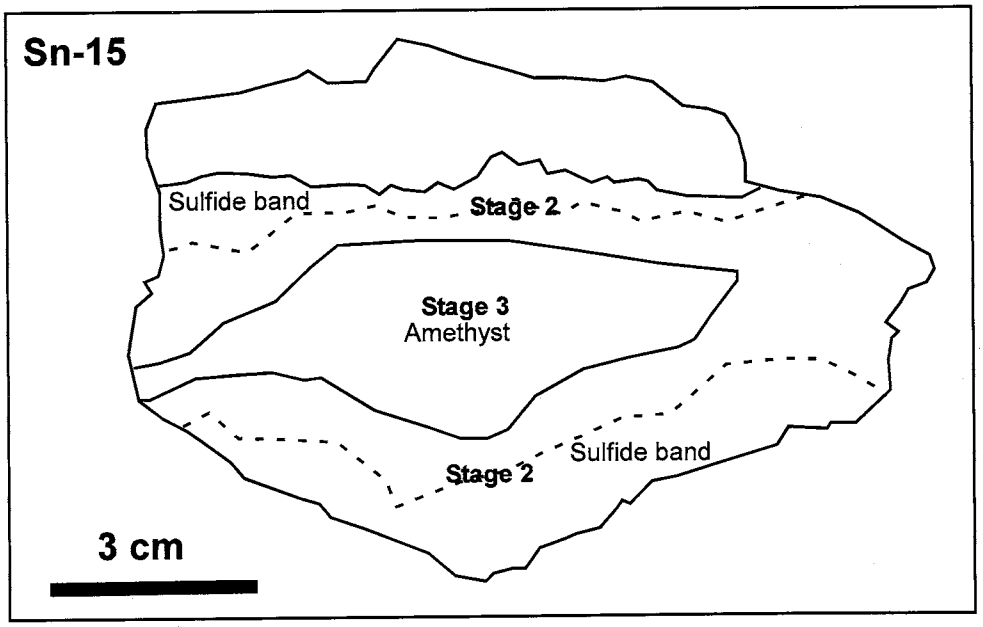

Figure 13. Sample (Sn-15; X:-1212, Y:-434) showing two stages of vein paragenesis.

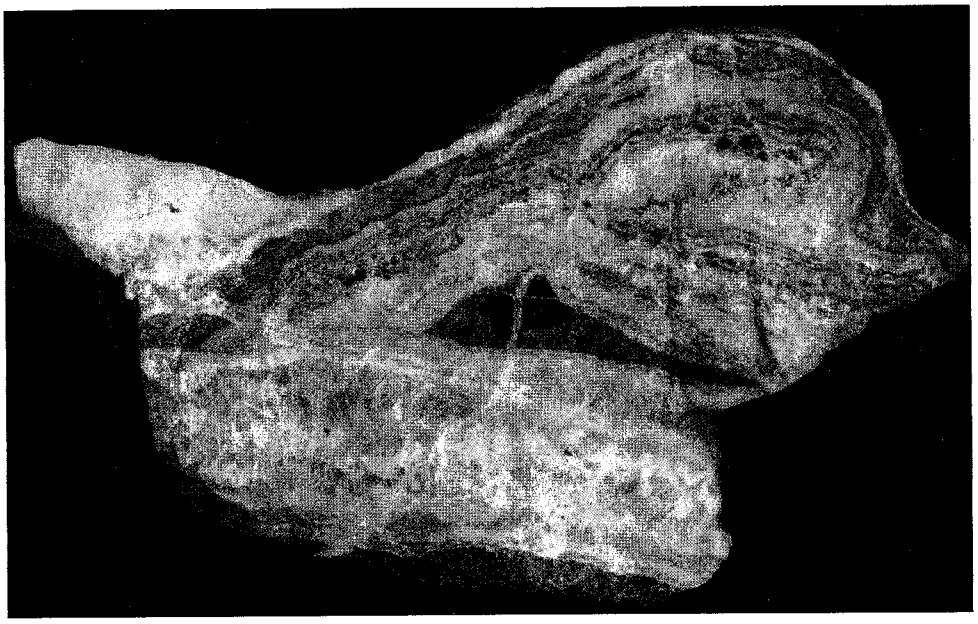

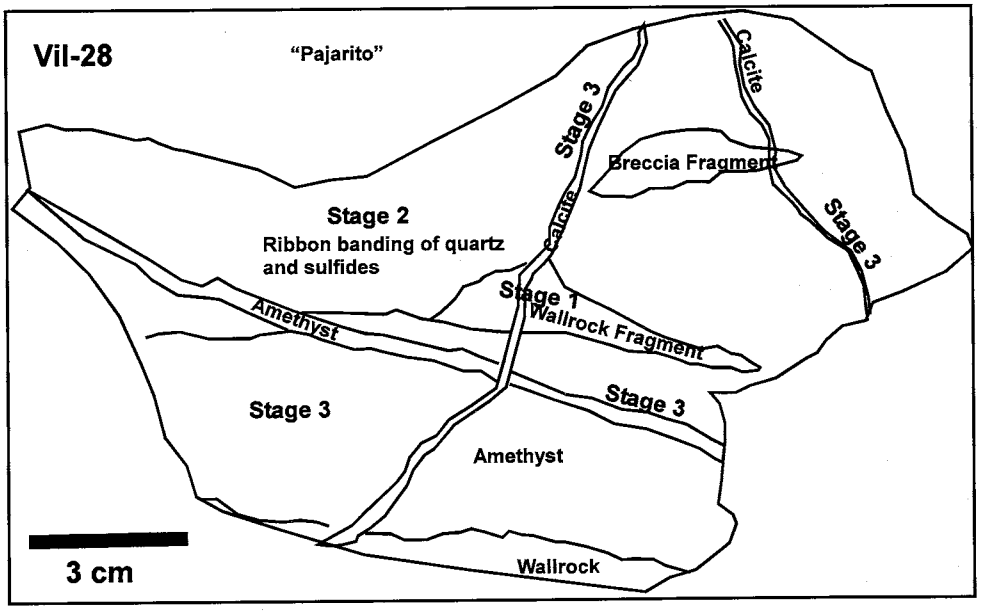

Figure 14. Handsample (Vil-28; X:406, Y:637) showing all three stages of vein paragenesis.

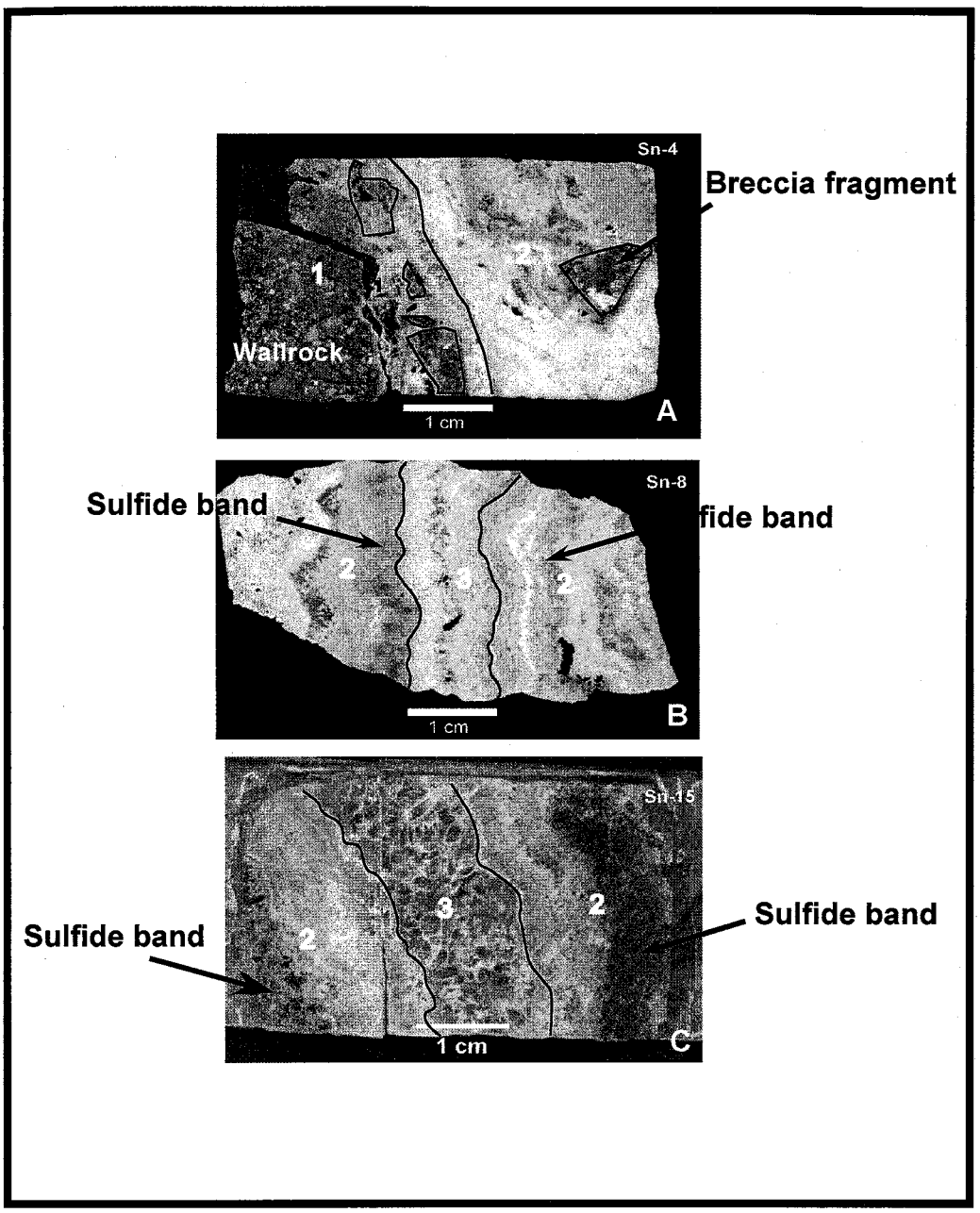

Figure 15. Paragenesis representing Stages I, II and III from samples (Sn-4, Sn-8 and Sn-15). Stages are separated by black lines.

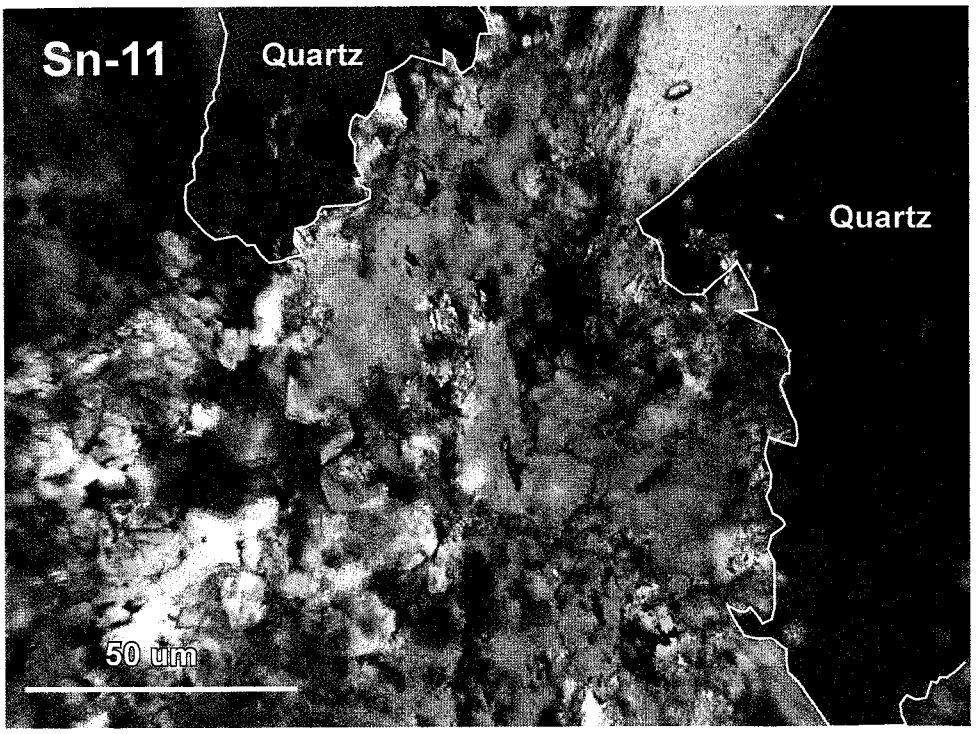

Figure 16. Photomicrograph of etched quartz (Sn-11; Stage 1 & preore Stage 2; X: -272, Y:-281) (20x magnification on polished thick section).

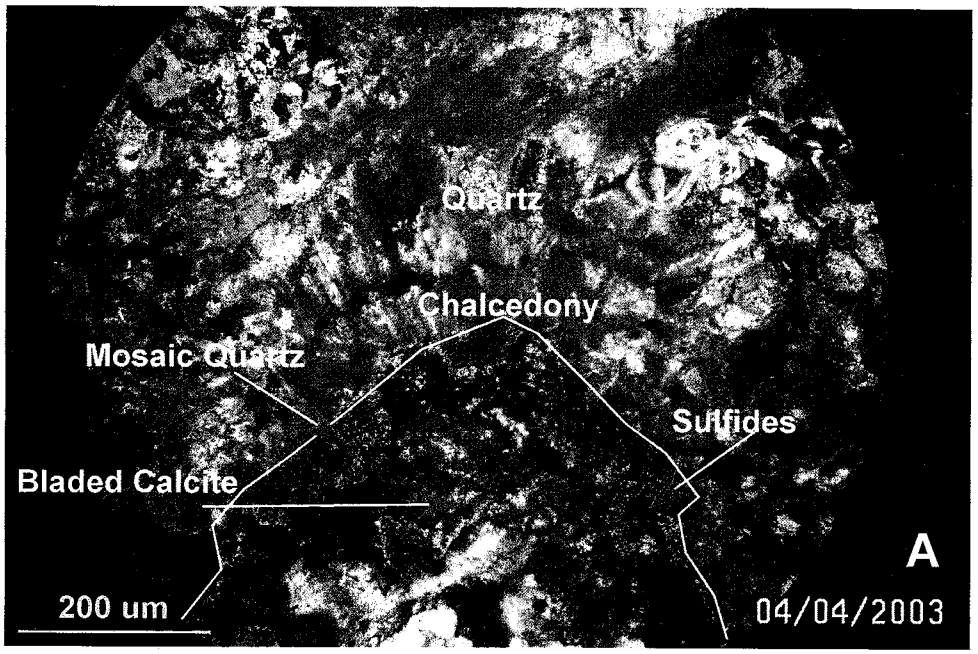

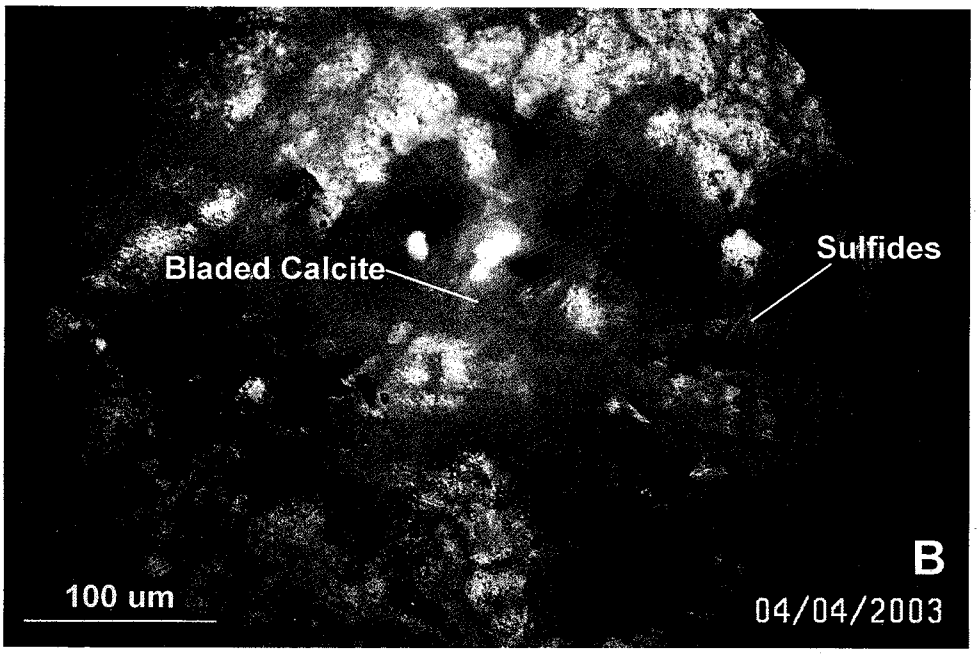

Figure 17. Photomicrographs of (Sn-6; Stage 2 ore and postore; X:-1124, Y: -330) sulfides intergrown with mosaic quartz and bladed calcite. Photo A (crossed polars) shows mosaic quartz, sulfides and bladed calcite grading to chalcedony followed by euhedral quartz. Photo B (plane polarized light) shows sulfides intergrown with bladed calcite. (10x magnification on polished thick section).

Stage III

Amethyst followed by blocky calcite are the last vein stages present in El Cubo veins **(Fig. 18).** They are either present as open-space filling, or crosscutting veins and veinlets **(Figs13 and 14).**

4.4 Alteration

A vertical zonation pattern is apparent in San Nicolas vein **(Fig. 19).** The vein is topographically positive due to silicification that is most abundant near the vein margins. Propylitic alteration that includes chlorite, pyrite and calcite is predominant below depths of 2400 m. At depths above 2400 meters green propylitic wallrock alteration grades into white, grey, yellow and sometimes green clay alteration. The clay alteration becomes stronger and clays become more intense and reddish-orange towards the topographic vein surface. The zonation pattern suggests a transition from a deep reduced (green Fe^{2+}) assemblage to an oxidized (orange-red Fe^{3+}) assemblage towards the vein surface. X-ray diffraction analyses of a sample from the lower grey-white clay (Sn-3) and a sample of the upper orange-red clay (Sn-74), indicate they are respectively illite and smectite **(Fig. 19).**

4.5 Geochemistry

Image maps were constructed to help visually understand the distribution of these elements along the length of these veins. Image maps of Au, Ag, Cu, Pb, Zn, As and Sb metal distributions from the Villalpando, Los Panchos and San Juan de Dios veins are included in this document for reference **(Appendix 2).** Tabulated geochemical data from these veins is included with San Nicolas geochemical data also in **(Appendix 2).**

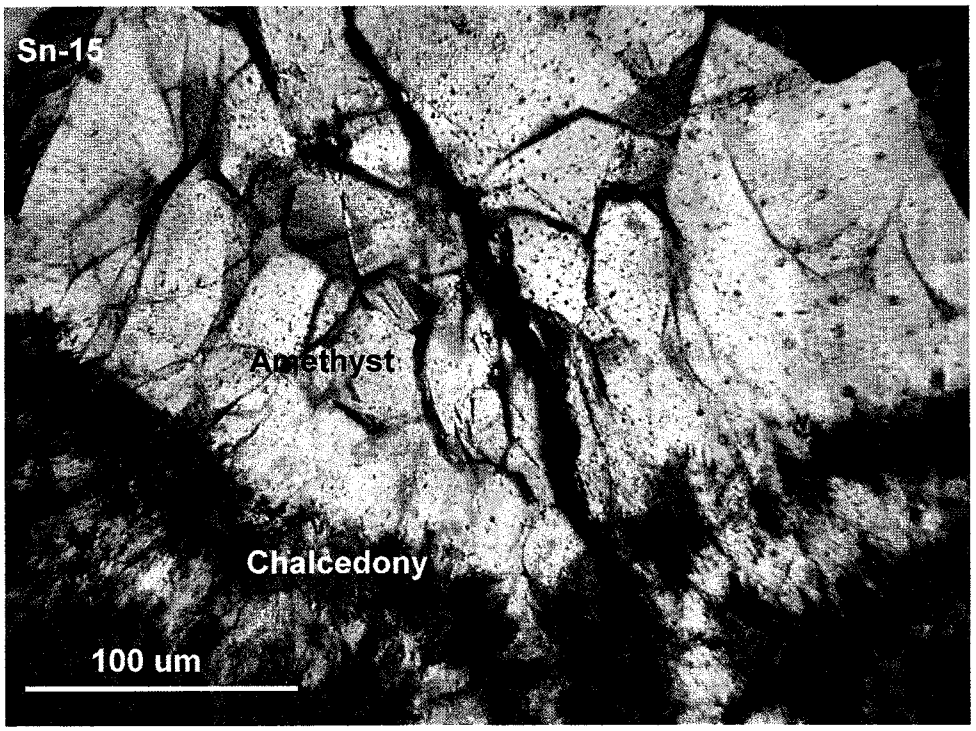

Figure 18. Chalcedony grading into amethyst (Sn-15; Stage 2 postore & early Stage 3; X:-1212, Y:-434) (plane polarized light).

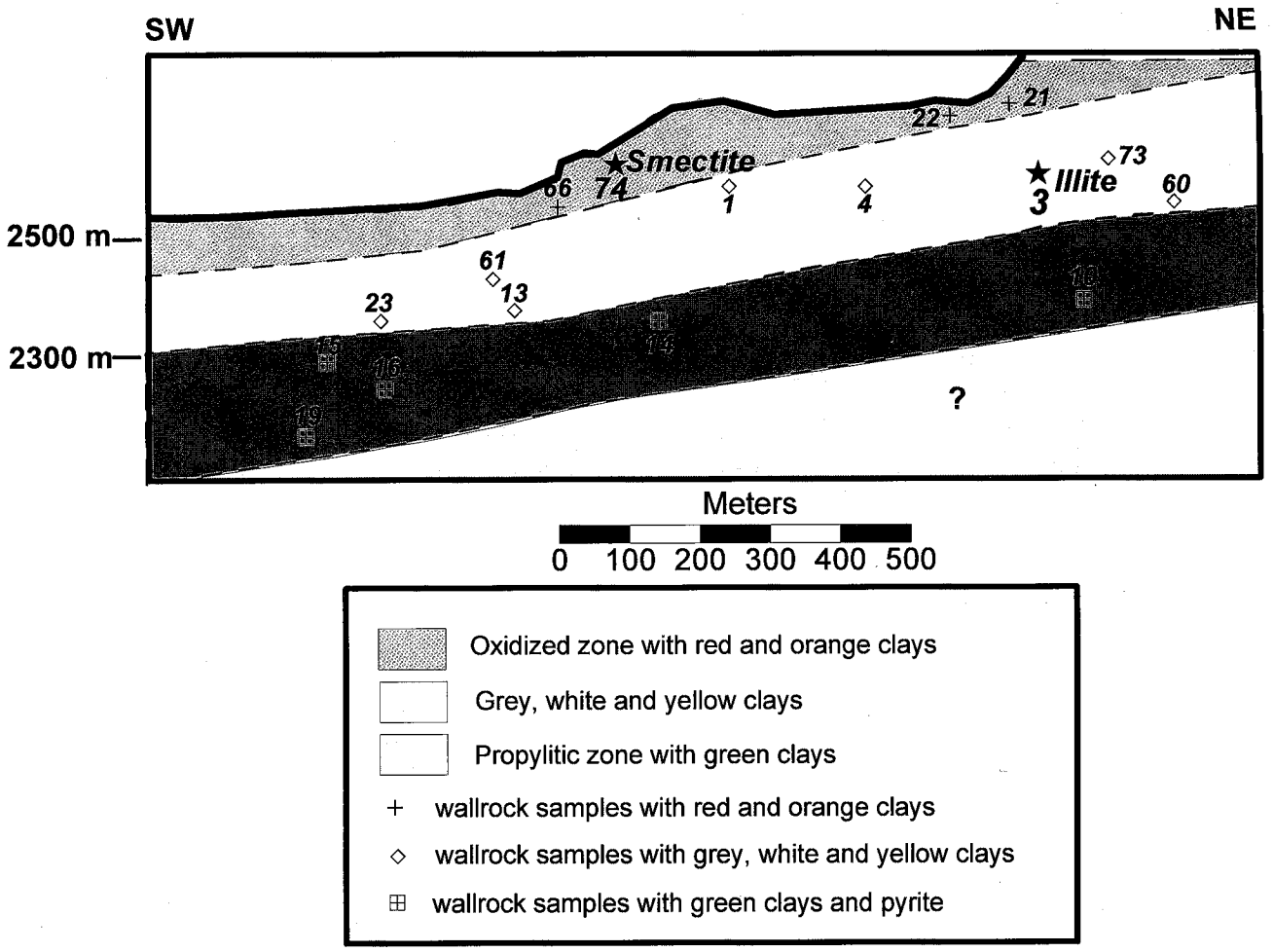

Figure 19. Longitudinal section of the San Nicolas vein showing wallrock alteration zones and results of XRD clay analyses on samples (Sn-3, predominately illite) and (Sn-74, predominately smectite).

A correlation matrix was calculated for all samples from all veins to evaluate the behavior of individual elements relative to one another. The data presented here is for the San Nicolas vein only.

4.5.1 Element Distributions (Image Maps)

The distribution of the precious metals (Au,Ag) **(Figs . 20 and 21)**, base metals (Cu, Pb and Zn) **(Figs. 22-24)**, pathfinder elements (As, Sb) and the element ratios (Au+Ag/Cu+Pb+Zn) **(Figs. 25-27)** are plotted. Gold and silver are most abundant in the northeast and southwest portions of the San Nicolas vein within the El Cubo property boundaries. Elevated trace element concentrations of Au and Ag are found proximal to the Villalpando, Contra and Alto de Villalpando vein intersections that are shown as red lines **(Figs. 20 and 21)**. Elevated distribution patterns of (Cu, Pb, Zn, As and Sb) coincide with that of gold and silver **(Figs. 22-26)**. Zinc shows a greater concentrations than both copper and lead. **(Figs. 22-25).** Values for arsenic and antimony are also elevated in the northeast and southwest parts of the vein **(Figs. 25 and 26)**. The ratio plot of precious metals to base metals (Au and Ag/Cu+Pb+Zn) shows a very distinct horizon where precious metals dominate over base metals **(Fig. 27)**

4.5.2 Element Correlations

An element correlation matrix created by the "StatMost" statistics software for the elements Au, Ag, As, Sb, Cu, Pb and Zn, numerically demonstrates how specific elements behave relative to one another **(Fig. 28).** In addition to determining a correlation factor,

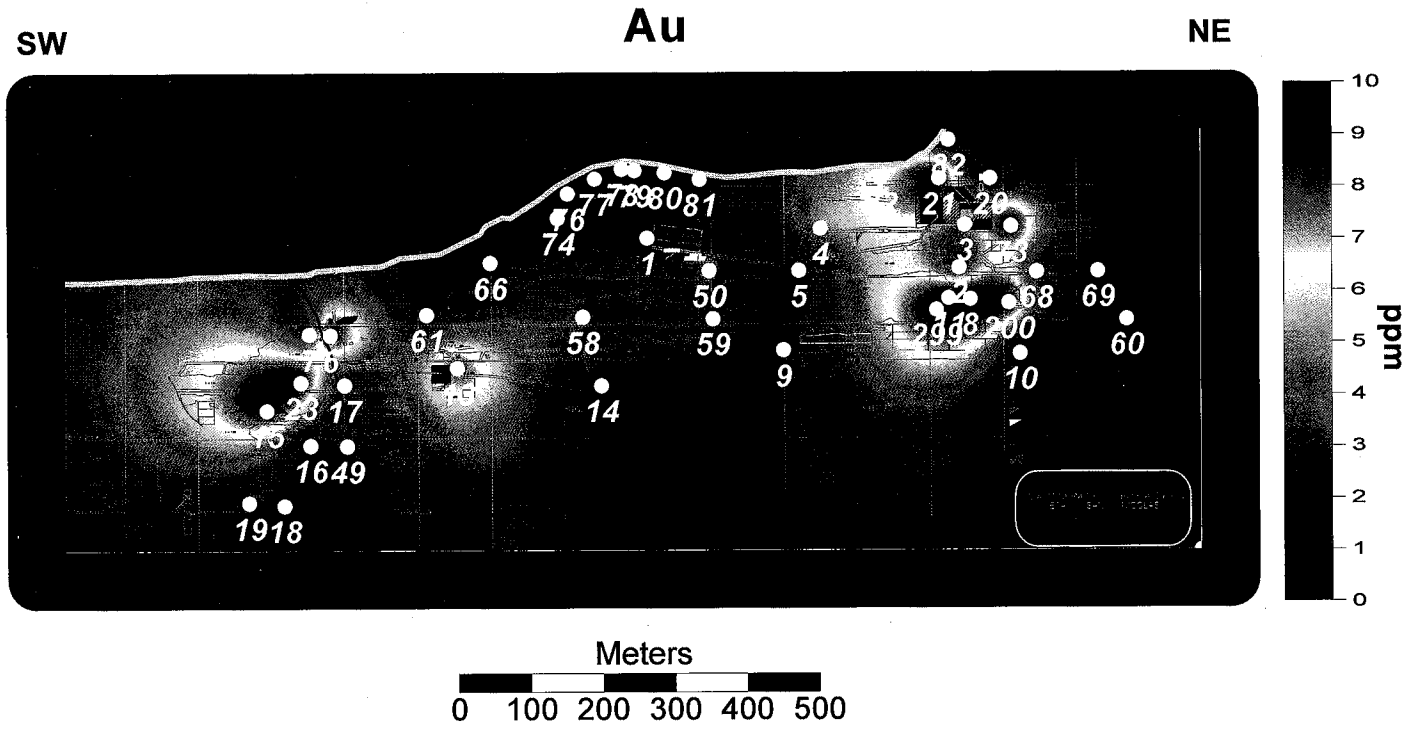

Figure 20. Geochemical sample locations and distribution of gold on the San Nicolas vein longitudinal section. Highest values for gold occur in northeastern and southwestern sections of the vein. Red lines are vein intersections.

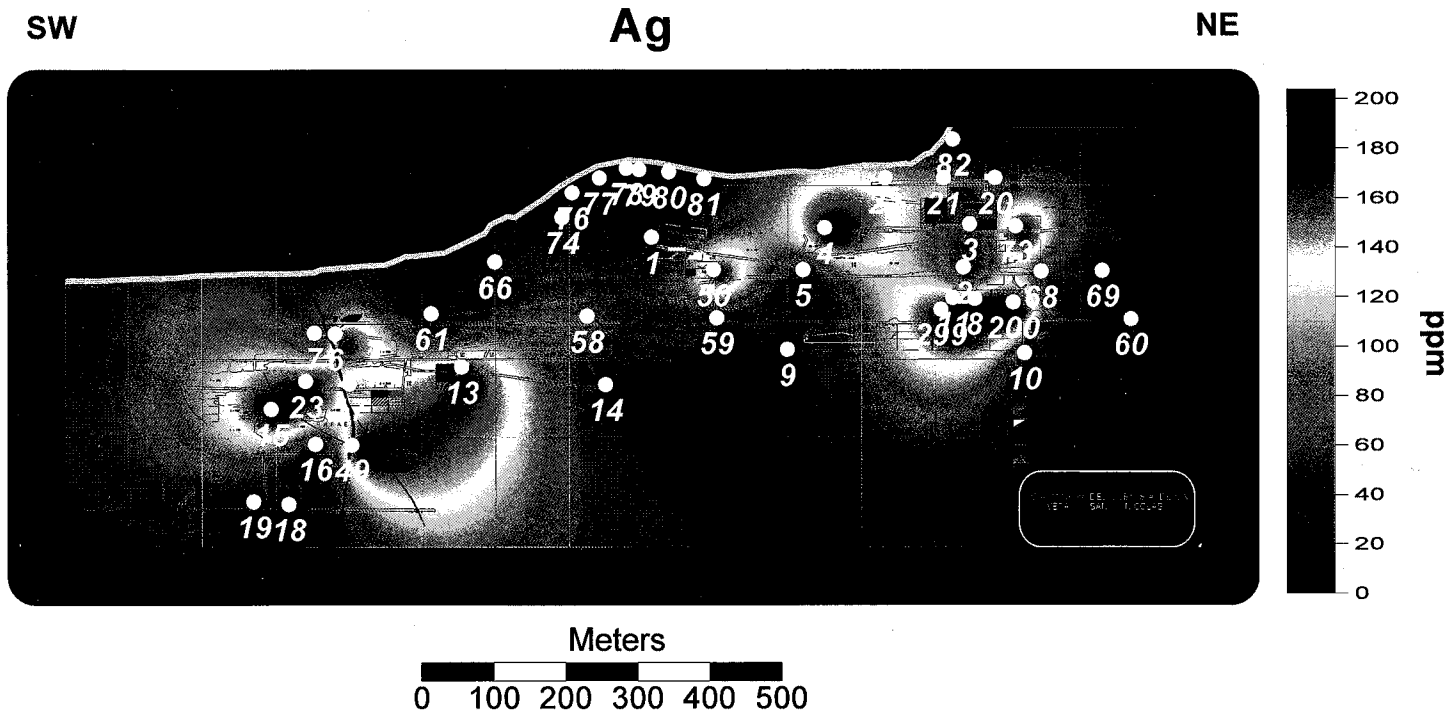

Figure 21. Geochemical sample locations and distribution of silver on the San Nicolas vein longitudinal section. Highest values for silver occur in northeastern and southwestern sections of the vein. Red lines are vein intersections.

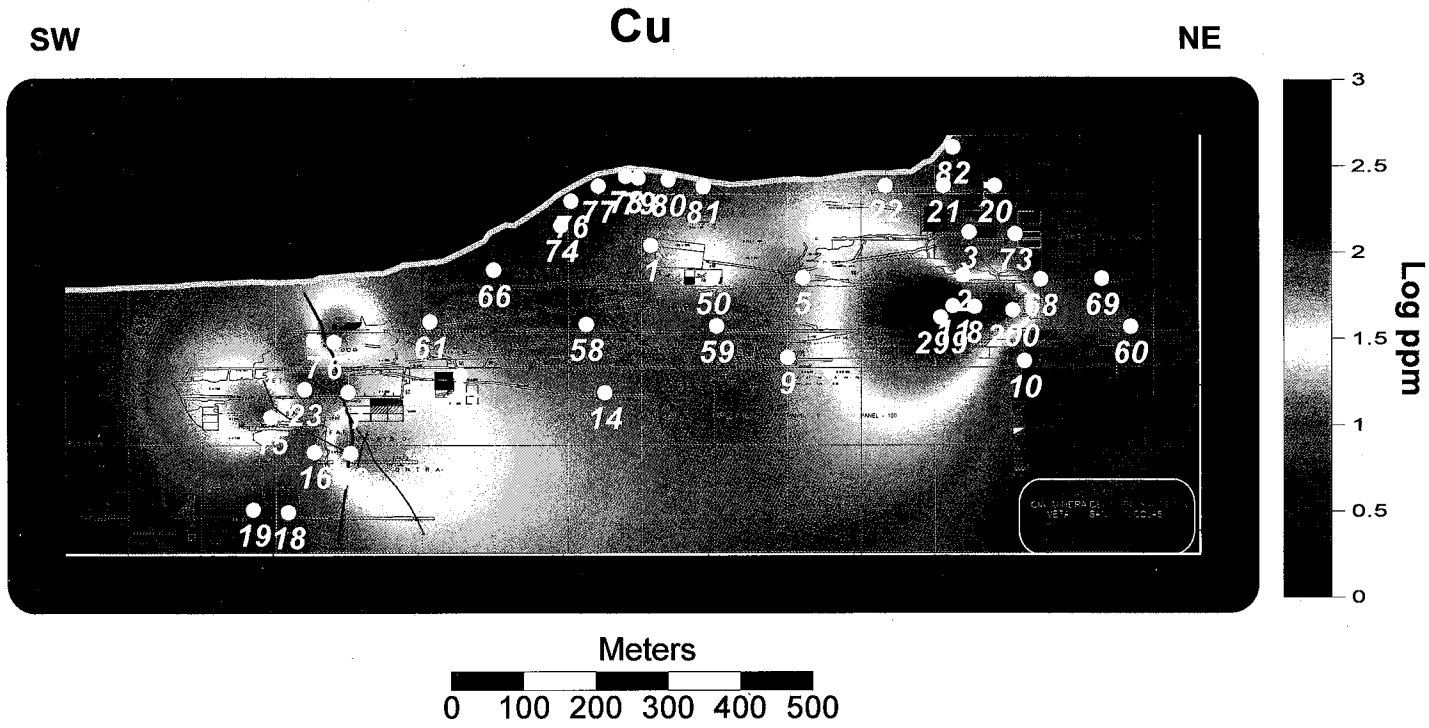

Figure 22. Geochemical sample locations and distribution of copper on the San Nicolas vein longitudinal section. Highest values for copper occur in northeastern and southwestern sections of the vein. Red lines are vein intersections.

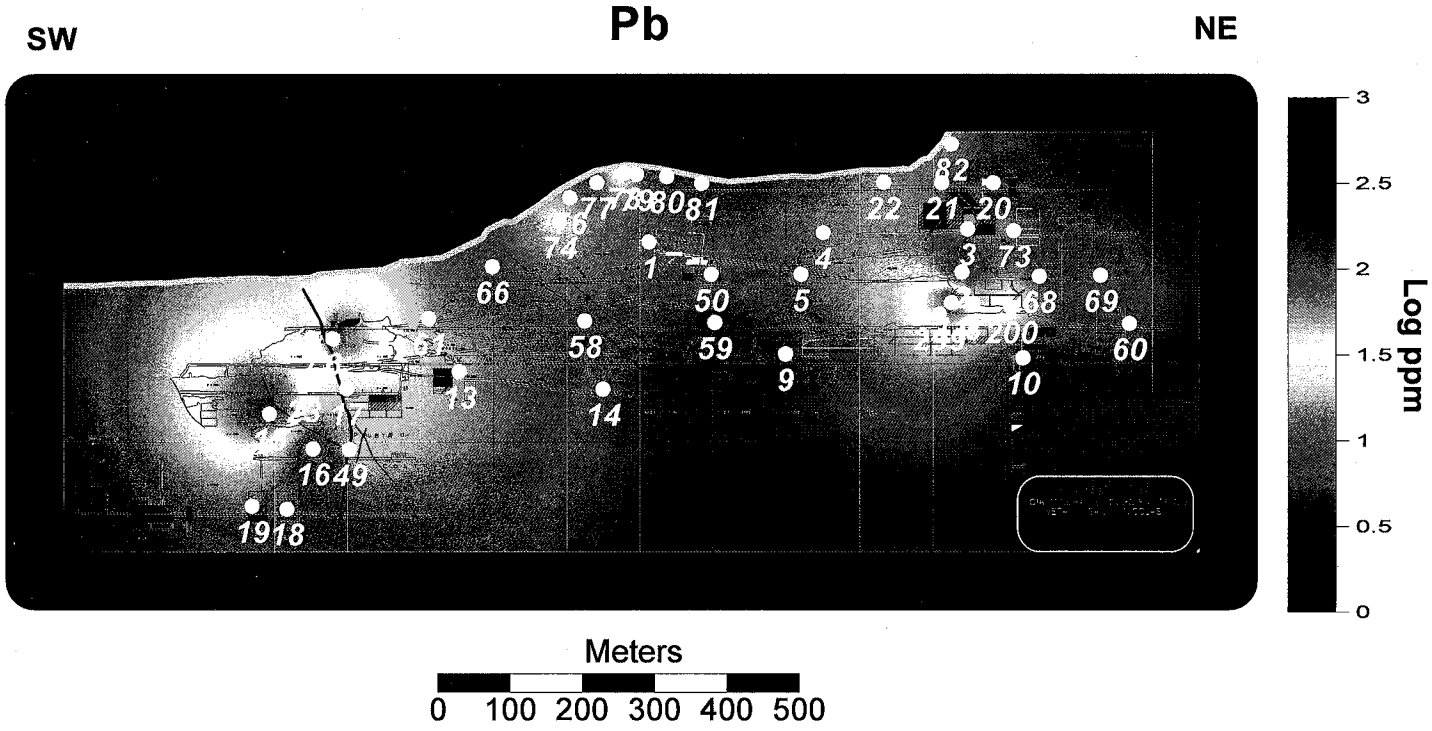

Figure 23. Geochemical sample locations and distribution of lead on the San Nicolas vein longitudinal section. Highest values for lead occur in northeastern and southwestern sections of the vein. Red lines are vein intersections.

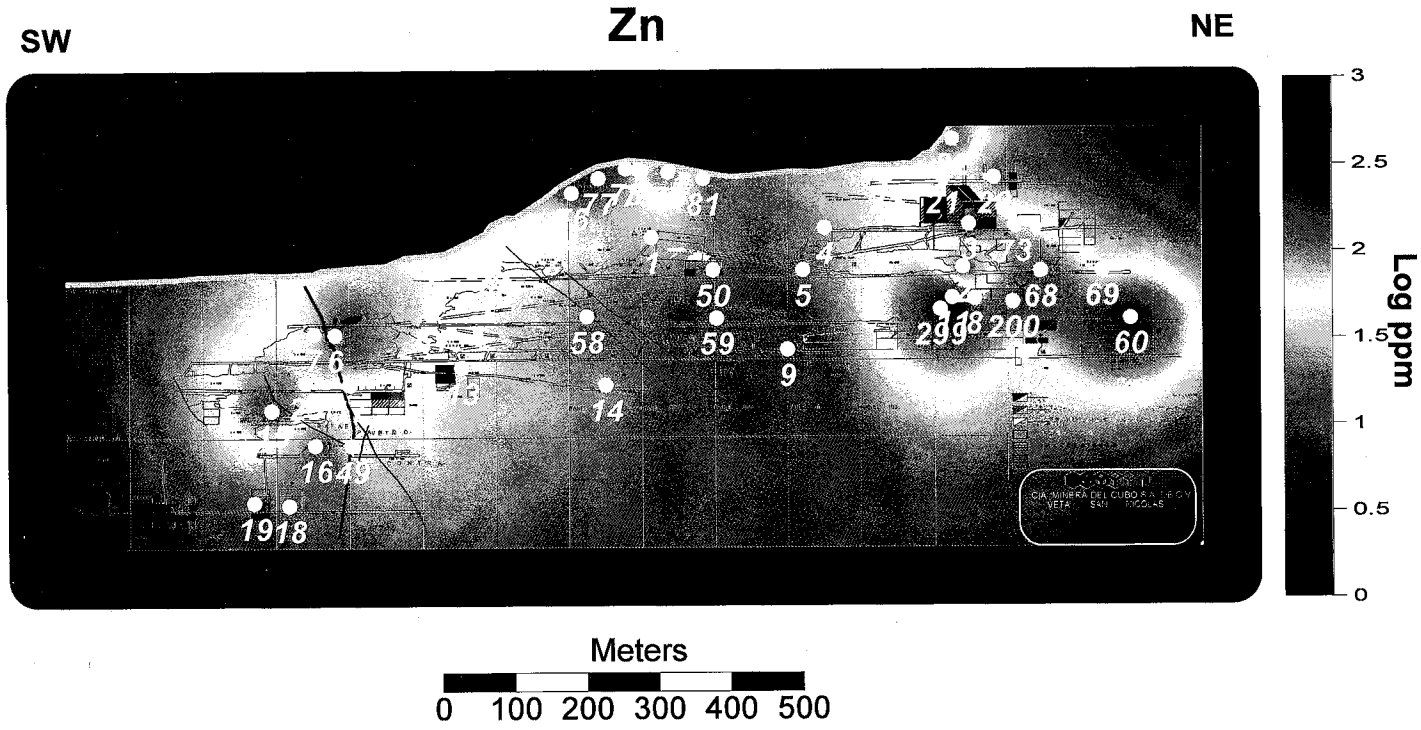

Figure 24. Geochemical sample locations and distribution of zinc on the San Nicolas vein longitudinal section. Highest values for zinc occur in northeastern and southwestern sections of the vein. Red lines are vein intersections.

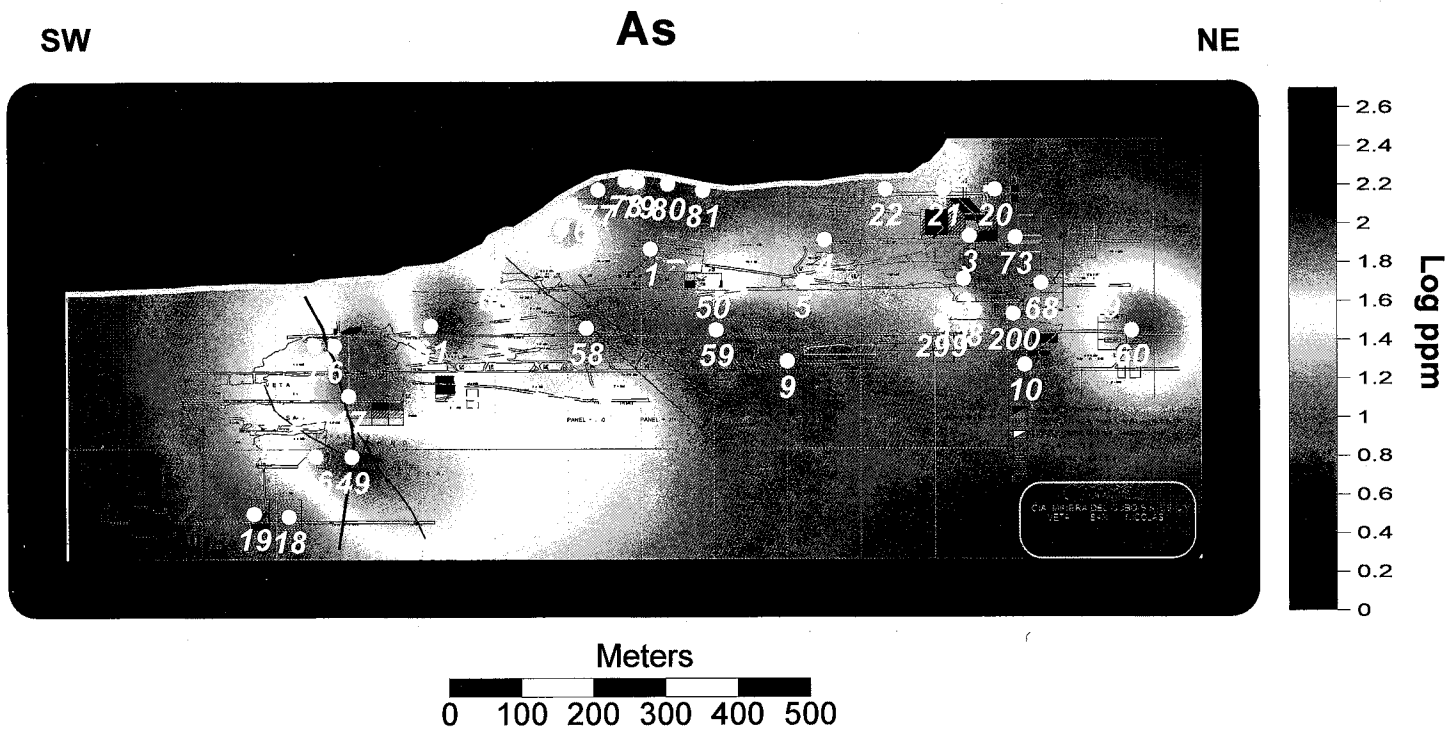

Figure 25. Geochemical sample locations and distribution of arsenic on the San Nicolas vein longitudinal section. Highest values for arsenic occur in northeastern and southwestern sections of the vein. Red lines are vein intersections.

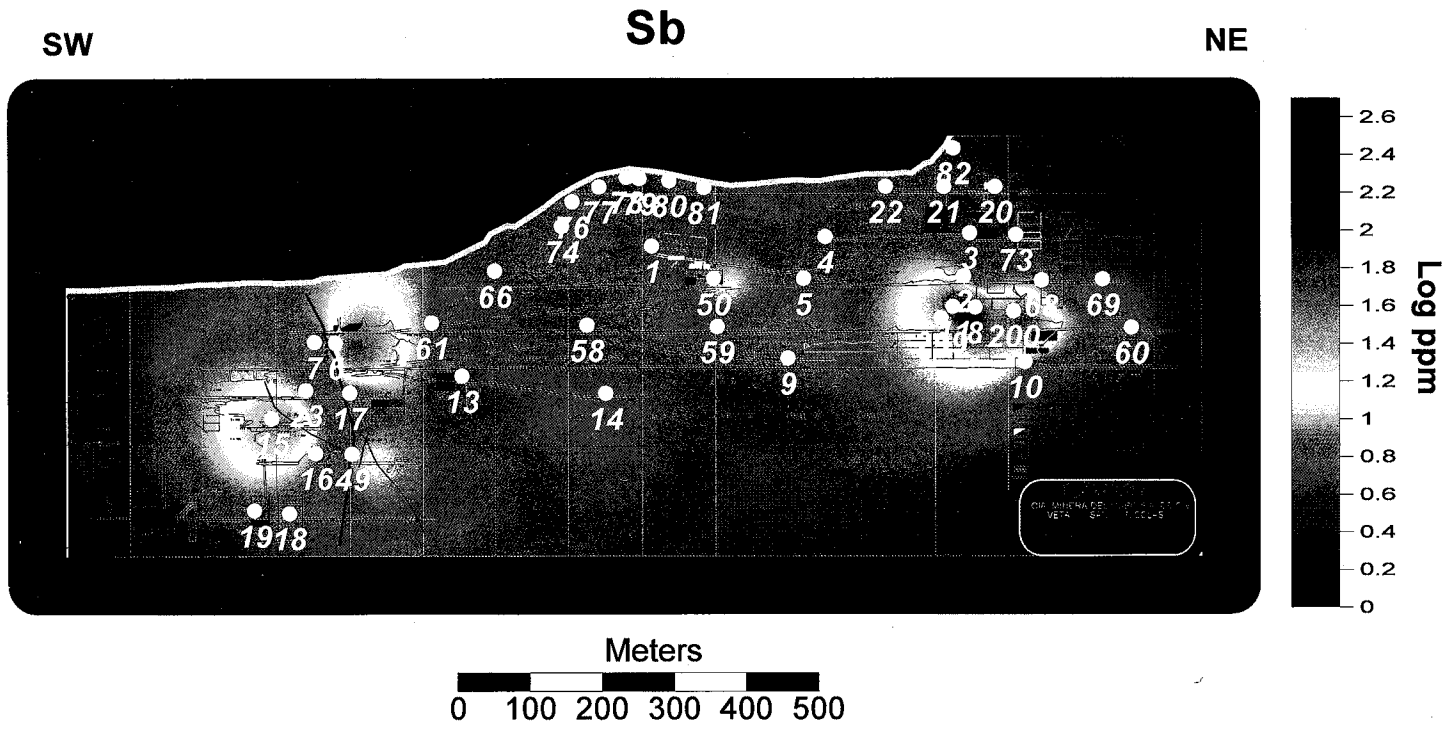

Figure 26. Geochemical sample locations and distribution of antimony on the San Nicolas vein longitudinal section. Highest values for antimony occur in northeastern and southwestern sections of the vein. Red lines are vein intersections.

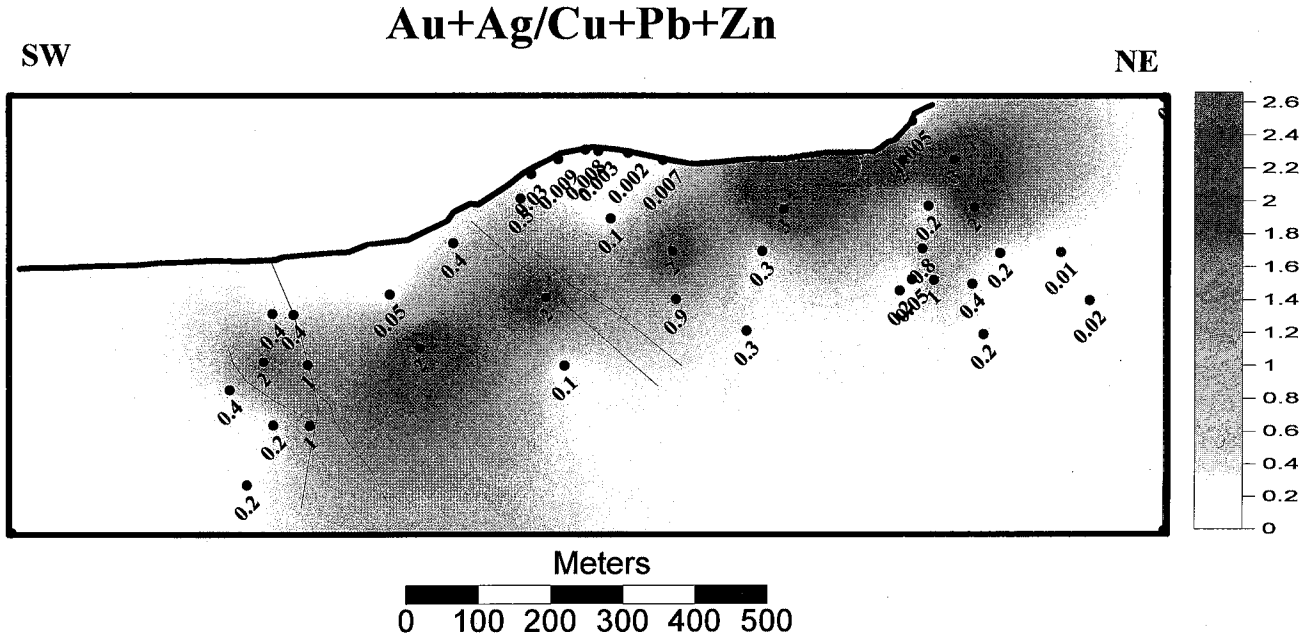

Figure 27. Geochemical sample locations and ratio distribution of precious metals (Au+Ag) over base metals (Cu+Pb+Zn) plotted on San Nicolas vein longitudinal section. Black lines are vein intersections.

	Au ppm	Ag ppm	Cu	Pb	Zn	As	Sb
Au ppm		0.9021 (82) 0.0000	0.2798 (82) 0.0109	0.4691 (82) 8.756E-006	0.3534 (82) 0.0011	-0.0784 (82) 0.4838	0.2423 (82) 0.0283
Ag ppm	0.9021 (82) 0.0000		0.2747 (82) 0.0125	0.5404 (82) 1.602E-007	0.3898 (82) 0.0003	-0.0751 (82) 0.5023	0.2209 (82) 0.0461
Cu	0.2798 (82) 0.0109	0.2747 (82) 0.0125		0.4694 (82) 8.644E-006	0.6977 (82) 3.260E-013	0.0345 (82) 0.7586	0.9799 (82) 0.0000
Pb	0.4691 (82) 8.756E-006	0.5404 (82) 1.602E-007	0.4694 (82) 8.644E-006		0.7379 (82) 2.615E-015	-0.0132 (82) 0.9064	0.4745 (82) 6.687E-006
Zn	0.3534 (82) 0.0011	0.3898 (82) 0.0003	0.6977 (82) 3.260E-013	0.7379 (82) 2.615E-015		0.0079 (82) 0.9435	0.6712 (82) 5.189E-012
As	-0.0784 (82) 0.4838	-0.0751 (82) 0.5023	0.0345 (82) 0.7586	-0.0132 (82) 0.9064	0.0079 (82) 0.9435		0.0367 (82) 0.7434
Sb	0.2423 (82) 0.0283	0.2209 (82) 0.0461	0.9799 (82) 0.0000	0.4745 (82) 6.687E-006	0.6712 (82) 5.189E-012	0.0367 (82) 0.7434	

*Values in the table are listed as follows:
correlation value
(sample size)
probability

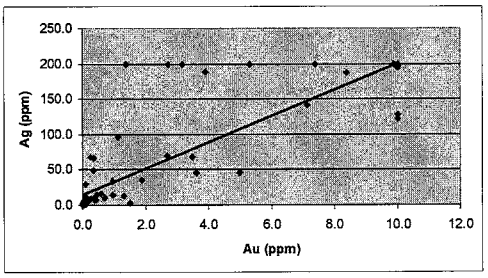

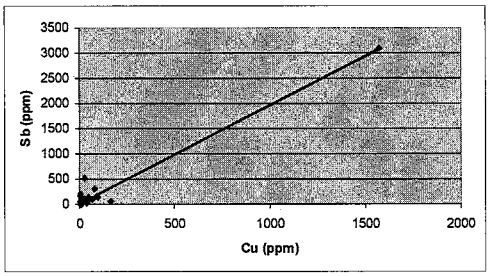

Figure 28. Geochemical element correlations including linear graphs for elements showing strong correlations. Linear graphs reveal that Cu and Sb only have a one point correlation and that Au and Ag are correlative.

the program also reports the sample size and probability. A perfect linear correlation between two elements will yield a value of "1.00". The poorer the correlation, the smaller their correlation coefficient. Elements that do not correlate will have a coefficient of zero. Elements that behave inversely to one another, will have a negative correlation.

The results of the correlation matrix calculation reveal four moderate correlations: Cu and Sb (.97), Au and Ag (.90), Pb and Zn (.74) and Cu and Zn (.70). Scatter plots of Au vs. Ag and Cu vs. Sb were made to determine the linearity of strongest correlations. They reveal that Cu and Sb only have a one point correlation. Without this point, the elements would have a correlation of (.4). The plots also show that gold and silver are linear and do correlate. The negative correlation values that exist between arsenic and gold, silver, and lead indicates that there is an inverse relationship between these elements. The correlation of Au and Ag and to a lesser extent Pb and Zn are evident in the in the image plots. Arsenic shows a halo of elevated arsenic values around elevated gold values.

4.6 Fluid Inclusions Microthermometry

4.6.1 Nature of Inclusions

Primary, secondary and pseudosecondary inclusions were observed in quartz, clear euhedral quartz, amethyst and calcite. Inclusion size ranges between 2 and 10 microns. Measurements were mostly made in clear euhedral quartz, amethyst and mosaic quartz. Small, irregular-shaped primary inclusions were generally found within quartz growth planes **(Fig. 29)**. Rounded secondary inclusions were dominately found in healed

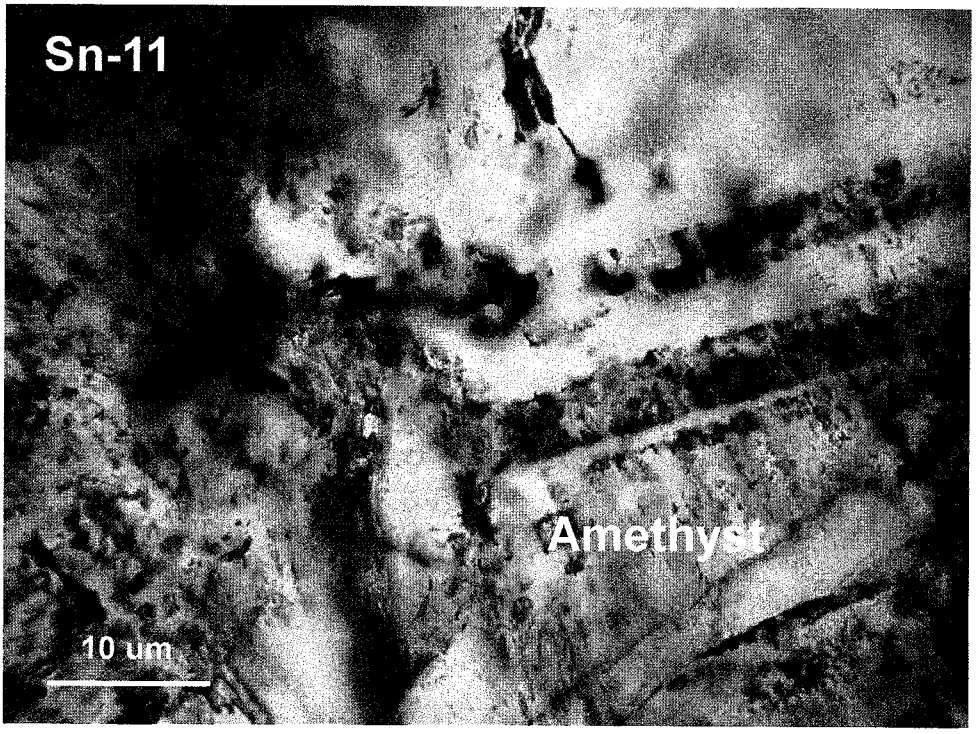

Figure 29. Quartz growth planes filled with vapor-rich (Type II) primary inclusions from Stage III amethyst (Sn-11; X:-272,Y:-281).

microfractures. Subrounded pseudosecondary inclusions were found in planes within crystal boundaries.

Fluid inclusions are either liquid-rich or vapor-rich at room temperature. No daughter minerals, were observed and no CO_2 clatherates were observed when inclusions were cooled. Based on these observations, fluid inclusions were classified into Type I and Type II inclusions. Type I inclusions are defined by the presence of a liquid and vapor with a ~.90 degree fill **(Fig. 30)**. Type II inclusions are vapor-dominated with a degree of fill from 0.0-0.3 **(Fig. 31)**. Coexisting Type I and Type II inclusions in a crystal growth plane or healed microfracture is the strongest evidence for fluid boiling (Bodnar et al, 1985) **(Fig. 32)**. Type II inclusions were observed in all the samples studied **(Table 3)**. Samples with both Type I and Type II fluid inclusions, that lack the coexistence of these two types of inclusions within the same plane are assumed to represent boiling at time during crystal growth.

4.6.2 Highest Temperature Fluid Inclusion Assemblages

The fluid inclusion study presented here is not a conventional fluid inclusion study in that fluid inclusions chosen for measurement were biased. Fluid inclusion populations chosen for measurement were chosen because they displayed characteristics of being the highest temperature fluid inclusions within the sample being analyzed. These highest temperature fluid inclusion assemblages were chosen to determine the maximum temperature in time and space. By determining maximum temperature, it is possible to determine the ore-fluid flow direction by plotting averages of fluid inclusion Th information on mine longitudinal sections (Albinson, pers. comm., 2000). These fluid

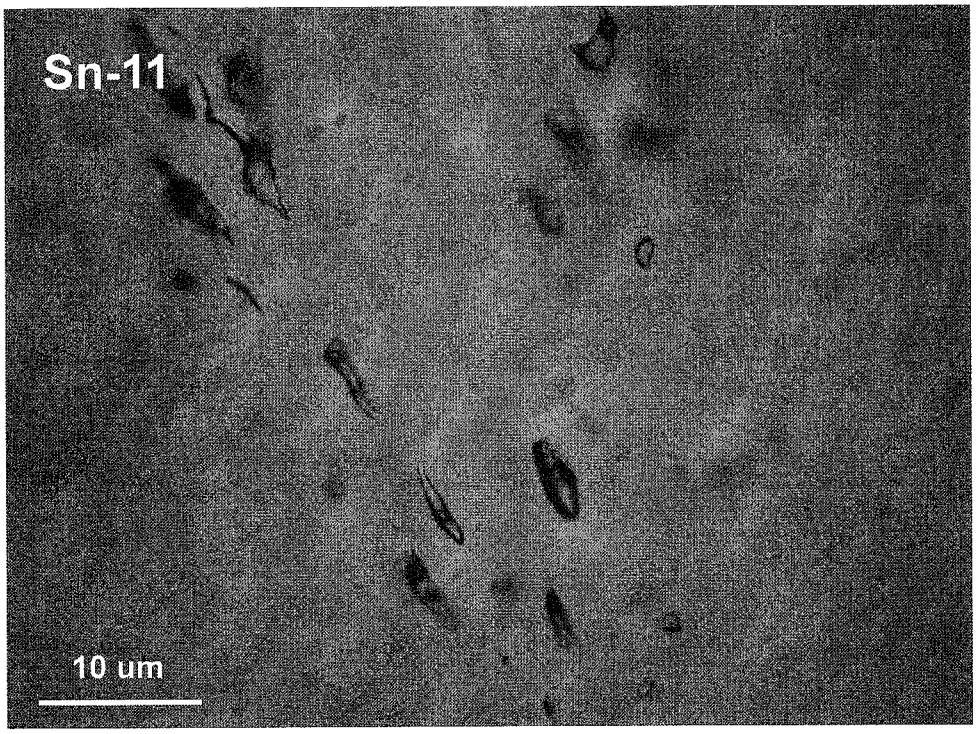

Figure 30. Photomicrograph of liquid-rich (Type 1) pseudosecondary inclusion plane from Stage III amethyst (Sn-11; X:-272 Y:-281).

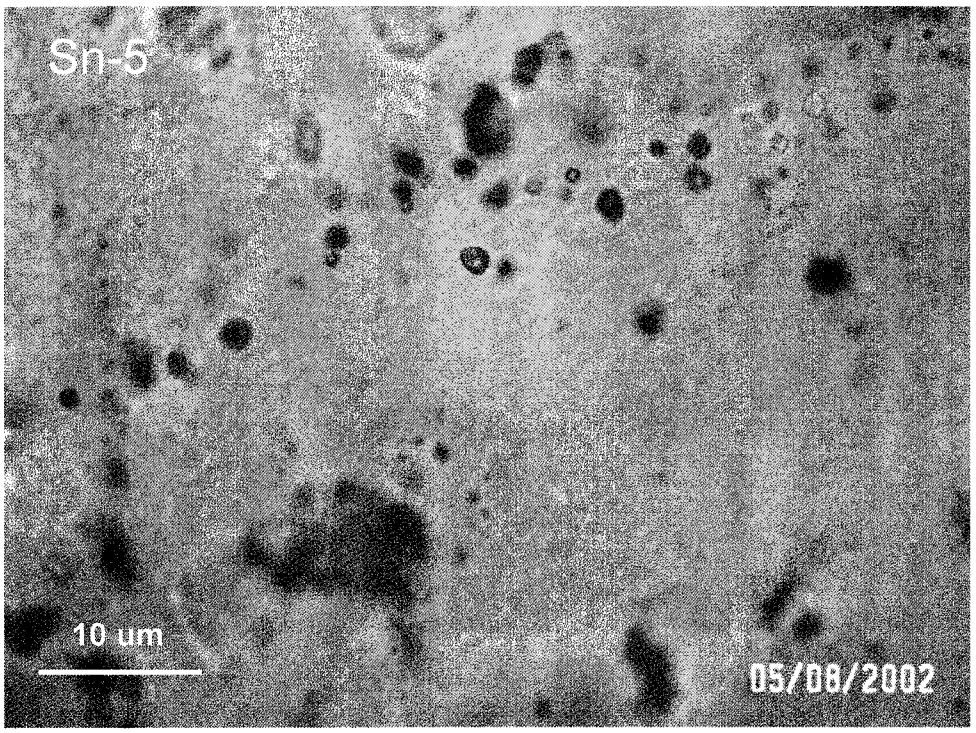

Figure 31. Photomicrograph of vapor-rich (Type II) secondary inclusion plane from Stage III amethyst (Sn-5; X: -478, Y: -242).

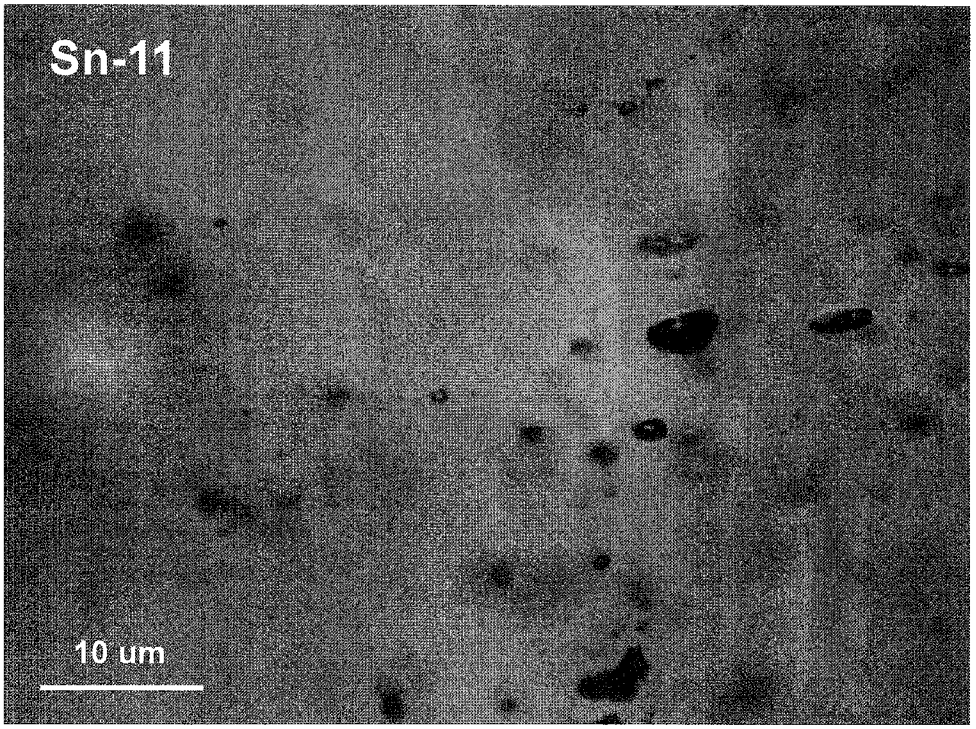

Figure 32. Photomicrograph of liquid-rich (Type I) fluid inclusions coexisting with vapor-rich (Type II) secondary inclusions suggesting boiling. (Sn-11; Stage III amethyst; X: -272, Y: -281).

Table 3. San Nicolas vein average, high temperature Fluid Inclusion Assemblage (FIA) data.

Sample #	Avg. Th	Avg. Tm	Host Mineral	Paragenetic Stage	Avg. Wt % NaCl	Type	Th range	# of inclusions	Tm deg C range	# of inclusions	Observations
Sn-1	230	-0.52	mosaic quartz	Stage II	0.9	P	208-245	5	-0.5 to -0.6	5	Type I and Type II
Sn-2	271	-1.32	quartz	Stage II	2.1	PS	261-282	5	-1.1 to -1.5	5	Type II
Sn-3	196	-1.32	crystalline quartz	Stage III	2.2	P	183-203	6	-1.3 to -1.4	6	**Type I, coexisting Type II**
Sn-4	240	-1.00	crystalline quartz	Stage II	1.7	S	239-243	5	-0.9 to -1.1	2	**Type I, coexisting Type II**
Sn-5	217	-0.41	crystalline quartz	Stage III	0.7	P	209-226	9	-0.4 to 0.5	9	Type I and Type II
Sn-6	255	-0.14	crystalline quartz	Stage III	0.2	P	240-277	8	-0.1 to -0.2	8	**Type I, coexisting Type II**
Sn-8	229	-0.10	mosaic quartz	Stage II	0.2	P	220-235	5	-0.2 to 0.2	5	**Type I, coexisting Type II**
Sn-9	223	-0.66	crystalline quartz	Stage III	1.1	P	194-245	7	-0.6 to 0.7	7	**Type I, coexisting Type II**
Sn-10	229	-0.53	quartz	Stage II	0.9	P	219-230	3	-0.5 to -0.6	3	Type I and Type II
Sn-13	250	-0.73	crystalline quartz	Stage III	1.2	PS	250-251	3	-0.7 to -0.8	3	**Type I, coexisting Type II**
Sn-14	250	-0.44	amethyst	Stage III	0.7	PS	234-260	7	-0.3 to -0.5	7	Type I and Type II
Sn-15	241	-0.35	crystalline quartz	Stage III	0.6	P	225-249	4	-0.2 to -0.5	4	**Type I, coexisting Type II**
Sn-19	216	-0.70	calcite	Stage III	1.2	PS	209-221	10	-0.6 to -0.9	10	Type I and Type II
Sn-22	223	-0.37	crystalline quartz	Stage III	0.6	P	216-225	3	-0.3 to -0.4	3	**Type I, coexisting Type II**
Sn-23	262	-0.33	quartz	Stage III	0.5	P	255-266	4	-0.2 to -0.4	4	Type I and Type II
Sn-49	232	-0.47	crystalline quartz	Stage III	0.8	P	227-237	7	-0.2 to -0.8	7	Type I and Type II
Sn-58	242	-0.10	calcite	Stage III	0.2	P	242-242	4	-0.1 to -0.1	4	**Type I, coexisting Type II**
Sn-60	223	-1.73	crystalline quartz	Stage II	2.8	PS	219-229	6	-1.7 to -1.8	6	**Type I, coexisting Type II**
Sn-61	237	-0.45	mosaic quartz	Stage II	0.5	P	237-238	2	-0.4 to -0.5	2	**Type I, coexisting Type II**
Sn-66	238	-0.20	quartz	Stage II	0.3	PS	234-244	3	-0.2 to -0.2	3	Type I and Type II
Sn-69	239	-0.60	crystalline quartz	Stage III	1.0	PS	212-258	5	-0.5 to -0.8	5	**Type I, coexisting Type II**
Sn-74	183	-0.10	calcite	Stage III	0.2	P	172-194	2	-0.1 to -0.1	2	**Type I, coexisting Type II**
Sn-82	181	-0.67	quartz veinlet	Stage I	1.1	P	168-198	3	-0.6 to 0.7	3	**Type I, coexisting Type II**

P-primary fluid inclusions
S-secondary fluid inclusions
PS-pseudosecondary fluid inclusions

coexisting-within a crystal grain both Type I and Type II inclusions exist within the same fluid inclusion assemblage
boiling- (indicated by bold lettering) the coexistence of Type I and Type II fluid inclusions within a primary growth plane, secondary or pseudosecondary healed microfracture (Bodnar et al., 1985)
Type I and Type II fluid inclusions within the same mineral or adjacent minerals

inclusions are known as the highest temperature Fluid Inclusion Assemblages (FIA's). Fluid Inclusion Assemblages were chosen based on the criteria defined by Bodner and others (1985). Inclusions that met this criteria have consistent liquid/vapor ratios, large vapor bubbles and negative crystal shapes. They number greater than two in a field of view and have small Th ranges. Lower temperature inclusions have variable liquid to vapor ratios, smaller vapor bubbles, irregular shapes and wide ranges in Th (Bodner et al., 1985). Inclusion assemblages with inconsistent liquid to vapor ratios were avoided as much as possible because these inclusions might have necked and would yield false high or low (Th's) (Bodner et al.,1985). Measurements are summarized in **Table 3**.

4.6.3 Temperatures of Homogenization

Temperatures of homogenization (Th) range from 103-282 °C with an average Th of 235 °C for all inclusions measured **(Appendix 3)**. Histograms of primary, secondary and pseudosecondary fluid inclusion Th from mosaic quartz, clear quartz, blocky calcite and bladed calcite (Stage II) are shown in **(Fig. 33).** Histograms of Th from amethyst and blocky calcite (Stage III) are also shown in **(Fig. 33)**. Stage I fluid inclusions were not plotted on histograms due to lack of data.

The majority of the fluid inclusions measured in Stage II were measured in clear quartz. The Th values range from 180-290 °C. Mosaic quartz recrystallized from amorphous silica has an average Th of 228 °C $\pm$ 1σ . Fluid inclusions measured in mosaic quartz may have formed during dewatering of amorphous silica as it crystallized to mosaic quartz. Therefore, fluid inclusion Th measured in mosaic quartz does not represent the primary deposition temperature of amorphous silica.. Stage II blocky calcite average Th is

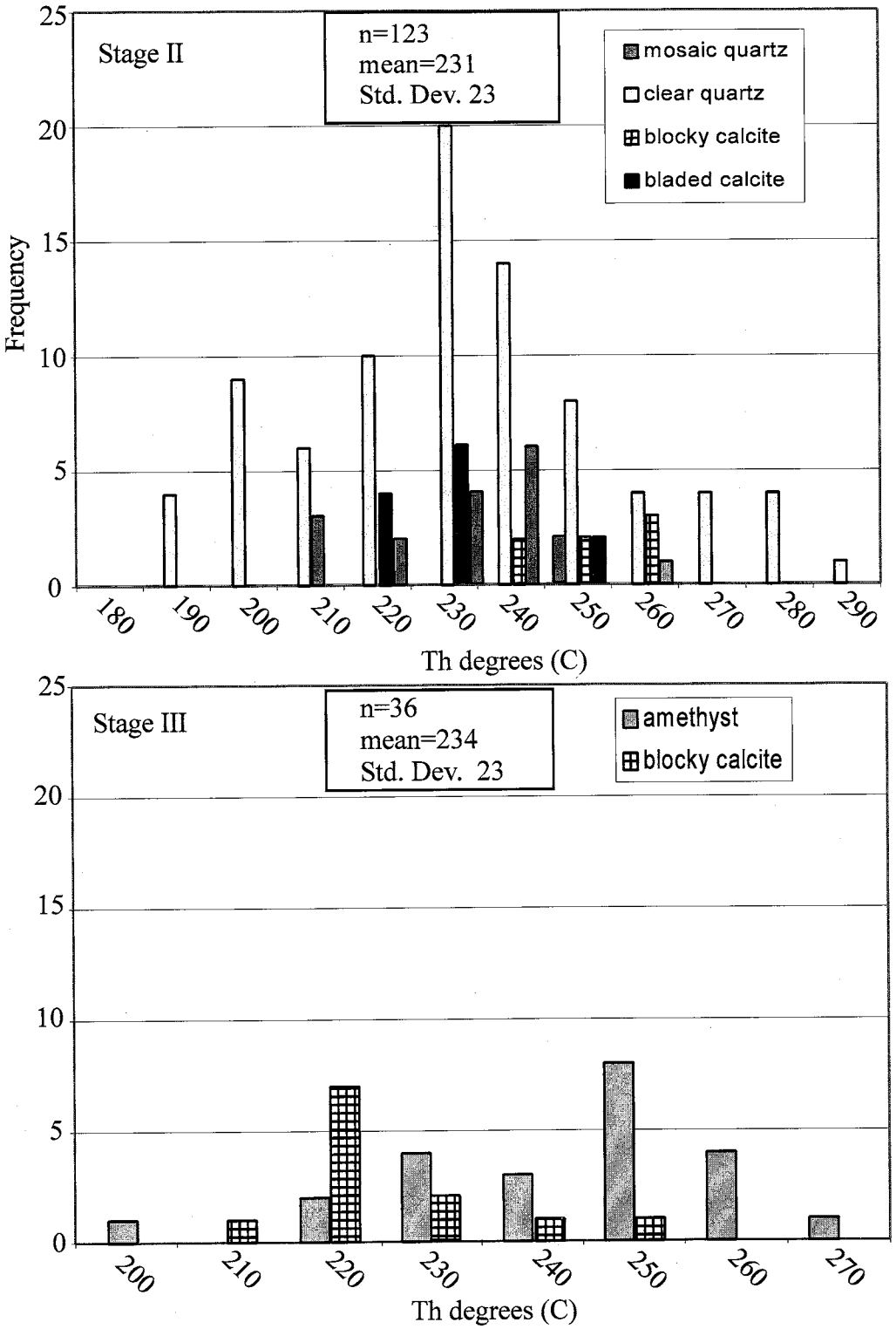

Figure 33. Histograms of Th measured in Stages II and III minerals.

245 °C ± 1σ. Fluid inclusion Th measured in bladed calcite average 225 °C ± 1σ. Stage III blocky calcite and amethyst average 221 °C ± 1σ and 238 °C ± 1σ.

A fluid inclusion assemblage with the highest average Th values was chosen for each sample studied to represent the maximum temperature in time or space. The averages for each sample were listed in **(Table 3).** They were plotted on the San Nicolas vein longitudinal section and hand contoured at twenty ° C intervals **(Fig. 34).**

4.6.4 Temperatures of Melting

Temperatures of melting Tm range from 0 – 0.8 °C with an average of -0.6 **(Appendix 3)** Melting temperatures were converted to salinities using the equation by Bodnar (1985). Salinities range from 0- 3 wt % NaCl eq. with an average of 1.0 wt % NaCl eq. **(Appendix 3).** Histograms of salinities from primary, secondary and pseudosecondary fluid inclusions measured in amorphous silica, clear quartz, blocky calcite, bladed calcite (Stage II), and amethyst and blocky calcite (Stage III) are presented in **(Fig. 35).** The majority of fluid inclusion Tm measurements were made in clear quartz. The calculated salinities range from 0.4 - 3 wt % NaCl eq. Amorphous silica salinities range from 0.4-2.4 wt % NaCl eq. Stage II blocky calcite ranges from 0-2.4 wt % NaCl eq. Bladed calcite ranges from 0-1.6 wt % NaCl eq. Stage III amethyst ranges from 1.4-1.2 wt % NaCl with the majority of the analyses within the 1.2 wt % NaCl eq. bin. Stage III blocky calcite salinities range from 0.4-1.6 wt%f NaCl eq.

Salinity values are plotted on the San Nicolas longitudinal section show that salinities generally increase downwards with the highest values in the northeast section of

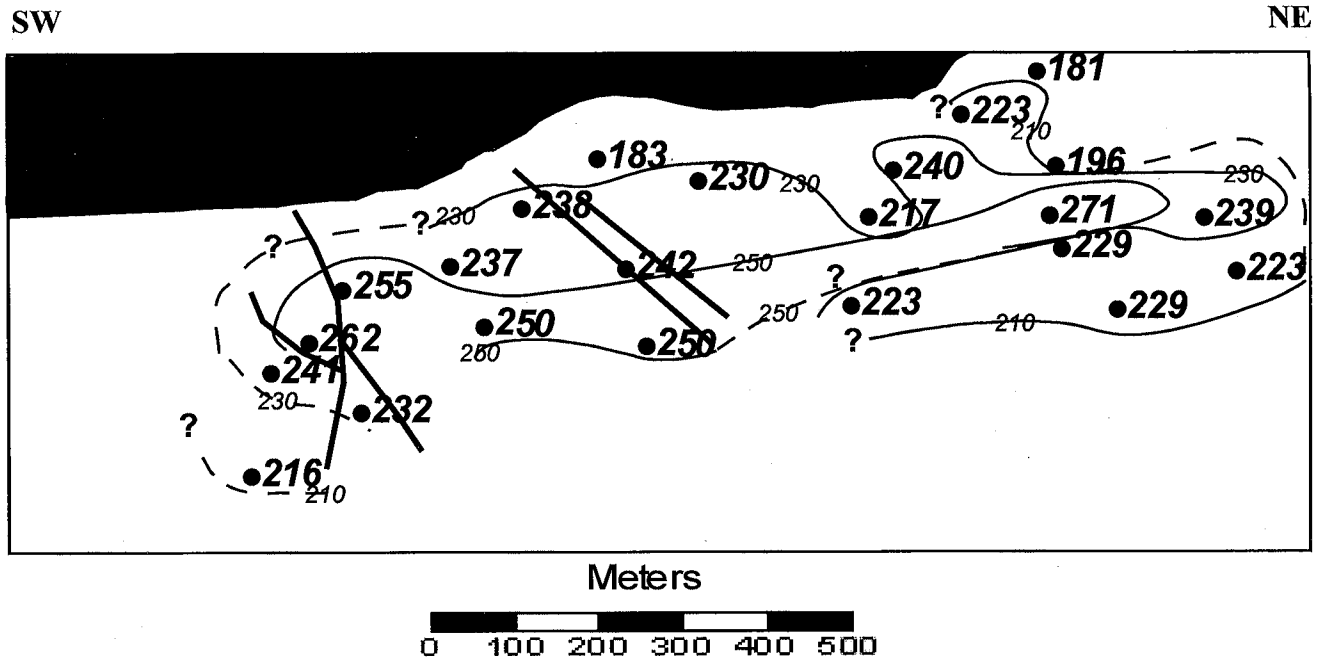

Figure 34. Average temperature contours from San Nicolas vein highest temperature Fluid Inclusion Assemblages (FIA's). Isograd lines drawn at 210, 230, and 250 degrees Celcius

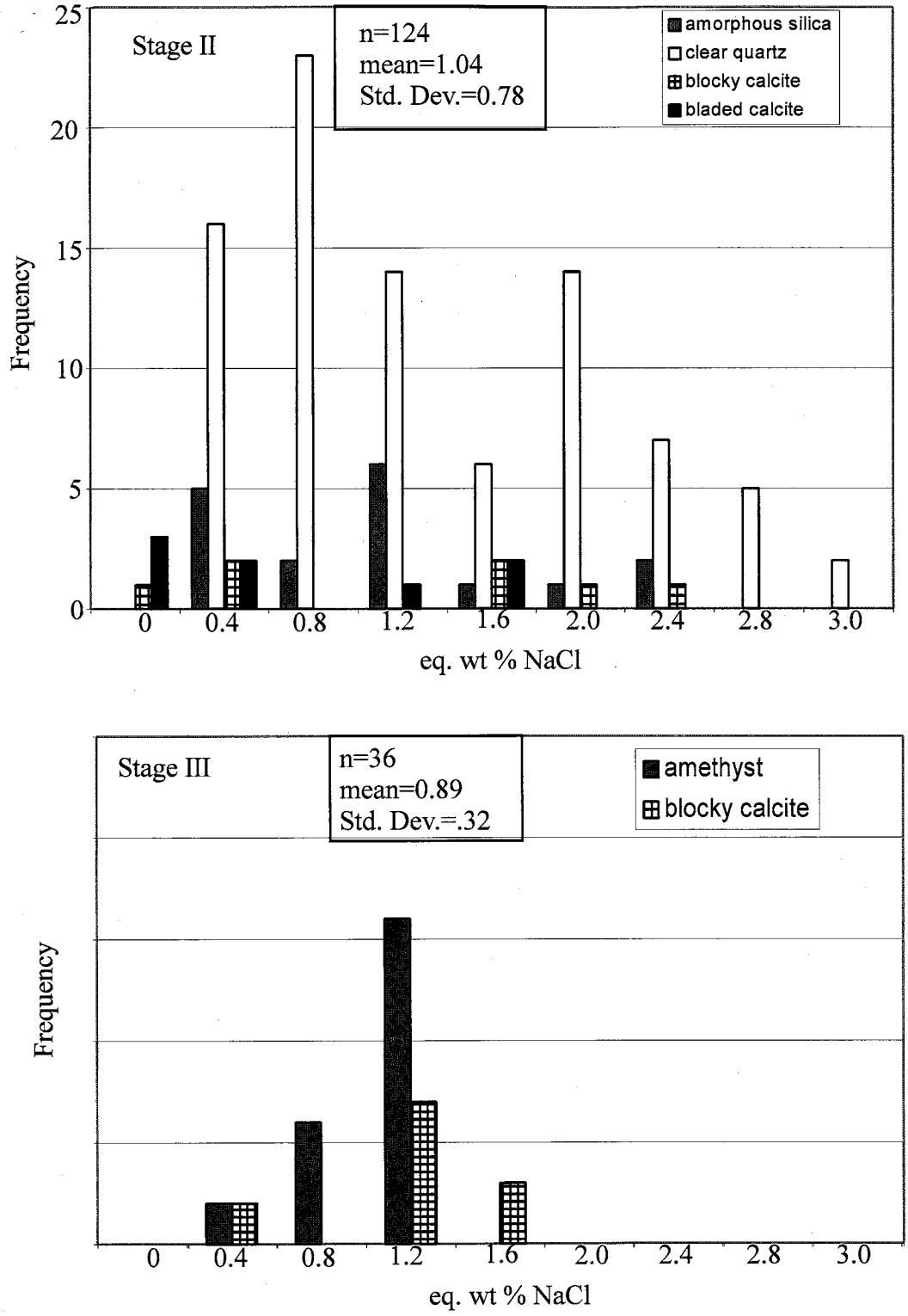

Figure 35. Histograms of salinities from different minerals within paragenetic Stages II and III.

the vein. Generally higher salinities are coincident with highest Th values **(Figs. 35 and 36)**.

A Th versus salinity scatter plot was made for all primary fluid inclusions **(Fig. 37)**. On this diagram are plotted four trends of fluid inclusion salinity and temperatures reported in studies from active geothermal system fluids. San Nicolas vein fluid inclusion data can be bound by two major trends (Trend 1 and Trend 2) determined by observations made on the Broadlands-Ohaaki geothermal system (Hedenquist an, 1985a; Simmons and Christenson, 1994). Trend 1 represents gas loss during boiling (Hedenquist and Henley, 1985). Trend 2 represents the dilution of a saline Cl- rich parent solution (composition A) with a CO_2 rich steam heated water (composition B) (Hedenquist and Henley, 1985). Intermediate compositions (Trend 3) may reflect mixing, gas loss, gas addition coupled with conductive cooling (Moore et al., 2000). Trend 4 represents boiling and evaporative steam loss of a gas-poor parent liquid (Simeone and Simmons, 1999 and Simmons et al., 2000).

The intersection of several trends may **(Fig. 37 point A)** provide the possible temperature and salinity of the parent water. However, trend 4 and trend 1 cannot occur from the same fluid. Although elements of the data appear to lie along a trend, analyses for no sample entirely lies along a single trend. Temperature verses salinity analyses from the Broadlands-Ohaaki geothermal system were plotted for comparison with San Nicolas analyses. Broadlands-Ohaaki fluid inclusion analyses show the same spread in salinity and temperature.

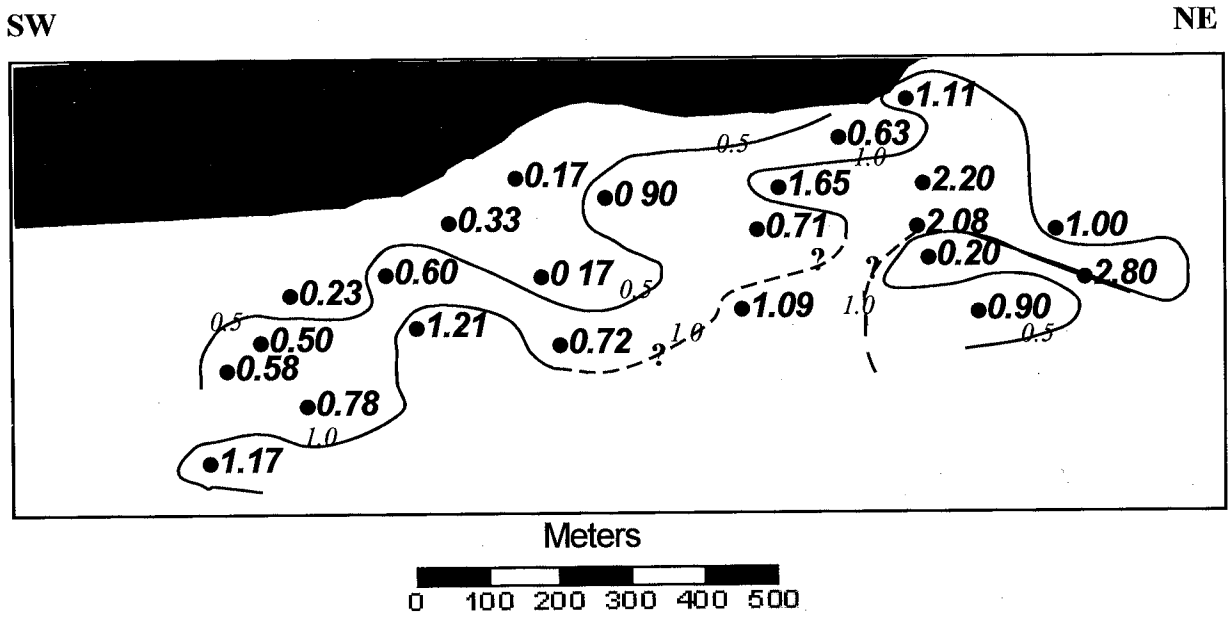

Figure 36. Average salinity contours from San Nicolas vein highest temperature Fluid Inclusion Assemblages (FIA's).

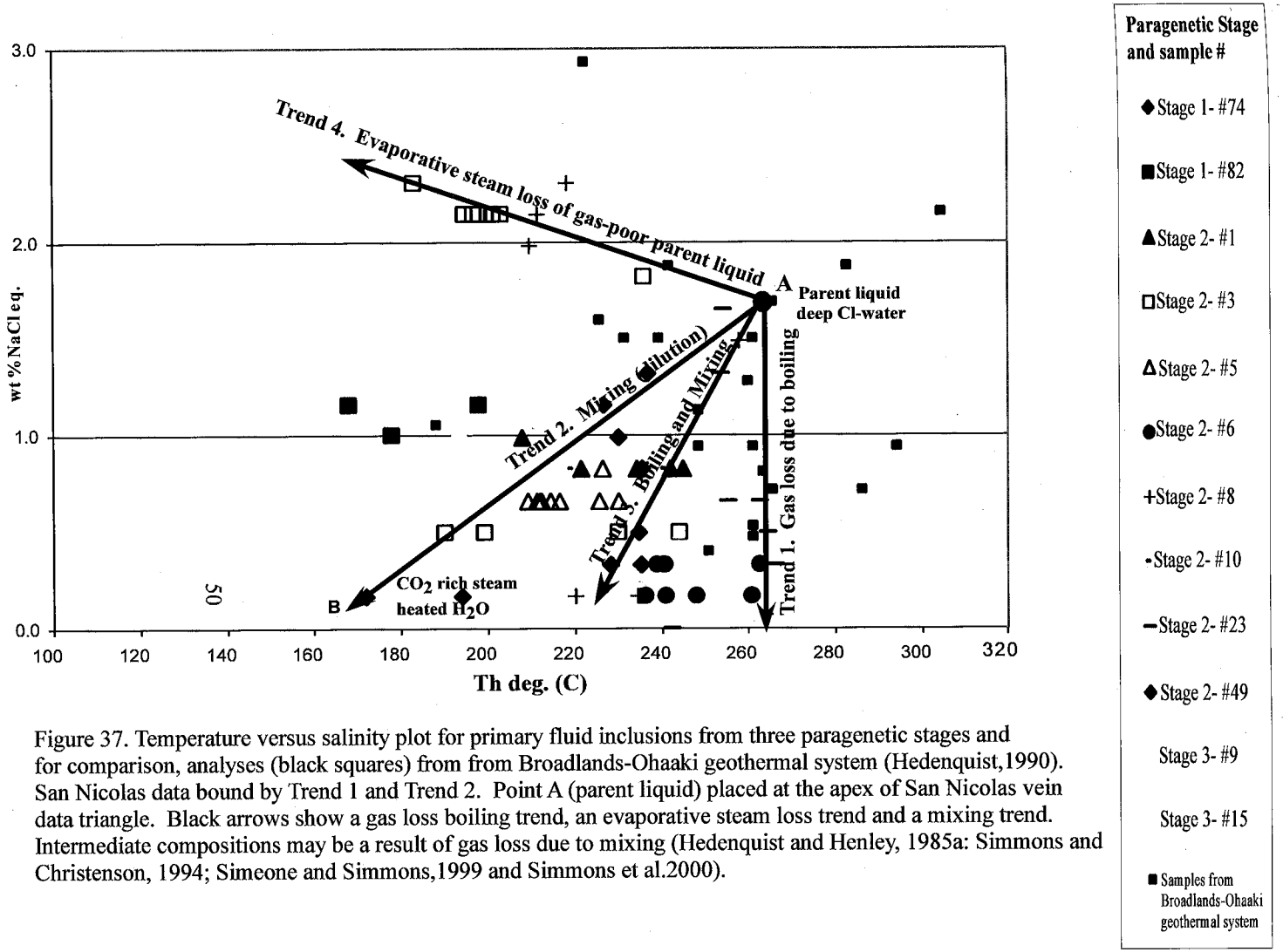

Figure 37. Temperature versus salinity plot for primary fluid inclusions from three paragenetic stages and for comparison, analyses (black squares) from from Broadlands-Ohaaki geothermal system (Hedenquist,1990). San Nicolas data bound by Trend 1 and Trend 2. Point A (parent liquid) placed at the apex of San Nicolas vein data triangle. Black arrows show a gas loss boiling trend, an evaporative steam loss trend and a mixing trend. Intermediate compositions may be a result of gas loss due to mixing (Hedenquist and Henley, 1985a: Simmons and Christenson, 1994; Simeone and Simmons,1999 and Simmons et al.2000).

Microthermometry measurements made on fluid inclusions from paragenetic bands in samples (Sn-8) and (Sn-15) **(Fig. 38)** are plotted on temperature verses salinity diagrams **(Fig. 38).** Data trends for (Sn-8) are boiling and mixing. Data trends for (Sn-15) are gas loss due to boiling and mixing.

4.6.5 Pressure and Depth to Boiling

The presence of bladed calcite and the coexistence of Type I and Type II fluid inclusions indicates that fluids San Nicolas fluids were boiling. Hence, they must have been trapped at or near conditions where liquid and vapor coexist therefore Th is considered equal to the trapping temperature (Th=Tt) and no presssure corrections were made.

A paleodepth reconstruction was created for hydrostatic and lithostatic pressures by plotting the averages and ranges of individual samples against present depth **(Fig. 39).** The depth scale and attendant depth to boiling curves were moved to best match the data. San Nicolas fluid inclusion pressures range from lithostatic to hydrostatic. The wide range in pressures is recorded in Stage I-III fluid inclusions. The data indicate mineralization depth was less than 600 meters below the water table, and that present depths are about the same as during mineralization.

4.7 Fluid Inclusion Gas Analyses

Tabulated gas values for H_2 He CH_4 H_2O, N_2 H_2S Ar, CO_2 , Total Gas and organics are included in **(Appendix 4).**

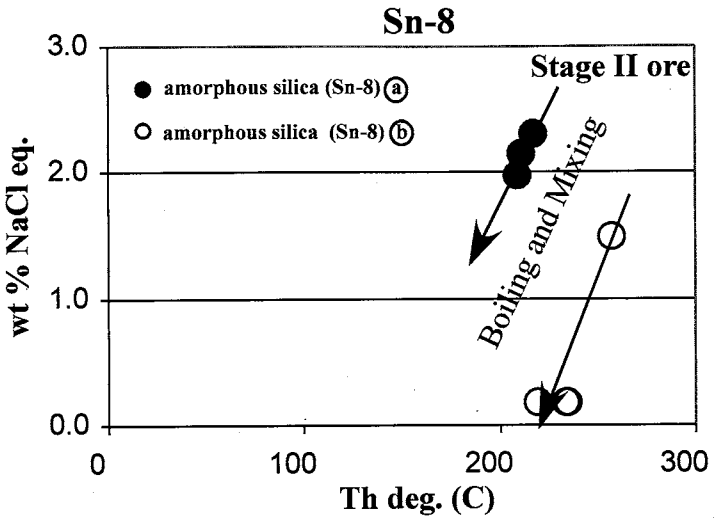

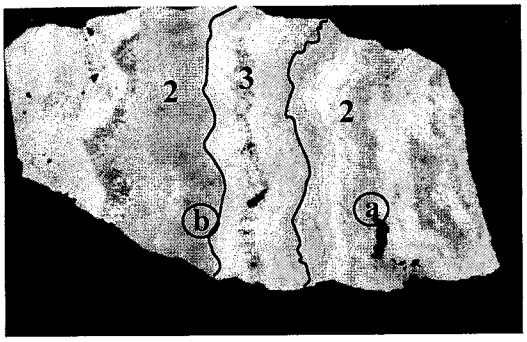

Fluid inclusion locations

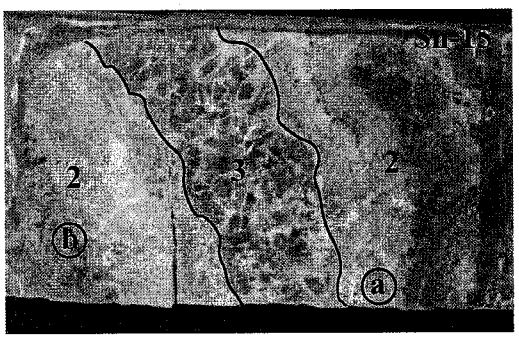

Fluid inclusion locations

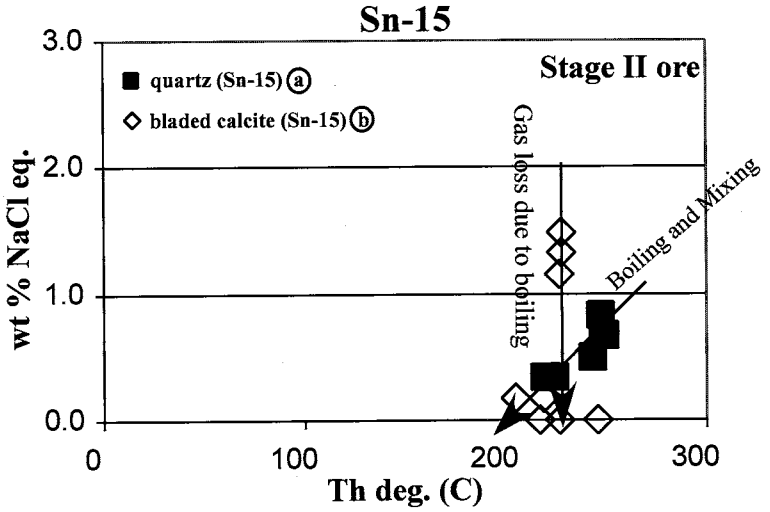

Figure 38. Temperature vs. salinity plots for paragenetically banded samples (Sn-8) and (Sn-15). Thick section photographs show fluid inclusion measurement locations (circled letters) and paragenetic stages from which fluid inclusions were measured. Fluid inclusion trends for for (Sn-8) are boiling and mixing trends. Trends for (Sn-15) are gas loss due to boiling and mixing Cooke and Simmons, 2000; Hedenquist and Henley, 1985a: Simmons and Christenson, 1994; Simeone and Simmons,1999 and Simmons et al.,2000).

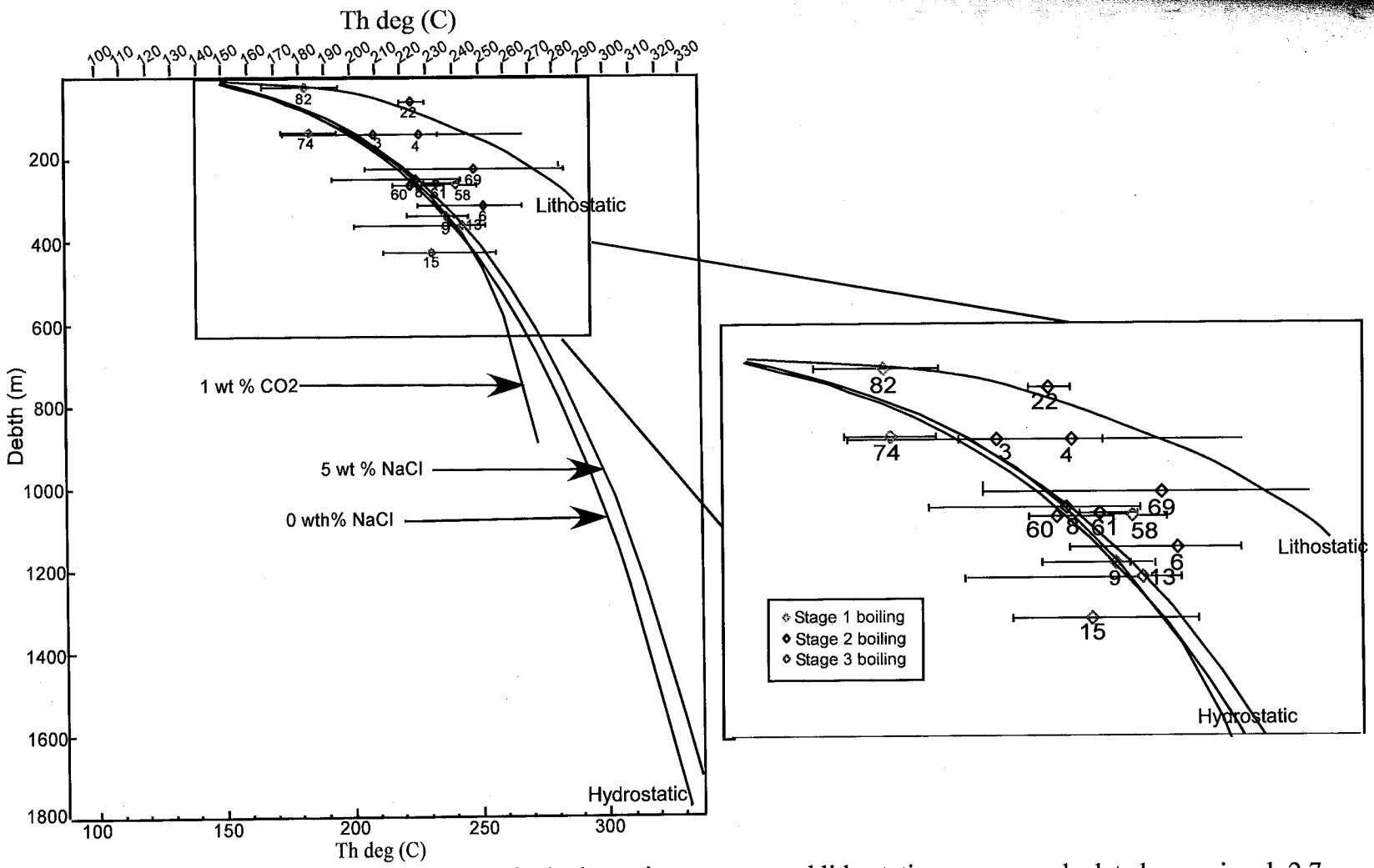

Figure 39. Boiling point to depth curves for hydrostatic pressures and lithostatic pressures calculated assuming d=2.7 g/cm^3 using the method of Henley and others (1984) pressures for 0 wt %, 5 wt % NaCl solutions (Hass, 1971) and 1 wt % CO_2 after (Hedenquist and Henley, 1985) Individual samples show average and range of Th. San Nicolas vein samples average 1 wt % NaCl eq.

4.7.1 CO_2/CH_4 vs. N_2/Ar Diagram

This diagram is used to help determine whether fluids are magmatic, crustal or some evolution of these fluid types (Norman and Moore, 1999) Magmatic fluids have high N_2/Ar ratios (100 - >1000). Shallow meteoric fluids have lower N_2/Ar ratios (25-105). Both magmatic and meteoric fluids initially have CO_2/CH_4 ratios ~ 1000 (Blamey and Norman, 2002). Upon circulation and interaction of these fluids with the crust and anaerobic crustal conditions, these fluids will equilibrate and produce CH_4, thus reducing CO_2/CH_4 ratios. (Blamey and Norman, 2002) Most of the San Nicolas gas analyses fall within the "Shallow Meteoric" field characterized by high CO_2/CH_4 values and low N_2/Ar values **(Fig. 40)**. A minor number of these analyses plot within the "Evolved Crustal" field . Overall, the data suggest variable meteoric and crustal sources for geothermal gaseous species and that Stage III fluids, show a slightly greater crustal component than Stage II fluids.

4.7.2 Ar/He vs. N_2/Ar Diagram

Blamey and Norman (2002), described this diagram as better suited than the CO_2/CH_4 vs. N_2/Ar diagram in determining the origin of gasses due to the less reactive nature of Ar/He compared to CO_2/CH_4. For the CO_2/CH_4 vs. N_2/Ar diagram, certain assumptions must be made about CO_2 and CH_4 that may not be geologically plausible in all situations. Argon will partition into the vapor phase much more readily that He and N_2 (Blamey and Norman, 2002) Upon degassing of a magmatic fluid, N_2/Ar and Ar/He ratios will decrease thus giving a negative slope to an evolving fluid as outlined by the box the "Calc-alkaline Magmatic" box **(Fig. 40)** All but five San Nicolas vein gas analyses

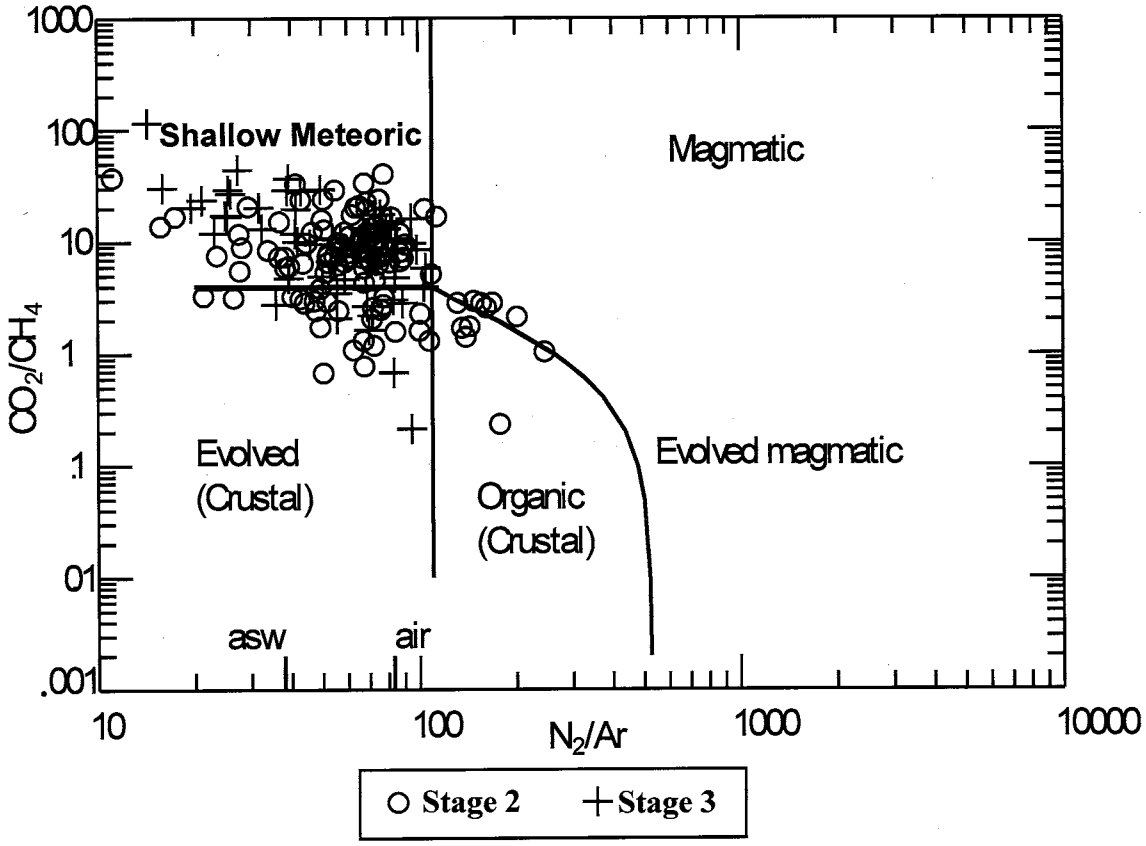

Figure 40. San Nicolas gas analyses plotted on Log N_2/Ar vs. Log CO_2/Ch_4 discrimination diagram showing magmatic and crustal fluid ranges (Norman and Moore, 1999).

fall outside the "Calc-alkaline Magmatic" box within an area of high Ar/He and low N_2/Ar ratios. Both **(Figs. 40 and 41)** indicate that gaseous species have a meteoric and crustal components with a possible weak addition of magmatic volatiles.

4.7.3 CO_2/CH_4 vs. H_2S Diagram

Equilibrium calculations made on geothermal fluids by Norman and others (1998) indicate that as temperature increases, hydrogen sulfide will also increase in fluids that are in equilibrium with pyrite and magnetite. The CO_2/CH_4 vs. H_2S diagram shows magnetite, pyrite and pyrrhotite stability fields for temperatures: 200, 250, 300, and 350 °C with 0 wt % NaCl eq. **(Fig. 42)**. San Nicolas gas analyses plotted on this diagram have been divided into their respective paragenetic stages. All analyses plotted on this diagram have a small positive slope (.15 ± .1) that suggests that H_2S concentrations were controlled by interaction with wallrocks. There is little difference between the samples with high gold content verses those with lower gold content. Samples that have less than 5 ppm Au and samples that have greater than 5 ppm gold have a wide range in H_2S values (.000001- <.1). There is also no major distinction between Stage II and Stage III fluid inclusion H_2S, however the highest H_2S concentrations were measured in Stage II fluid inclusions. Equilibrium calculations indicate that fluid measurements from San Nicolas Stage II and III fluids were generally >250 °C. Elevated H_2S will react with magnetite in the host-rock to form pyrite and CH_4. The reaction is:

$$2\ Fe_3O_4 + 12\ H_2S + CO_2 = 6\ FeS_2 + 10\ H_2O + CH_4$$

Conversely, fluids with minor H_2S and bearing Ch_4 may react with pyrite thus acquiring H_2S. If this reaction controls H_2S in solution a log plot of H_2S vs. CO_2/CH_4

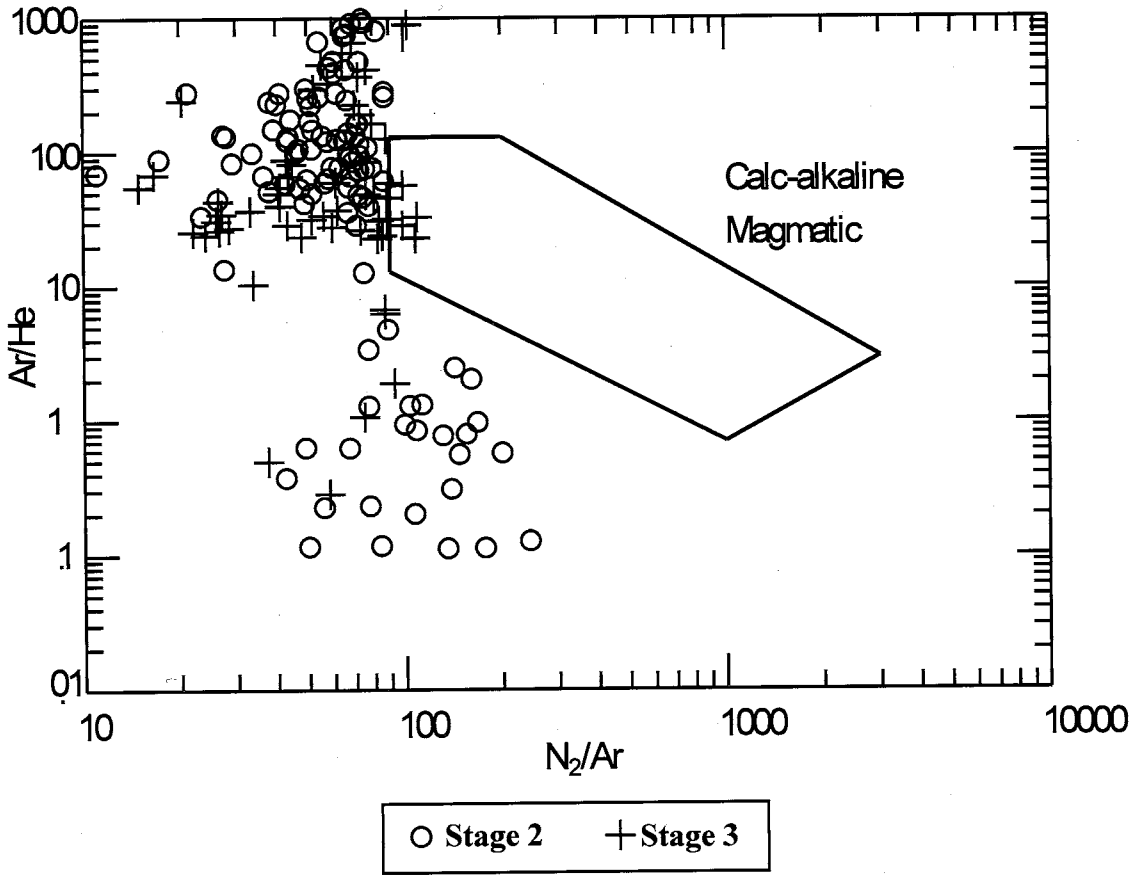

Figure 41. San Nicolas gas analyses plotted on Ar/He vs. N/Ar discrimination diagram showing Calc-alkaline Magmatic field (Blamey and Norman, 2002)

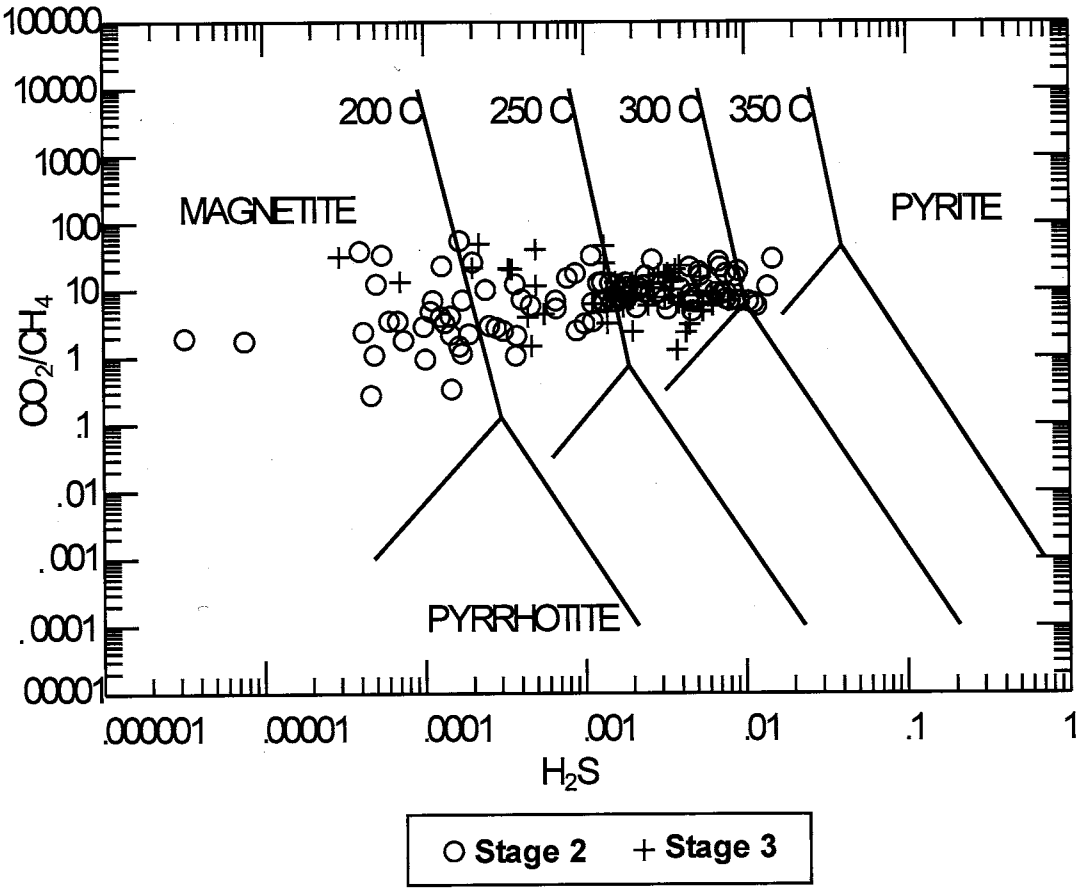

Figure 42. San Nicolas gas analyses plotted on Log CO_2/CH_4 vs. Log H_2S discrimination diagram showing the stability fields for magnetite, pyrite and pyrrhotite at 200, 250, 300 and 350 degrees Celcius (Norman et al.,1998).

should have a positive slope. San Nicolas vein fluid inclusions show this slope as do inclusions analyzed from the Geysers and Broadlands geothermal system (Norman et al., 1998).

4.7.4 CO_2/N_2 vs. Total Gas (100-H_2O) Diagram

This diagram discriminates between fluids that are boiling or condensing (Norman, et al., 2002). Analyses that are boiling will plot on a negative slope. As the amount of total gas decreases due to volatile loss in the vapor phase, the CO_2 concentration increases as N_2 more readily partitions into the vapor phase. A condensation trend will behave conversely to the boiling trend and form a positive slope. Total gas content will increase in areas that have undergone condensation due gasses dissolving in the fluid phase. An increase in CO_2 will occur in the liquid due its' greater solubility than N_2. Analysis from all but two samples (Sn-8 and Sn-15) plot along a negative slope **(Fig. 43)** (Norman, Blamey and Moore, 2002).

4.7.5 Fluid Evolution

Mineralogic banding sequences from samples (Sn-8) and (Sn-15) were analyzed to evaluate the evolution of fluid inclusion gas content through time. Analysis of inclusions from six mineralogic bands from (Sn-8) and three mineralogic bands from (Sn-15) are plotted in **(Figures 44 and 45)**.

Gas analyses from (Sn-8) **(Figure 44A and 44C)** do not show that early Stage II fluids differ from later stage fluids. **Figure (44 A and 44B)** shows a decrease in CO_2/CH_4 and Ar/He ratios from preore to postore. Diagram **(D)** shows an early preore condensation trend (Sn-8a) followed by boiling trends (Sn-8b-f). Since quartz that once was amorphous

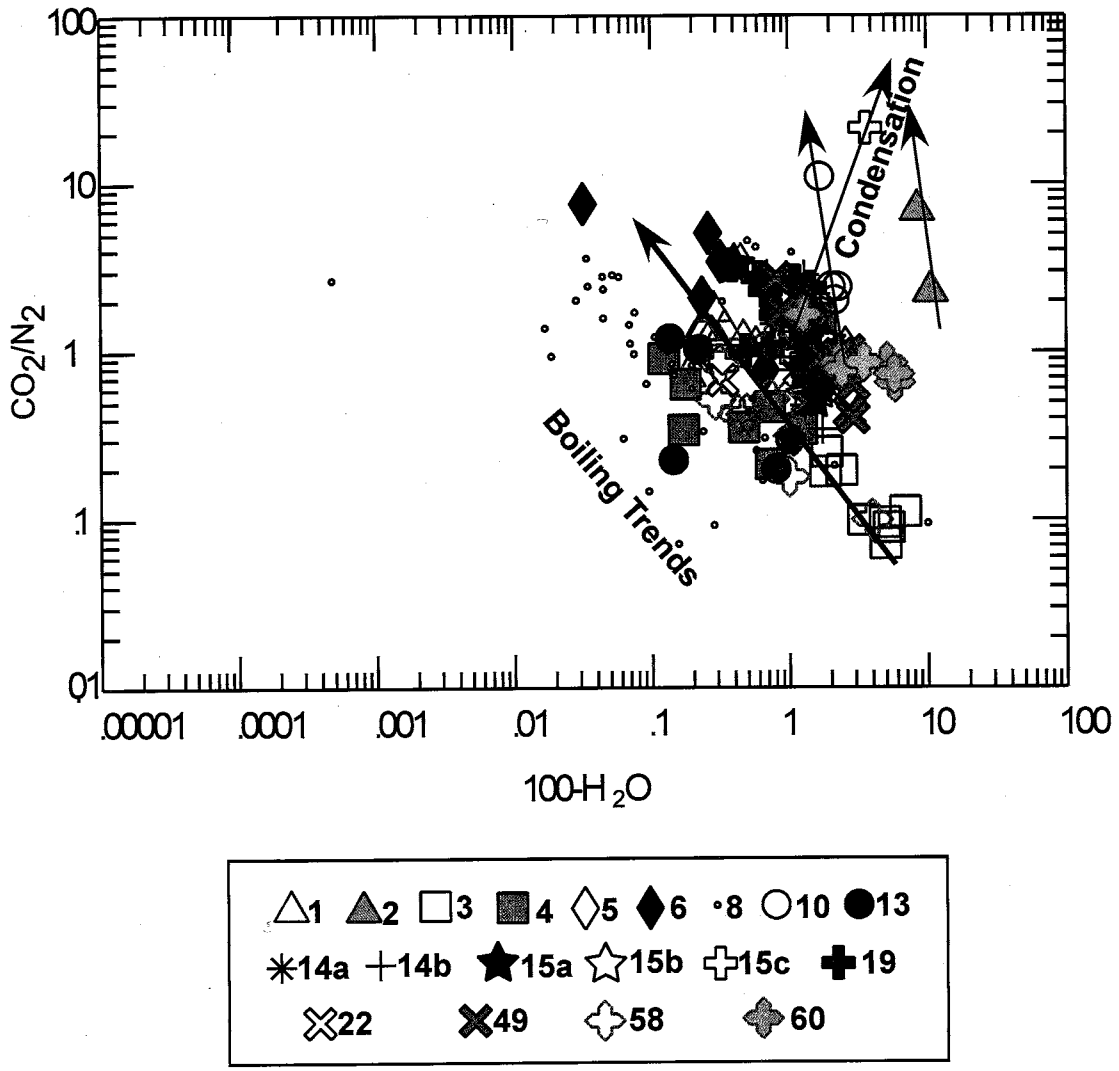

Figure 43. San Nicolas gas analyses for all samples plotted on a CO_2/N_2 vs. Total Gas ($100\text{-}H_2O$) discrimination diagram showing boiling and condensation trends (Norman, et al. 2002).

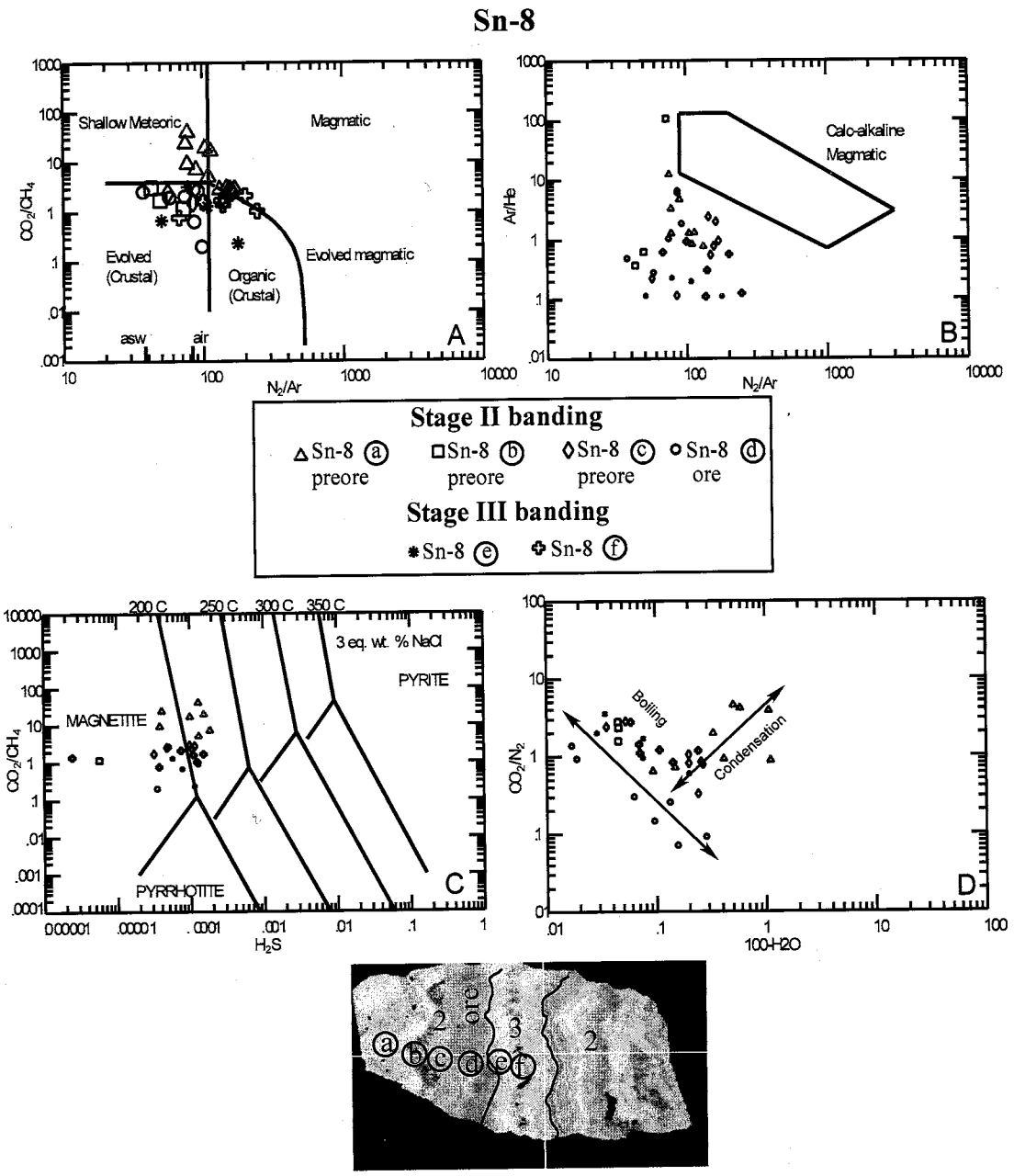

Figure 44. San Nicolas gas analyses from paragenetic banding (Sn-8a-f) plotted on four different discrimination diagrams show evolution of fluid inclusion gas content. Gas analyses sample locations are shown on thick section photograph. A. CO_2/CH_4 vs. N_2/Ar diagram showing a general progression from shallow meteoric to evolved crustal water signatures. B. Ar/He vs. N_2/Ar diagram showing the progression from high Ar/He ratios to low Ar/He ratios. C. CO_2/CH_4 vs. H_2S showing a little change in H_2S with time. D. CO_2/N_2 diagram showing a condensation trend in early Stage II banding with boiling trends during the rest of Stage II and Stage III paragenetic banding.

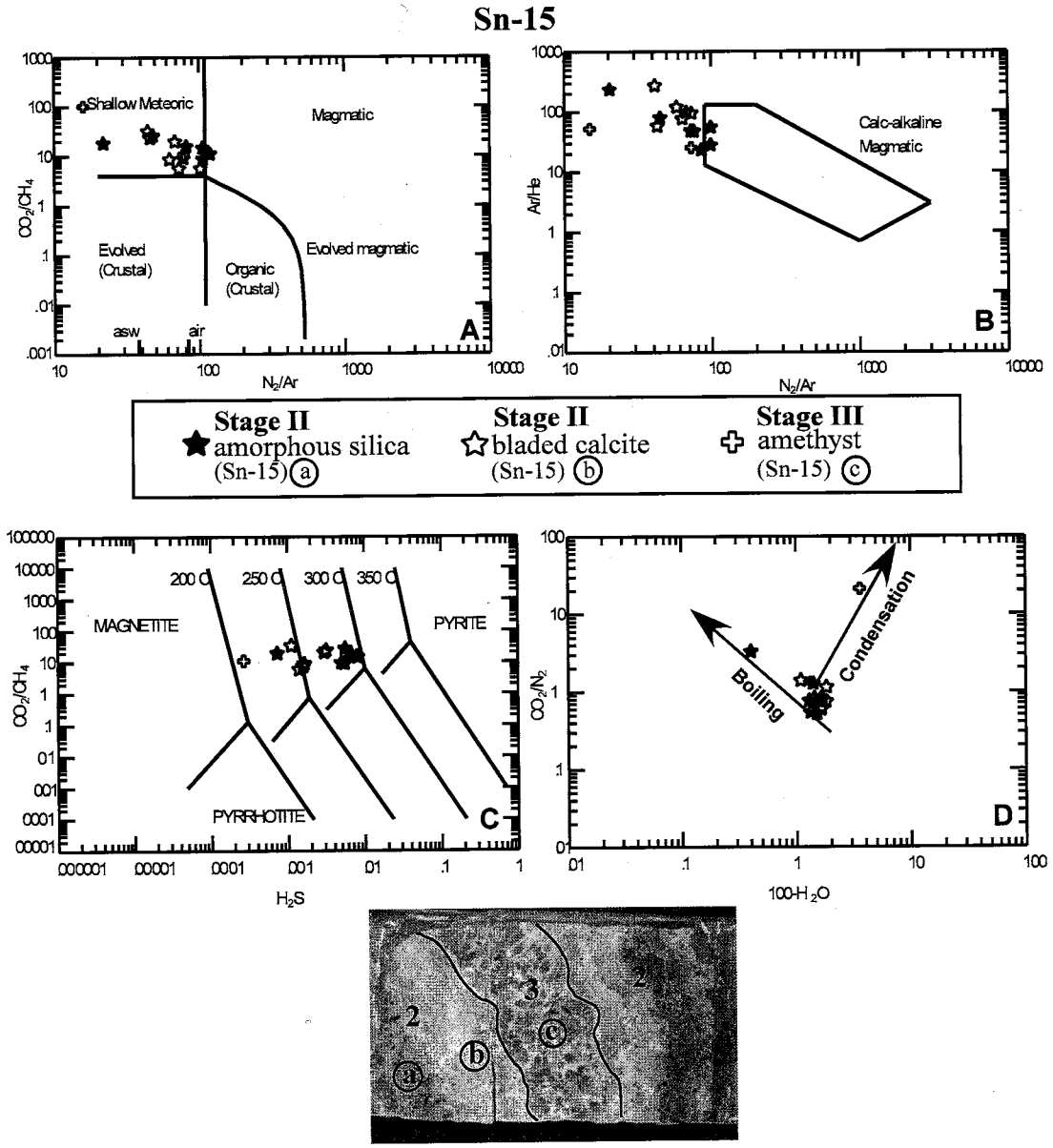

Figure 45. San Nicolas gas analyses from paragenetic banding (Sn-15-a-c) plotted on four different gas discrimination diagrams showing the progression of fluid inclusion gas content through time. Gas analyses sample locations are shown in thick section photograph. A. CO_2/CH_4 vs. N_2/Ar diagram showing progression from Stage II magmatic to Stage III shallow meteoric signatures. B. Ar/He vs. N_2/Ar diagram showing the progression away from "calc-alkaline magmatic" signatures. C. CO_2/CH_4 vs H_2S diagram showing the decrease in H_2S content from ore Stage II to barren Stage III. D. CO_2/N_2 diagram showing Stage 2 boiling and Stage 3 condensation trends.

silica and chalcedony, has only secondary inclusions, it is suggested that fluids in these stages are similar to fluids measured in Stage III minerals. Gas analyses from (Sn-15) **(Figure 45)** show a decrease in N_2/Ar ratios in diagrams **(A)** and **(B)** and a trend that moves away from magmatic fluid signatures. **Figure (45C)** shows a decrease in H_2S with time. **Figure (45D)** shows boiling in Stage II ore (Sn-15a) and in early Stage III bladed calcite (Sn-15b). Stage III amethyst (Sn-15 c) **(Figure 45D)** shows a condensing trend.

5.0 DISCUSSION

5.1 Boiling

San Nicolas vein fluids were boiling. The most important physical evidence is the coexistence of Type I (liquid dominated) with Type II (vapor dominated) fluid inclusions within mineral growth planes or healed microfractures throughout Stages I to III. The presence of excess gas > 1mol %, predominately in northeastern San Nicolas, suggests that gas analyses were made on populations of gas-rich, vapor dominated fluid inclusions that were formed in a boiling environment (Norman et al., 1996) **(Fig. 46).** Further evidence for boiling is the presence of Stage II bladed calcite intergrown with ore mineralization **(Fig. 17).** Bladed calcite is very common in modern boiling geothermal systems and forms at the onset of boiling as CO_2 is released (Simmons and Browne, 2000)

Additional evidence for fluid boiling is shown on temperature verses salinity diagrams (Stages II and III) **(Figs. 37 and 38).** Open-system boiling results in gas loss without significant temperature decrease (Hedenquist and Henley, 1985a; Simmons and Christenson 1994). The CO_2/N_2 vs. Total Gas discrimination diagram shows boiling trends for all but two analyses (Sn-8a; Sn-15c) **(Figs. 43, 44D and 45D).** Loss of gas that is principally CO_2 will lower the apparent salinity of trapped fluids. Salinity values generally increase upward along the San Nicolas vein as would be expected in an open-system fluid boiling with continual gas loss. The highest salinities are measured in

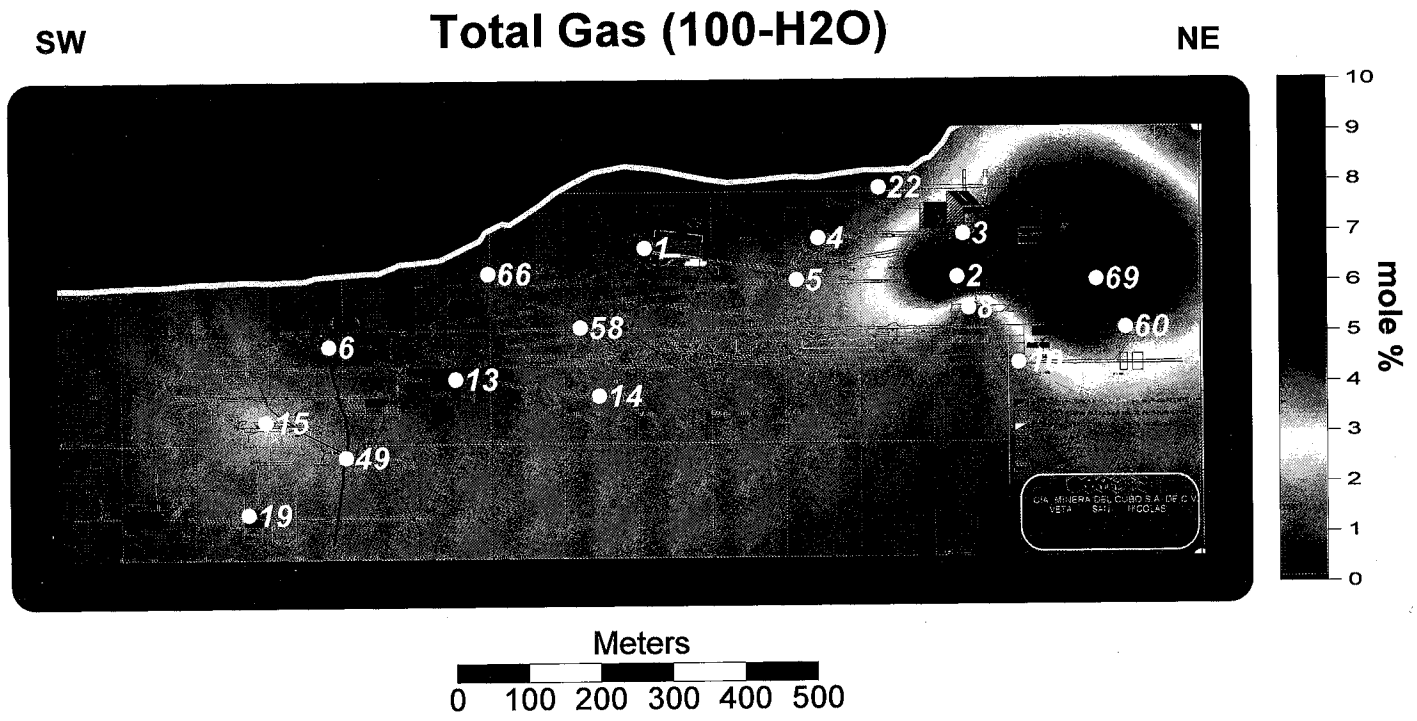

Figure 46. Longitudinal section showing total gas distribution.

samples from the upper northeast section of the vein that also exhibits the highest total gas values **(Fig. 46)**.

5.2 Fluid Mixing

Mineralogic and fluid inclusion evidence for fluid mixing exists in San Nicolas vein samples. Mineralogic evidence is found in the presence of blocky calcite in early Stage II and late Stage III paragenetic banding **(Fig. 12)**. Blocky calcite precipitates upon heating as CO_2-rich steam-heated waters mix with hot, Cl-rich ascending solutions (Fournier, 1985b). The CO_2-rich steam heated waters are located on the periphery of the geothermal system and form as gas and steam from boiled solutions condense (Reed and Spycher, 1985). Condensation trends are apparent in samples (Sn-8a and Sn-15c) on CO_2/N_2 vs. Total Gas discrimination diagrams **(Figs 43-45).** Stage III blocky calcite and massive calcite veins found on the deepest levels of the vein, signifies the collapse of a mixing geothermal system (Fournier, 1985b). Fluid inclusion Th vs. salinity diagrams reveal that the bulk of the fluid inclusion analyses plot between boiling and mixing trends **(Figs. 37 and 38)** Gas loss due to boiling, and temperature loss due to mixing are believed to be the dominant fluid processes for analyses that plot between these two trends (Hedenquist and Henley, 1985a; Simons and Christenson, 1994). Mixing is a common process and occurs in many active geothermal systems like the Broadlands-Ohaaki geothermal system (Simmons and Browne, 2000).

5.3. Temperatures and Salinities of Fluids

Fluid inclusion measurements made in bladed calcite associated with ore mineralization indicate San Nicolas vein ore was deposited from ~ 225 °C boiling

solutions. The few temperatures of homogenization <150 °C and >280 °C may represent temperatures from necked fluid inclusions or fluid inclusions with a significant amount of dissolved gasses (Bodnar et al., 1985; Cooke and Simmons, 2000).

San Nicolas vein apparent salinities range 0-2.95 wt % NaCl eq. Hedenquist and Henley (2000) showed that most apparent salinity between 0-2.5 wt % NaCl eq., could be entirely attributed to the presence dissolved CO_2 rather than dissolved salts. True San Nicolas vein salinities are likely between 0-.2 wt % NaCl eq. Samples with elevated salinities (Sn-3 and Sn-8) **(Figure 39 Trend 4)** > 1.5 wt % NaCl, may be explained by evaporative concentration of NaCl under open-system conditions (Cooke and Simmons, 2000).

5.4 Fluid Source

Fluid inclusion gas analyses suggest that San Nicolas vein fluids are dominantly meteoric with a very minor magmatic component **(Figs 40 ,41, 42A and 43A).** Analyses from (Sn-8) suggest a more evolved fluid signature for this sample, as some analyses plot in the "Evolved Crustal" and "Organic Crustal" fields. Oxygen isotopic analysis of the Veta Madre mineralization agrees with the interpretation (Mango, 1991).

5.5 Paragenesis and Fluid Processes

The San Nicolas vein has three major stages of vein paragenesis with the major ore- bearing stage residing in Stage II. The ore-bearing stage is preceded by initial brecciation of the wallrock and possible propylitic alteration and silicification of the vein selvages. Late Stage I into Stage II is dominated by repetitive sequences of quartz, chalcedony and amorphous silica with minor variations in this sequence occurring after

ore deposition when chalcedony grades to quartz and back to chalcedony again. Fluid inclusion analysis suggests

ore fluid temperature increased through paragenesis. Chalcedony is a product of amorphous silica recrystallization (Fournier, 1985 and Bogie and Lawless, 2001) Chalcedony from Stage II grades into amethystine quartz and onto blocky calcite from Stage III **(Fig. 18)**. The order of these forms of silica, quartz, chalcedony and amorphous sequences suggests that catastrophic processes influencing silica solubility affected San Nicolas mineralization. Two mechanisms for depositing amorphous silica from an initial solution in equilibrium with quartz are extreme fluid cooling by either boiling or mixing (Simmons and Browne, 2000) or by catastrophic boiling (flashing) caused by rapid depressurization and with minimal to no heat loss because wallrocks remain hot (Moore, pers. comm., 2003) **(Fig. 47)**.

Cooling by boiling would not produce enough heat loss to decrease the temperature by ~80° C to produce amorphous silica, because the dominant heat source is in the wallrock and not in the fluid itself (Moore, pers. comm., 2003). Fluid inclusion Th measurements, especially those performed on bladed calcite do not indicate that fluid temperatures were below 180 °C. Cooling by mixing would produce condensate minerals such as blocky calcite and/or anhydrite from the heating of CO_2 rich steam descending water (Fournier, 1985). These minerals were not precipitated together with amorphous silica and bladed calcite. Evidence for fluid mixing is present in San Nicolas vein fluids **(Figs. 37 and 38)**, however it is not genetically linked to gold mineralization. Hence, the presence of gold intergrown with bladed calcite and amorphous silica along

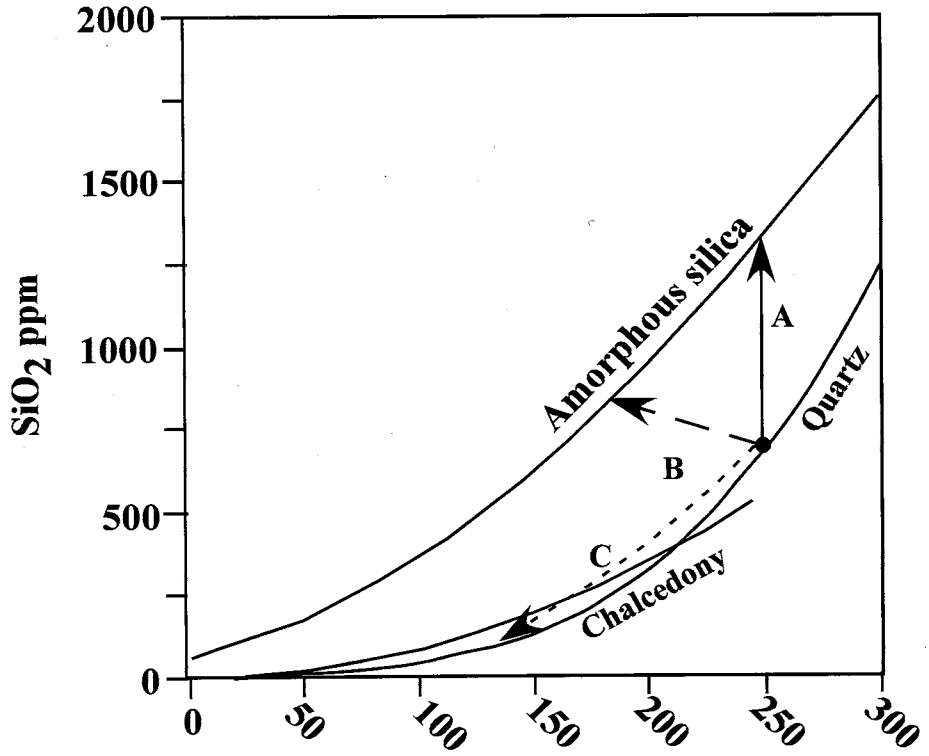

Figure 47. Solubility curves of amorphous silica, chalcedony and quartz (maximum steam loss) (Fournier, 1985). Reaction path A shows the change in fluid silica concentration resulting from rapid depressurization (flashing) and boiling of with minimal to no heat loss. Reaction path B is boiling with accompanied heat loss. Reaction path C is mixing and cooling while maintaining equilibrium.

indicates that gold deposition occurred in response to catastrophic depressurization and extreme boiling.

5.6 Gold Complexation and Precipitation

The hydrosulfide ligands are the most common gold complexes in reduced sulfur, low-temperature environments (<350°C) (Seward, 1973). Gold chloride complexes are generally not stable at temperatures below (300°C) unless fluids are oxidized, acidic and/or saline (Henley, 1973). The $Au(HS)^-_2$ complex dominates in dilute, reduced, near-neutral pH waters present in most low sulfidation epithermal deposits, similar to the San Nicolas vein (Cooke and Simmons, 2000). Gold deposition due to boiling in the epithermal environment is a complex process dominated by the following reaction (Reed and Spycher, 1985):

$$Au(HS)^-_2 + H^+ + 0.5\ H_{2\ (aq)} \Rightarrow Au_{\ (s)} + 2H_2S_{\ (g)}$$

At the initiation of boiling, the immediate loss of CO_2 causes an abrupt increase in pH according to the following equation (Reed and Spycher, 1985):

$$HCO^-_3\ (aq) + H^+ \Rightarrow H_2O\ (aq) + CO_2\ (g)$$

This pH increase causes the disassociation of H_2S to HS^- and drives reaction (1) to the left, thus increasing the solubility of gold as a $Au(HS)^-_2$ complex. The CO_2 loss during boiling acts in opposition to H_2S loss in controlling Au solubility. The gas partitioning constant for CO_2 is greater than for H_2S, hence initially CO_2 loss is greater than H_2S loss (Henley and Brown, 1985). Hydrogen sulfide gas loss as a continued consequence of boiling will dominate, driving the reaction to the right causing Au deposition (Reed and Spycher, 1985). Hence, gold deposition due to open-system boiling is predominately a function of

H_2S loss rather than pH increase and to be effective requires extreme or a long period of boiling.

Fluids from the San Nicolas vein were compared to those of the Broadlands-Ohaaki geothermal system. San Nicolas fluids are remarkably similar in H_2S (max ~100 ppm) **(Fig. 42)** and in salinity 0-.2 wt % NaCl (considering the effects of dissolved CO_2) to those fluids of Broadlands-Ohaaki (100 ppm H_2S and 10000 ppm Cl (0.2 wt % NaCl eq.). Calculations by Henley (1985) indicate that Broadlands fluids with the given H_2S and Cl compositions are capable of creating a 1.3 Moz Au deposit in 10,000 years at a discharge rate 10 kg/s. By comparison, the data shows that the San Nicolas vein with > 0.5 Moz Au has ore fluids of low salinity and sufficient H_2S capacity to create a similar type to that calculated by Henley (1985).

5.7 Fluid Flow Direction

San Nicolas vein fluids never reached the vein surface because there is no outcropping of vein material on the surface. Hence, they must have flowed laterally. The presence of vertical alteration zones **(Fig. 19)** suggest lateral fluid flow as well. Temperature contours and the enrichment of gold suggest the fluids may have originated from the Villalpando vein intersection and flowed laterally to the northeast **(Fig. 34)**.

5.8 Why is there higher gold grades in the San Nicolas vein than in other veins in the Guanajuato district?

1) San Nicolas vein fluids underwent catastrophic boiling (flashing) which ultimately led to gold deposition. In well BR22 at Broadlands-Ohaaki geothermal site, all precious metal mineralization occurs within the first few seconds of flashing (Browne, 1985). Fluid inclusion studies of the deeper veins found no evidence of fluid boiling. Hence, boiling essential to the deposition of a significant amount of Au, did not occur in deeper fluids.

2) There is a sufficient amount of H_2S in San Nicolas fluids to complex gold as a $Au(HS)^-_2$ complex **(Fig. 42)**. The immediate loss of H_2S after the initiation of boiling will quickly destroy the HS- complex and deposit Au and sulfides.

3) San Nicolas fluids are lower in salinity (0-3 wt % verses 3-5 wt %) than Guanajuato Ag veins. Albinson and others (2001) demonstrate empirically the inverse relationship between salinity and Au mineralization. Henley and Brown (1985) show by calculations that Au transport is favored in low Cl thermal fluids.

4) San Nicolas vein was preserved. The El Cubo mine is located stratigraphically above the top of the major silver ore veins, and survived erosion since mineralization.
If upper gold-rich (possibly boiling) horizons from the La Luz and Veta Madre vein systems existed , it is possible that they were eroded away.

5.9 Model of San Nicolas Vein Ore Genesis

Convection of near neutral pH, low salinity chloride rich- fluids leached Au and S from the organic-rich and sulfide-rich La Luz Formation (Randall et al., 1984). Hydrogen sulfide disassociated to form a HS^- ion that complexed Au. Lateral-flowing gold-bearing solutions began to boil. A near surface pH decrease caused by the condensation of CO_2-rich steam heated waters and formation of carbonic acid, altered the wallrock to form a clay-mineral alteration blanket. An abrupt change in pressure caused fluids to flash. This abrupt change in pressure was either caused by a switch from lithostatic to hydrostatic pressures, a landslide, faulting, hydrothermal eruption or drop in the water table. Flashing caused the immediate loss of CO_2 gas and a pH increase which ultimately led to the increase in gold solubility. Continued boiling and loss of H_2S destabilized the $Au(HS)^-_2$ complex and ultimately deposited gold, amorphous silica and bladed calcite. Boiled steam and gas (dominantly CO_2 and H_2S) condensed to form CO_2 rich waters, that accumulated on the periphery of the system. Carbon-dioxide rich steam heated waters mixed with

ascending near neutral pH, chloride waters and deposited blocky calcite. This process continued to cycle until the hydrothermal system began to loose heat towards the termination its' geothermal life span. At this stage, oxidized CO_2-rich descending meteoric waters dominated fluid flow . The incursion of these oxidized waters led to the deposition of amethyst and massive calcite as the hydrothermal system collapsed.

6.0 CONCLUSIONS

The following conclusions are made from this study:

1 Catastrophic decompression and extreme fluid boiling (flashing) caused gold deposition.

2. Low salinity fluids and sufficient H_2S enabled San Nicolas fluids to carry gold in solution as a $(HS)^-$ complex.

3. There are three major paragenetic stages to San Nicolas vein formation. All stages are boiling.

4 Mixing of CO_2 -rich steam- heated waters with hot ascending waters played a role in San Nicolas vein formation, but it did not cause gold deposition.

5. San Nicolas vein temperatures range 172-282 °C and average 229° C. Ore mineralization occurred at ~225 °C. Apparent salinities range from 0-.2.95 wt % NaCl eq. and average 1 wt % NaCl eq. True salinites are likely between 0-.2 wt % NaCl.

6. Correlation calculations indicate that gold correlates strongly with Ag and weakly with Pb, Cu, Zn and Sb.

7. Gas analyses reveal that San Nicolas fluids are dominantly meteoric with possible small magmatic component.

REFERENCES CITED

Albinson, T., Norman, D. I., Cole, D., and Chomiak, B., 2001, Controls on formation of low-sulfidation epithermal deposits in Mexico; constraints from fluid inclusion and stable isotope data: New mines and discoveries in Mexico and Central America, v. 8, p. 1-32.

Aranda g., J. J., Aranda G.,J.M., and Nieto S., A.F., 1989, Consideraciones acerca de la evolucion tectonica durante el Cenozoico de la Sierra de Guanajuato y la porcion meridional de la Mesa Central: Universidad Nacional Autonoma de Mexico, Instituto de Geologia, v. 8, p. 33-46.

Bodnar, R. J., Reynolds, T. J., and Kuehn, C. A., 1985, Fluid-inclusion systematics in epithermal systems: Geology and geochemistry of epithermal systems, Reviews in Economic Geology, v. 2, p. 73-97.

Bogie, I., and Lawless, J. V., 2001, Precipitation of gold in a low-sulfidation epithermal gold deposit; insights from submillimeter-scale oxygen isotope analysis of vein quartz; discussion: Economic Geology and the Bulletin of the Society of Economic Geologists, v. 96, p. 1701-1702.

Browne, P. R. L., and Ellis, A. J., 1970, The Ohaki-Broadlands hydrothermal area, New Zealand; mineralogy and related geochemistry: American Journal of Science, v. 269, p. 97-131.

Buchanan, L. J., 1980, Ore controls of vertically stacked deposits, Guanajuato, Mexico: Society of Mining Engineers, 80-82, 27p.

Clark, K. F., Foster, C. T., and Damon, P. E., 1982, Cenozoic mineral deposits and subduction-related magmatic arcs in Mexico, *in* Gastil, G., and Phillips, R. P., eds. Relationships between variations in the subduction of oceanic plates and variations in the magmatic and mineralogic substances believed to be the products of subduction, 93, Geological Society of America (GSA), p. 533-544.

Cooke, D. R., and Simmons, S. F., 2000, Characteristics and genesis of epithermal gold deposits: Gold in 2000, v. 13, p. 221-244.

Davila A., V. M. a. M. R. J., 1987, Un edad Cretacia para las rocas de la Sierra de Guanajuato:: Universidad Nacioonal Autonoma de Mexico, Simposio sobre la Geologia de la Region de la Sierra, Guanajuato, Guanajuato, April 28-30, 1987, p. Resumen , p. 19-20.

Fournier, R. O., 1985, The behavior of silica in hydrothermal solutions: Geology and geochemistry of epithermal systems, Reviews in Economic Geology, v. 2, p. 45-61.

Fournier, R. O., 1985, Carbonate transport and deposition in the epithermal environment: Geology and geochemistry of epithermal systems, Reviews in Economic Geology, v. 2, p. 63-72.

Girnius, R., 1993, Deposition of the upper ore in the El Cubo Mine, Guanajuato Mining District, Mexico: Dartmouth College, unpublished Bachelor's Honor Thesis, p. 18.

Gross, W. H., 1975, New ore discovery and source of silver-gold veins, Guanajuato, Mexico: Proceedings of Gold and Money Session and Gold Technical Session, v. no. 5, p. 164.

Guoyi, D., Morrison, G., Jaireth, S., 1995, Quartz textures in epithermal veins, Queensland-classification, origin and implication: Economic Geology, v. 90 p, p. 1841-1856.

Haas, J. L., Jr., 1971, The effect of salinity on the maximum thermal gradient of a hydrothermal system at hydrostatic pressure: Economic Geology and the Bulletin of the Society of Economic Geologists, v. 66, p. 940-946.

Hedenquist, J. W., and Henley, R. W., 1985, The importance of CO_2 on freezing point measurements of fluid inclusions; evidence from active geothermal systems and implications for epithermal ore deposition: Economic Geology and the Bulletin of the Society of Economic Geologists, v. 80, p. 1379-1406.

Hedenquist, J.W., 1990, The Thermal and Geochemical Structure of the Broadlands-Ohaaki Geothermal System, New Zealand: Geothermics Vol. 19, No. 2, pp. 151-185.

Henley, R. W., and Brown, K. L., 1985, A practical guide to the thermodynamics of geothermal fluids and hydrothermal ore deposits: Geology and geochemistry of epithermal systems, Reviews in Economic Geology v. 2, p. 25-44.

Mango, H., Zantop, H., and Oreskes, N., 1991, A fluid inclusion and isotope study of the Rayas Ag-Au-Cu-Pb-Zn mine, Guanajuato, Mexico: Economic Geology and the Bulletin of the Society of Economic Geologists, v. 86, p. 1554-1561.

Martinez, M., J.A., 1991, Magmatismo Oligoceno, una guia para la exploracion por oro y plata en Guanajuato, Mexico:: Asociacion de Ingenieros de Minas, Metalurgistas y Geologos de Mexico Convencion Nacional, 1991, p. p. 61-78.

Martinez, R. J., 1987, Resumen de la Geologia de la Sierra de Guanajuato: Universidad Nacional Autonoma de Mexico, Instituto de Geologia, Simposio sobre la Geologia de la Region de la Sierra de Guanajuato,Guanajuato „ p. 50-91.

Moore, J. N., and Adams, M. C. A. A. J., 2000, The fluid inclusion and mineralogic record of the transition from liquid- to vapor-dominated conditions in The Geysers geothermal system, California: Economic Geology and the Bulletin of the Society of Economic Geologists, v. 95, p. 1719-1737.

Moore, J. N., Powell, T. S., Heizler, M. T., and Norman, D. I., 2000, Mineralization and hydrothermal history of the Tiwi geothermal system, Philippines: Economic Geology and the Bulletin of the Society of Economic Geologists, v. 95, p. 1001-1023.

Norman, D. I., Blamey N., Moore J.N, 2002, Interpreting geothermal processes and fluid sources from fluid inclusion organic compounds and CO_2/N_2 ratios, v. Proceedings from the Twenty-Seventh Workshop on Geothermal Resevoir Engineering, Stanford University, California, January 28-30, 2002.

Norman, D. I., and Moore, J. N., 1997, Gaseous species in fluid inclusions; a fluid tracer and indicator of fluid processes, *in* Boiron, M.-C., and Pironon, J., eds., XIVth European current research on fluid inclusions; XIV ECROFI, 14, p. 243-244.

Norman, D. I., Moore, J.N., 1999, Methane and excess N2 and Ar in geothermal fluid inclusions: 24th Workshop Geotherm. Reservoir Eng., Stanford University, 1999, p. 196-2002.

Petruk, W., and Owens, D., 1974, Some Mineralogical Characteristics of the Silver Deposits in the Guanajuato Mining District, Mexico: Economic Geology and the Bulletin of the Society of Economic Geologists, v. 69, p. 1078-1085.

Querol, F., and Navarro, R., 1990, Ore deposits of the Guanajuato mining district, Mexico, *in* Clark, K. F., ed., Mexican silver deposits, 6, Society of Economic Geologists, p. 201-211.

Randall R, J. A., 1982, Contacto entre el Terciario y el Mesozoico en el distrito minero de Guanajuato: Sociedad Geologica Mexicana, Convencion Nacional 6th, Mexico City, 1982, p. Resumen , p. 89.

Randall R, J. A., 1987, Emplazamiento y Origen del acimiento Auro-Argentifero de "El Cubo", Gunajuato: Universidad Nacional Autonoma de Mexico, Simposio sobre la Geologia de la Region de la Sierra Guanajuato, Guanajuato, p. 35-37.

Randall R, J. A., 1989, Cause of gold distribution in veins, Guanajuato, Mexico: Gold '89 in Europe, Toulouse, France,, p. 15.

Randall R, J. A., Saldana A, E., and Clark, K. F., 1994, Exploration in a volcano-plutonic center at Guanajuato, Mexico: A special issue on volcanic centers as targets for mineral exploration, Economic Geology, v. 89, p. 1722-1751.

Reed, M. H., and Spycher, N. F., 1985, Boiling, cooling, and oxidation in epithermal systems; a numerical modeling approach: Geology and geochemistry of epithermal systems, Reviews in Economic Geology, v. 2, p. 249-272.

Saldana A, E., 1990, Gold-silver geothermal systems of the central part of the Sierra de Guanajuato, Mexico:: Unpublished M.S.c. thesis, p. 127 p.
Sedlock, T. L., Ortega G.,F., and Speed, R.C., 1993, Tectonostratigraphic terranes in Mexico and tectonic evolution of Mexico: Geologic Society of America Special Paper, v. 278, p. 153.

Seward, T.M., 1973, Thio complexes of gold and the transport of gold in hydrothermal ore solutions: Geochimica et Cosmochimica Acta, v. 37, p. 379-399.

Seward, T. M., 1988, The hydrothermal chemistry of gold and its implications for ore formation, *in* Goode, A. D. T., and Bosma, L. I., eds., Bicentennial gold; 1988, 22, Geological Society of Australia, p. 197-198.

Simeone, R., and Simmons, S. F., 1999, Mineralogical and fluid inclusion studies of low-sulfidation epithermal veins at Osilo (Sardinia), Italy: Mineralium Deposita, v. 34, p. 705-717.

Simmons, S. F., Arehart, G., Simpson, M. P., and Mauk, J. L., 2000, Origin of massive calcite veins in the Golden Cross low-sulfidation, epithermal Au-Ag deposit, New Zealand: Economic Geology and the Bulletin of the Society of Economic Geologists, v. 95, p. 99-112.

Simmons, S. F., and Browne, P. R. L., 2000, Hydrothermal minerals and precious metals in the Broadlands-Ohaaki geothermal system; implications for understanding low-sulfidation epithermal environments: Economic Geology and the Bulletin of the Society of Economic Geologists, v. 95, p. 971-999.

Simmons, S. F., and Christenson, B. W., 1990, Platy calcite as an indicator of boiling in epithermal deposits; evidence from New Zealand geothermal systems, *in*

Anonymous, ed., Geological Society of America, 1990 annual meeting, 22, Geological Society of America (GSA), p. 42.

Simmons, S. F., and Christenson, B. W., 1994, Origins of calcite in a boiling geothermal system: American Journal of Science, v. 294, p. 361-400.

Wandke, A., and Martinez, J., 1928, The Guanajuato mining district, Guanajuato, Mexico: Economic Geology and the Bulletin of the Society of Economic Geologists, v. 23, p. 1-44.

Appendix 1:
Handsample Descriptions

Sample #	Vein	Handsample description
1	San Nicolas	Massive milky white quartz
2	San Nicolas	Massive milky white quartz
3	San Nicolas	Massive milky white quartz
4	San Nicolas	Banded milky white quartz
5	San Nicolas	Clay rich wallrock with banded milky whitequartz and chaldedony
6	San Nicolas	Calcite and quartz
7	SN/Vill intersection	Banded milky white quartz containing sulfides
8	San Nicolas	Banded milky whitequartz containing sulfides and late amethyst
9	San Nicolas	Quartz and chalcedony
10	San Nicolas	Massive quartz vein
11	San Nicolas	Banded milky white quartz
12	San Nicolas	Calcite with minor quartz
13	San Nicolas	Calcite
14	San Nicolas	Amethyst and calcite
15	San Nicolas	Banded milky white quartz, amethyst and calcite
16	San Nicolas	Amethyst and calcite
17	San Nicolas	Quartz and amethyst
18	San Nicolas	Calcite and amethyst
19	San Nicolas	Banded milky white quartz and calcite
20	San Nicolas	Milky white quartz
21	San Nicolas	Milky white quartz
22	San Nicolas	Milky white quartz
23	San Nicolas	Milky white quartz
24	Villalpando	Quartz, bladed calcite and amethyst

Sample #	Vein	Handsample description
25	Villalpando	Banded milky white quartz containing sulfides and late amethyst
26	Villalpando	Banded milky white quartz, bladed calcite, amethyst and sulfides
27	Villalpando	Banded milky white quartz containing sulfides
28	Villalpando	Banded milky white quartz, amethyst, sulfides and late blocky calcite
29	Villalpando	Quartz
30	Villalpando	Quartz vein material with wallrock breccia clasts
31	Villalpando	Sugary quartz with bladed calcite and amethyst
32	Villalpando	Quartz and bladed calcite
33	Los Panchos	Banded milky white quartz containing sulfides and late amethyst
34	Los Panchos	Sugary quartz, bladed calcite and blocky calcite
35	Los Panchos	Quartz, chalcedony and bladed calcite
36	Los Panchos	Sugary quartz and sulfids (pyrargyrite)
37	Villalpando	Banded milky white quartz containing sulfides and late amethyst
38	Los Panchos	Milky white quartz containing sulfides, calcite and banded chlorite
39	Los Panchos	Quartz and brecciated wallrock fragments
40	Los Panchos	Calcite and minor quartz
41	Los Panchos	Banded milky white quartz and calcite
42	Los Panchos	Quartz and calcite with brecciated, chloritized wallrock fragments
43	Villalpando	Quartz veinlet
44	Villalpando	Quartz and calcite
45	Villalpando	Quartz
46	Villalpando	Quartz veinlets
47	Villalpando	Quartz, chalcedony and calcite
48	Villalpando	Milky white quartz

Sample #	Vein	Handsample description
49	San Nicolas	Surgary quartz and late amethyst
50	Villalpando	Brecciated wallrock and milky white quartz
53	San Juan de Dios	Quartz
54	San Juan de Dios	Coarse crystalline quartz
55	San Juan de Dios	Late-stage masssive calcite
56	Villalpando (Peregrina Mine)	Massive calcite
57	Villalpando (Peregrina Mine)	Banded quartz and massive calcite
58	San Nicolas	Quartz and calcite
59	San Nicolas	Massive milky white quartz and calcite
60	San Nicolas	Quartz
61	San Nicolas	Minor quartz and bladed calcite
66	San Nicolas	Quartz
67	San Juan de Dios	Sugary quartz and amethyst
68	San Juan de Dios	Sugary quartz and amethyst
69	San Nicolas	Quartz
70	San Juan de Dios	Banded quartz containing sulfides
71	San Juan de Dios	Milky white, sugary and euhedral quartz
72	San Juan de Dios	Banded milky white quartz containing sulfides
73	San Nicolas	Banded milky white quartz containing sulfides and late amethyst
74	San Nicolas	Calcite and quartz
76	San Nicolas	Clay altered Peregrina wallrock
77	San Nicolas	Silicified Peregrina wallrock
78	San Nicolas	Clay altered Peregrina wallrock
79	San Nicolas	Clay altered Caldedrones formation wallrock

Sample #	Vein	Handsample description
80	San Nicolas	Clay altered Caldedrones formation wallrock
81	San Nicolas	Clay altered Caldedrones formation wallrock
82	San Nicolas	Silicified Chichindaro Rhyolite breccia with quartz veinlets
83	Los Panchos	Crystalline quartz veinlets with silicified Peregrina wallrock
84	Los Panchos	Clay-altered wallrock
85	Los Panchos	Milky white quartz and coarse crystalline quartz
87	San Juan de Dios	Quartz and wallrock
88	San Juan de Dios	Clay-altered wallrock
89	San Juan de Dios	Quartz veinlets in brecciated wallrock
90	San Juan de Dios	Silicified wallrock
250	Villalpando	Banded milky white quartz and calcite
200	San Nicolas	Banded milky quartz containing sulfides
299	San Nicolas	Clay rick wallrock with banded quartz and chaldedony

Appendix 2
Geochemical Data
Results are listedn in (ppm) unless otherwise specified

Run #	Sample #	X	Y	Vein	Au 30 (ppb)	Ag (ppb)	Au (ppm)	Ag (ppm)	Cu	Pb	Zn	Log Cu	Log Pb	Log Zn	Mo	Ni	Co	Cd	Bi	As	Sb	Log As	Log Sb	Hg
386551	1	-688	-198	San Nicolas	106	32000	0.1	6.9	13	11	32	1.11	1.04	1.51	4	8	1	0.2	5	13	5	1.11	0.70	0.2
386552	2	-257	-239	San Nicolas	965	9000	1.0	14.5	8	3	9	0.90	0.48	0.95	2	8	1	0.2	5	5	5	0.70	0.70	0.2
386553	3	-249	-180	San Nicolas	4989	207000	5.0	45.7	10	22	207	1.00	1.34	2.32	5	15	1	0.2	5	18	5	1.26	0.70	0.2
386554	4	-448	-185	San Nicolas	5320	27000	5.3	200.0	33	13	27	1.52	1.11	1.43	4	6	1	0.3	5	13	5	1.11	0.70	0.2
386555	5	-478	-242	San Nicolas	104	21000	0.1	11.8	12	11	21	1.08	1.04	1.32	3	15	4	0.4	5	33	5	1.52	0.70	0.2
386556	6	-1124	-330	San Nicolas	10000	185000	10.0	195.1	156	118	185	2.19	2.07	2.27	1	1	1	2.4	5	5	94	0.70	1.97	3.1
386557	7	-1153	-329	SN/Vill	973	60000	1.0	34.1	11	19	60	1.04	1.28	1.78	3	4	1	1.6	5	61	5	1.79	0.70	0.2
386558	8	-242	-282	San Nicolas	9884	92000	9.9	200.0	105	21	92	2.02	1.32	1.96	4	7	1	0.4	5	10	26	1.00	1.41	0.2
386559	9	-500	-352	San Nicolas	392	7000	0.4	6.7	13	4	7	1.11	0.60	0.85	1	6	1	0.2	5	5	5	0.70	0.70	0.2
386560	10	-173	-357	San Nicolas	345	39000	0.3	9.9	5	4	39	0.70	0.60	1.59	4	7	1	0.2	5	8	5	0.90	0.70	0.2
386561	11	-272	-281	San Nicolas	10000	740000	10.0	200.0	3094	216	740	3.49	2.33	2.87	2	4	1	4.2	5	92	1571	1.96	3.20	1.9
386562	13	-950	-376	San Nicolas	8371	39000	8.4	186.9	26	18	39	1.41	1.26	1.59	3	8	3	0.4	5	32	5	1.51	0.70	0.2
386563	14	-751	-400	San Nicolas	185	26000	0.2	5.5	13	6	26	1.11	0.78	1.41	2	21	8	0.2	5	45	5	1.65	0.70	0.2
386564	15	-1212	-434	San Nicolas	10000	173000	10.0	200.0	140	204	173	2.15	2.31	2.24	2	4	1	1.3	5	38	48	1.58	1.68	0.2
386565	16	-1152	-482	San Nicolas	69	13000	0.1	5.3	5	4	13	0.70	0.60	1.11	2	7	2	0.2	5	86	5	1.93	0.70	0.2
386566	17	-1105	-399	San Nicolas	1126	50000	1.1	96.8	8	21	50	0.90	1.32	1.70	3	5	1	0.6	5	5	5	0.70	0.70	0.2
386567	18	-1188	-565	San Nicolas	37	21000	0.0	5.8	4	10	21	0.60	1.00	1.32	2	2	1	0.2	5	13	5	1.11	0.70	0.2
386569	20	-214	-116	San Nicolas	259	17000	0.3	68.5	4	5	17	0.60	0.70	1.23	4	6	1	0.4	5	8	5	0.90	0.70	0.2
386570	21	-285	-116	San Nicolas	10000	36000	10.0	122.0	7	12	36	0.85	1.08	1.56	2	5	2	0.4	5	24	5	1.38	0.70	0.2
378963	12	-750	-359	San Nicolas	435	13000	0.4	14.5	18	6	13	1.26	0.78	1.11	1	7	2	0.2	5	11	5	0.2	1.04	0.2
386571	23	-1165	-395	San Nicolas	10000	70000	10.0	200.0	9	34	70	0.95	1.53	1.85	4	6	1	0.8	5	22	5	1.34	0.70	0.2
386572	24	879	637	Villalpando	10000	43000	10.0	200.0	25	17	43	1.40	1.23	1.63	3	3	1	0.3	5	46	39	1.66	1.59	0.2
386573	25	1133	622	Villalpando	7403	86000	7.4	200.0	45	56	86	1.65	1.75	1.93	2	5	1	0.9	5	16	8	1.20	0.90	0.2
386574	26	716	620	Villalpando	10000	47000	10.0	200.0	70	27	47	1.85	1.43	1.67	3	3	1	0.5	5	7	25	0.85	1.40	0.2
386575	27	540	626	Villalpando	10000	63000	10.0	200.0	42	26	63	1.62	1.41	1.80	1	4	1	0.4	5	14	18	1.15	1.26	0.3
386576	28	406	627	Villalpando	10000	116000	10.0	200.0	108	66	116	2.03	1.82	2.06	3	9	1	1	5	14	71	1.15	1.85	0.3
386577	29	571	787	Villalpando	584	50000	0.6	16.2	4	21	50	0.60	1.32	1.70	4	5	1	0.6	5	55	5	1.74	0.70	0.2
386578	30	1108	790	Villalpando	373	26000	0.4	8.1	13	17	26	1.11	1.23	1.41	3	4	1	0.3	5	32	5	1.51	0.70	0.2

ppm- parts per million
ppb-parts per billion

Run #	Sample #	X	Y	Vein	Au 30 (ppb)	Ag (ppb)	Au (ppm)	Ag (ppm)	Cu	Pb	Zn	Log Cu	Log Pb	Log Zn	Mo	Ni	Co	Cd	Bi	As	Sb	Log As	Log Sb	Hg
386579	31	834	827	Villalpando	7142	29000	7.1	141.8	9	14	29	0.95	1.15	1.46	6	5	1	0.2	5	6	5	0.78	0.70	0.2
386580	32	707	842	Villalpando	148	5000	0.1	7.1	1	2	5	0.00	0.30	0.70	2	1	1	0.2	5	10	5	1.00	0.70	0.2
386581	33	-110	-88	Los Panchos	10000	203000	10.0	200.0	111	148	203	2.05	2.17	2.31	5	5	1	2.2	5	37	55	1.57	1.74	0.2
386582	34	-399	-69	Los Panchos	252	38000	0.3	9.5	5	15	38	0.70	1.18	1.58	4	3	1	0.3	5	62	5	1.79	0.70	0.2
386583	35	-716	-83	Los Panchos	87	43000	0.1	7.1	6	12	43	0.78	1.08	1.63	13	8	1	0.3	5	32	5	1.51	0.70	0.2
386584	36	-873	-161	Los Panchos	10000	322000	10.0	200.0	71	173	322	1.85	2.24	2.51	20	6	2	6.1	5	32	162	1.51	2.21	0.2
386585	37	750	625	Villalpando	10000	44000	10.0	195.8	14	14	44	1.15	1.15	1.64	4	23	6	0.8	5	27	5	1.43	0.70	0.2
386586	38	-1	14	Los Panchos	10000	124000	10.0	127.5	17	84	124	1.23	1.92	2.09	2	1	1	1.8	5	7	18	0.85	1.26	0.8
386587	40	-198	-15	Los Panchos	697	37000	0.7	9.7	12	13	37	1.08	1.11	1.57	10	9	1	0.4	5	60	5	1.78	0.70	0.2
386588	41	-389	-215	Los Panchos	3153	305000	3.2	200.0	212	126	305	2.33	2.10	2.48	5	4	1	5.2	5	27	5	1.43	0.70	3.9
386589	42	-280	-212	Los Panchos	400	11000	0.4	7.5	3	8	11	0.48	0.90	1.04	7	6	1	0.2	5	5	5	0.70	0.70	0.2
386590	43	854	471	Villalpando	1303	18000	1.3	13.2	16	11	18	1.20	1.04	1.26	23	23	5	3.4	5	1173	5	3.07	0.70	0.2
386591	44	965	504	Villalpando	2695	24000	2.7	69.4	12	14	24	1.08	1.15	1.38	5	4	1	0.3	5	29	5	1.46	0.70	0.2
386592	45	1548	935	Villalpando	36	282000	0.0	5.9	19	69	282	1.28	1.84	2.45	3	14	8	1.8	5	9	5	0.95	0.70	0.2
386593	46	1404	944	Villalpando	13	7000	0.0	1.2	7	2	7	0.85	0.30	0.85	10	10	1	0.2	5	5	5	0.70	0.70	0.2
386594	47	1773	904	Villalpando	136	14000	0.1	8.0	10	8	14	1.00	0.90	1.15	10	10	2	1.2	5	13	5	1.11	0.70	0.2
386595	48	1893	872	Villalpando	383	10000	0.4	10.0	10	4	10	1.00	0.60	1.00	6	7	1	0.2	5	6	5	0.78	0.70	0.2
386596	49	-1101	-483	San Nicolas	1389	45000	1.4	200.0	107	21	45	2.03	1.32	1.65	3	22	9	0.8	5	140	14	2.15	1.15	2.3
386597	50	820	690	Villalpando	3900	21000	3.9	188.4	47	13	21	1.67	1.11	1.32	7	9	2	0.4	5	48	13	1.68	1.11	0.2
386598	53	270	270	San Juan de Dios	366	72000	0.4	66.5	29	40	72	1.46	1.60	1.86	5	8	2	0.9	5	74	5	1.87	0.70	0.2
386599	54	245	268	San Juan de Dios	84	17000	0.1	2.1	10	5	17	1.00	0.70	1.23	7	8	1	0.3	5	17	5	1.23	0.70	0.2
386600	55	303	250	San Juan de Dios	85	13000	0.1	8.1	1	9	13	0.00	0.95	1.11	1	2	1	0.2	5	15	5	1.18	0.70	0.2
386601	56	269	309	Villalpando	1517	9000	1.5	3.0	16	2	9	1.20	0.30	0.95	5	8	2	0.2	5	9	5	0.95	0.70	0.2
386602	57	351	305	Villalpando	2706	366000	2.7	200.0	71	227	366	1.85	2.36	2.56	3	15	3	3.3	5	39	28	1.59	1.45	1.3
386603	58	-777	-306	San Nicolas	3495	19000	3.5	68.3	5	9	19	0.70	0.95	1.28	6	5	1	0.2	5	6	5	0.78	0.70	0.2
386604	59	-597	-309	San Nicolas	1309	9000	1.3	13.2	5	3	9	0.70	0.48	0.95	6	6	1	0.2	5	5	5	0.70	0.70	0.2
386605	60	-26	-310	San Nicolas	139	412000	0.1	6.5	7	7	412	0.85	0.85	2.61	4	5	2	0.6	5	120	5	2.08	0.70	0.3
386606	61	-992	-303	San Nicolas	114	60000	0.1	4.1	6	14	60	0.78	1.15	1.78	6	8	3	0.6	5	141	5	2.15	0.70	0.2

Run #	Sample #	X	Y	Vein	Au 30 (ppb)	Ag (ppb)	Au (ppm)	Ag (ppm)	Cu	Pb	Zn	Log Cu	Log Pb	Log Zn	Mo	Ni	Co	Cd	Bi	As	Sb	Log As	Log Sb	Hg
386611	**66**	-904	-232	San Nicolas	83	55000	0.1	29.2	5	7	55	0.70	0.85	1.74	3	5	1	0.4	5	21	5	1.32	0.70	0.2
386612	**67**	321	125	San Juan de Dios	3604	17000	3.6	46.6	7	6	17	0.85	0.78	1.23	9	8	1	0.2	5	5	5	0.70	0.70	0.2
386613	**68**	-150	-245	San Juan de Dios	1872	154000	1.9	35.8	5	6	154	0.70	0.78	2.19	3	4	1	0.2	5	18	5	1.26	0.70	0.6
386614	**69**	-66	-244	San Nicolas	12	47000	0.0	0.7	4	11	47	0.60	1.04	1.67	3	4	1	0.4	5	36	5	1.56	0.70	0.3
386615	**70**	498	184	San Juan de Dios	10000	159000	10.0	197.6	106	43	159	2.03	1.63	2.20	6	6	1	1.3	5	46	12	1.66	1.08	0.2
386616	**71**	420	187	San Juan de Dios	10000	24000	10.0	200.0	72	13	24	1.86	1.11	1.38	4	5	1	0.3	5	7	5	0.85	0.70	1.6
386617	**72**	284	186	San Juan de Dios	10000	18000	10.0	200.0	160	15	18	2.20	1.18	1.26	7	8	1	0.4	5	5	6	0.70	0.78	1.1
386618	**73**	-185	-182	San Nicolas	10000	75000	10.0	200.0	7	14	75	0.85	1.15	1.88	6	7	1	0.3	5	10	5	1.00	0.70	0.5
386619	**74**	-811	-170	San Nicolas	341	61000	0.3	49.1	5	25	61	0.70	1.40	1.79	10	5	1	0.5	5	72	5	1.86	0.70	0.2
386621	**76**	-797	-137	San Nicolas	38	15000	0.0	1.0	2	15	15	0.30	1.18	1.18	2	2	1	0.2	5	18	5	1.26	0.70	0.2
386622	**77**	-760	-116	San Nicolas	17	14000	0.0	0.2	1	8	14	0.00	0.90	1.15	1	1	1	0.2	5	5	5	0.70	0.70	0.2
386623	**78**	-722	-103	San Nicolas	22	16000	0.0	0.7	4	76	16	0.60	1.88	1.20	5	4	1	0.2	5	36	5	1.56	0.70	0.2
386624	**79**	-705	-105	San Nicolas	10	58000	0.0	0.2	2	10	58	0.30	1.00	1.76	1	1	1	0.2	5	5	5	0.70	0.70	0.2
386625	**80**	-664	-108	San Nicolas	13	127000	0.0	0.3	13	10	127	1.11	1.00	2.10	2	8	3	0.2	5	5	5	0.70	0.70	0.2
386626	**81**	-615	-117	San Nicolas	7	19000	0.0	0.2	5	5	19	0.70	0.70	1.28	1	2	1	0.2	5	6	5	0.78	0.70	0.2
386627	**82**	-272	-63	San Nicolas	14	146000	0.0	0.8	9	16	146	0.95	1.20	2.16	3	7	3	0.3	5	27	5	1.43	0.70	1.0
386628	**83**	-698	-17	Los Panchos	10	19000	0.0	0.2	3	15	19	0.48	1.18	1.28	3	3	1	0.2	5	27	5	1.43	0.70	0.2
386629	**84**	-726	-25	Los Panchos	5	38000	0.0	0.2	3	11	38	0.48	1.04	1.58	3	3	1	0.2	5	11	5	1.04	0.70	0.2
386630	**85**	-840	-48	Los Panchos	11	13000	0.0	0.2	2	14	13	0.30	1.15	1.11	3	4	1	0.2	5	17	5	1.23	0.70	0.2
386632	**87**	336	287	San Juan de Dios	15	124000	0.0	3.7	23	26	124	1.36	1.41	2.09	4	30	17	2.2	5	16	5	1.20	0.70	0.2
386633	**88**	395	292	San Juan de Dios	5	121000	0.0	0.2	5	24	121	0.70	1.38	2.08	2	4	2	0.3	5	95	13	1.98	1.11	0.4
386634	**89**	425	306	San Juan de Dios	5	15000	0.0	0.2	6	7	15	0.78	0.85	1.18	1	4	1	0.2	5	16	10	1.20	1.00	0.7
386635	**90**	489	299	San Juan de Dios	5	29000	0.0	0.2	5	5	29	0.70	0.70	1.46	2	3	1	0.2	5	7	5	0.85	0.70	0.2
378955	**250**	1143	788	Villalpando	10000	219000	10.0	200.0	62	184	219	1.79	2.26	2.34	1	3	1	2.7	5	33	34	1.52	1.53	0.2
378958	**200**	-189	-287	San Nicolas	10000	176000	10.0	200.0	316	58	176	2.50	1.76	2.25	2	7	1	0.7	5	17	79	1.23	1.90	1.2
378959	**299**	-288	-297	San Nicolas	10000	325000	10.0	200.0	511	49	325	2.71	1.69	2.51	2	3	1	2	5	23	24	1.36	1.38	0.2

Run #	Sample #	X	Y	Vein	Fe %	Mn	Te	Ba	Cr	V	Sn	W	La	Al %	Mg %	Ca %	Na %	K %	Sr	Y	Ga	Li	Nb	Sc	Ta	Ti	Zr	S
386579	31	834	827	Villalpando	0.59	331	10	10	126	4	20	20	10	0.31	0.11	2.13	0.01	0.09	23	5	2	4	1	5	10	0.01	1	0.11
386580	32	707	842	Villalpando	0.18	4079	10	3	13	1	20	20	6	0.09	0.03	10	0.01	0.02	240	23	2	1	1	5	10	0.01	1	0.26
386581	33	-110	-88	Los Panchos	0.58	730	10	1	114	3	20	20	1	0.08	0.04	2.48	0.01	0.04	14	3	2	3	1	5	10	0.01	1	0.37
386582	34	-399	-69	Los Panchos	0.95	644	10	12	67	2	20	20	18	0.09	0.01	4.97	0.01	0.12	73	15	2	1	1	5	10	0.01	3	1.02
386583	35	-716	-83	Los Panchos	1.07	95	10	10	179	4	20	20	12	0.08	0.04	0.1	0.01	0.04	4	6	2	3	1	5	10	0.01	2	0.82
386584	36	-873	-161	Los Panchos	0.99	117	10	1	122	12	20	20	2	0.22	0.22	0.59	0.01	0.02	10	1	2	8	1	5	10	0.01	1	0.72
386585	37	750	625	Villalpando	1.49	532	10	3	122	40	20	20	2	1.05	1.08	1.91	0.02	0.04	30	3	2	39	3	5	10	0.082	1	0.33
386586	38	-1	14	Los Panchos	0.60	644	10	1	33	8	20	20	3	0.25	0.43	3.36	0.01	0.03	51	7	5	32	1	5	10	0.01	1	0.12
386587	40	-198	-15	Los Panchos	0.98	349	10	33	211	7	20	20	18	0.33	0.05	1.54	0.06	0.2	43	9	2	12	1	5	10	0.027	3	0.57
386588	41	-389	-215	Los Panchos	0.55	785	10	3	88	3	20	20	3	0.08	0.15	10	0.01	0.01	237	3	2	4	1	5	10	0.01	1	0.5
386589	42	-280	-212	Los Panchos	0.24	652	10	2	132	4	20	20	3	0.07	0.04	10	0.01	0.02	110	11	2	4	1	5	10	0.01	1	0.08
386590	43	854	471	Villalpando	0.85	1381	10	2	190	24	20	20	3	0.3	0.31	10	0.01	0.02	54	7	2	10	2	5	10	0.01	1	0.65
386591	44	965	504	Villalpando	0.21	797	10	1	92	3	20	20	2	0.04	0.03	7.77	0.01	0.01	52	1	2	2	1	5	10	0.01	1	0.07
386592	45	1548	935	Villalpando	2.49	689	10	53	34	19	20	20	21	1.56	0.42	0.09	0.03	0.2	7	19	3	27	1	5	10	0.01	2	0.01
386593	46	1404	944	Villalpando	0.52	34	10	9	261	7	20	20	8	0.19	0.01	0.08	0.01	0.04	3	1	2	2	1	5	10	0.01	2	0.01
386594	47	1773	904	Villalpando	1.16	44	10	27	220	10	20	20	3	0.39	0.02	0.05	0.01	0.1	4	2	2	11	1	5	10	0.01	3	0.01
386595	48	1893	872	Villalpando	0.62	46	10	33	151	5	20	20	4	0.28	0.03	0.02	0.01	0.06	3	2	2	2	1	5	10	0.01	2	0.01
386596	49	-1101	-483	San Nicolas	2.39	261	10	10	135	47	20	20	2	1.09	1.03	0.17	0.01	0.06	4	3	2	46	3	5	10	0.01	1	0.54
386597	50	820	690	Villalpando	0.62	464	10	1	133	7	20	20	2	0.15	0.17	1.82	0.01	0.03	9	2	2	7	1	5	10	0.01	1	0.36
386598	53	270	270	San Juan de Dios	1.53	43	10	64	149	9	20	20	12	0.45	0.05	0.06	0.01	0.1	9	5	2	4	1	5	10	0.01	3	0.38
386599	54	245	268	San Juan de Dios	1.11	59	10	26	180	10	20	20	10	0.33	0.05	0.05	0.03	0.08	12	3	2	7	1	5	10	0.01	5	0.01
386600	55	303	250	San Juan de Dios	0.29	4477	10	6	4	1	20	20	9	0.37	0.07	10	0.01	0.04	855	10	2	1	1	5	10	0.01	1	0.4
386601	56	269	309	Villalpando	0.49	384	10	3	50	14	20	20	2	0.18	0.15	10	0.01	0.03	70	1	2	10	1	5	10	0.01	1	0.16
386602	57	351	305	Villalpando	0.97	897	10	2	90	12	20	20	2	0.23	0.25	8.83	0.05	0.02	79	2	2	11	1	5	10	0.01	1	0.88
386603	58	-777	-306	San Nicolas	0.37	507	10	5	125	4	20	20	5	0.22	0.05	6.79	0.01	0.05	42	4	2	3	1	5	10	0.01	1	0.17
386604	59	-597	-309	San Nicolas	0.27	113	10	1	157	2	20	20	1	0.02	0.01	0.44	0.01	0.01	3	1	2	1	1	5	10	0.01	1	0.02
386605	60	-26	-310	San Nicolas	0.83	50	10	9	135	3	20	20	7	0.31	0.03	0.11	0.01	0.15	4	7	2	2	1	5	10	0.01	1	0.64
386606	61	-992	-303	San Nicolas	1.56	354	10	15	104	6	20	20	15	0.37	0.1	4.27	0.03	0.1	91	8	2	11	1	5	10	0.01	1	1.06

Run #	Sample #	X	Y	Vein	Fe %	Mn	Te	Ba	Cr	V	Sn	W	La	Al %	Mg %	Ca %	Na %	K %	Sr	Y	Ga	Li	Nb	Sc	Ta	Ti	Zr	S
386611	**66**	-904	-232	San Nicolas	0.59	79	10	5	130	2	20	20	10	0.24	0.03	0.16	0.01	0.03	5	10	2	1	1	5	10	0.01	1	0.42
386612	**67**	321	125	San Juan de Dios	0.39	123	10	4	213	5	20	20	2	0.1	0.06	0.24	0.01	0.01	8	2	2	10	1	5	10	0.01	1	0.03
386613	**68**	-150	-245	San Juan de Dios	0.45	137	10	1	126	1	20	20	2	0.05	0.02	0.04	0.01	0.01	2	3	2	1	1	5	10	0.01	1	0.2
386614	**69**	-66	-244	San Nicolas	0.73	57	10	17	65	2	20	20	7	0.57	0.03	0.08	0.01	0.34	4	7	2	1	1	5	10	0.01	1	0.57
386615	**70**	498	184	San Juan de Dios	1.52	31	10	3	202	4	20	20	2	0.15	0.01	0.03	0.01	0.11	2	2	2	1	1	5	10	0.01	1	0.69
386616	**71**	420	187	San Juan de Dios	0.44	29	10	8	123	3	20	20	2	0.13	0.02	0.06	0.01	0.08	3	5	2	1	1	5	10	0.01	1	0.05
386617	**72**	284	186	San Juan de Dios	0.42	27	10	3	162	5	20	20	1	0.15	0.02	0.08	0.01	0.03	3	4	2	2	1	5	10	0.01	1	0.06
386618	**73**	-185	-182	San Nicolas	0.53	87	10	6	177	3	20	20	3	0.13	0.01	0.04	0.01	0.1	2	2	2	4	1	5	10	0.01	1	0.21
386619	**74**	-811	-170	San Nicolas	0.94	1252	10	12	83	2	20	20	17	0.69	0.04	7.92	0.01	0.06	21	20	2	2	1	5	10	0.01	2	0.77
386621	**76**	-797	-137	San Nicolas	0.52	24	10	28	35	2	20	20	25	0.9	0.02	0.1	0.03	0.26	10	14	3	1	1	5	10	0.01	3	0.01
386622	**77**	-760	-116	San Nicolas	0.53	18	10	27	24	2	20	20	21	0.5	0.01	0.04	0.02	0.23	5	9	2	2	1	5	10	0.01	2	0.01
386623	**78**	-722	-103	San Nicolas	0.73	128	10	205	60	2	20	20	31	0.59	0.01	0.06	0.04	0.27	22	8	3	3	1	5	10	0.01	4	0.06
386624	**79**	-705	-105	San Nicolas	0.76	40	10	46	17	3	20	20	32	1.64	0.04	0.02	0.01	0.33	5	7	4	11	1	5	10	0.01	9	0.01
386625	**80**	-664	-108	San Nicolas	1.35	74	10	76	31	13	20	20	37	1.8	0.27	0.14	0.01	0.35	22	11	4	3	1	5	10	0.01	3	0.01
386626	**81**	-615	-117	San Nicolas	0.54	20	10	30	17	6	20	20	11	0.87	0.07	0.11	0.01	0.25	15	4	3	1	1	5	10	0.01	2	0.01
386627	**82**	-272	-63	San Nicolas	3.19	13	10	63	82	23	20	20	13	0.46	0.01	0.01	0.01	0.14	8	6	2	2	1	5	10	0.01	5	0.02
386628	**83**	-698	-17	Los Panchos	1.22	69	10	396	74	2	20	20	18	0.6	0.01	0.03	0.05	0.08	17	4	2	8	1	5	10	0.01	6	0.07
386629	**84**	-726	-25	Los Panchos	1.19	47	10	53	40	4	20	20	15	1.34	0.03	0.03	0.02	0.2	7	7	3	1	1	5	10	0.01	7	0.01
386630	**85**	-840	-48	Los Panchos	1.17	23	10	41	84	2	20	20	10	0.42	0.02	0.06	0.01	0.23	9	3	2	3	1	5	10	0.01	2	0.02
386632	**87**	336	287	San Juan de Dios	3.18	694	10	1701	61	40	20	20	104	1.99	0.83	0.18	0.02	0.37	32	33	6	1	2	5	10	0.01	2	0.05
386633	**88**	395	292	San Juan de Dios	3.88	30	10	73	19	20	20	20	29	0.58	0.01	0.08	0.01	0.2	9	181	3	2	1	5	10	0.016	18	0.01
386634	**89**	425	306	San Juan de Dios	0.54	30	10	44	67	2	20	20	14	0.29	0.01	0.02	0.01	0.14	3	8	2	2	1	5	10	0.01	10	0.01
386635	**90**	489	299	San Juan de Dios	0.69	32	10	152	43	16	20	20	12	0.39	0.01	0.02	0.01	0.21	15	7	2		1	5	10	0.01	7	0.01
378955	**250**	1143	788	Villalpando	0.73	949	10	2	94	1	20	20	4	0.14	0.05	6.53	0.01	0.09	97	8	2	2	1	5	10	0.01	3	0.44
378958	**200**	-189	-287	San Nicolas	0.46	54	10	4	255	1	20	20	1	0.09	0.01	0.11	0.01	0.09	4	1	2	1	1	5	10	0.01	1	0.11
378959	**299**	-288	-297	San Nicolas	0.64	72	10	3	66	1	20	20	4	0.2	0.03	0.27	0.01	0.09	5	5	2	1	1	5	10	0.01	1	0.34

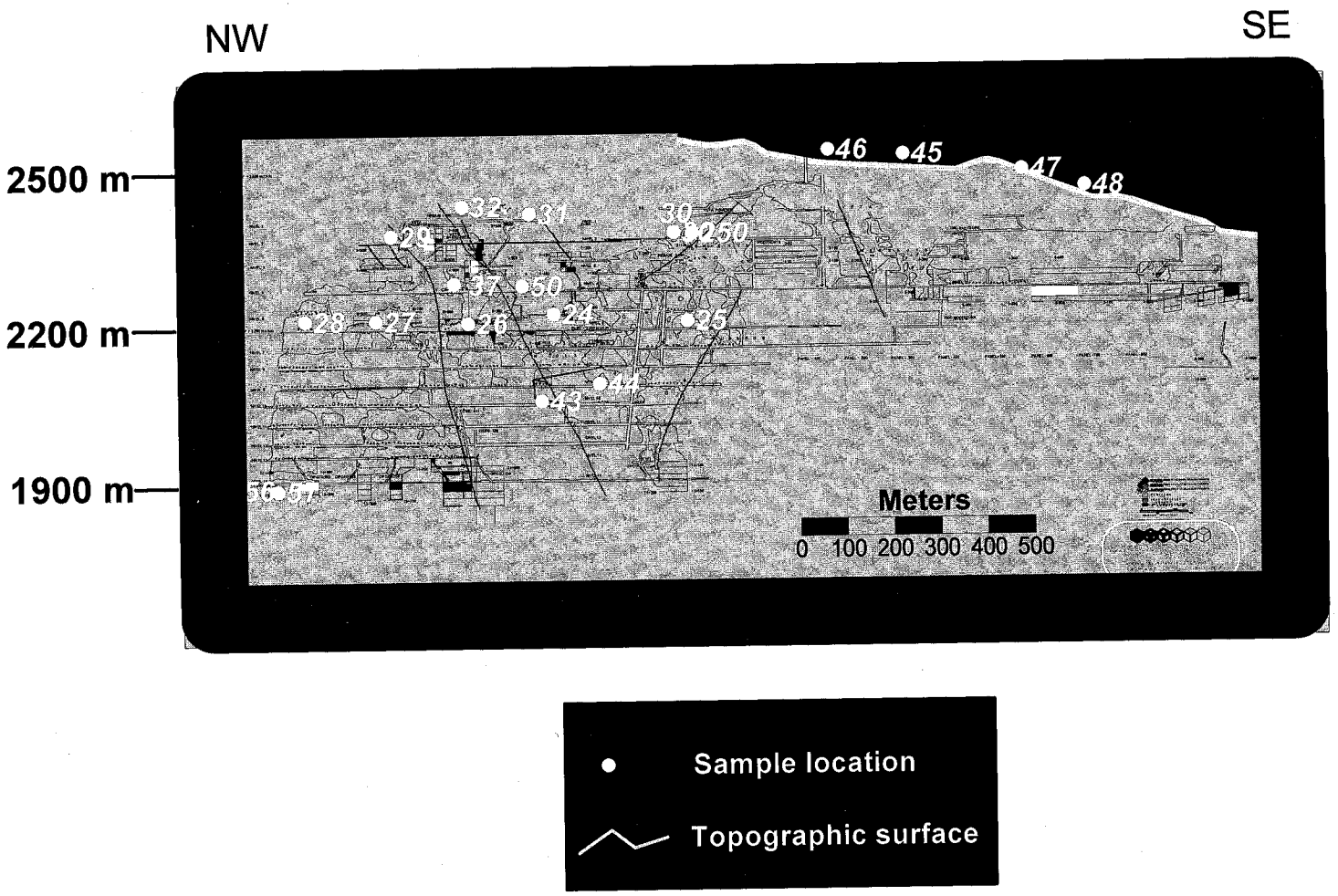

Appendix 2-1. Sample location map along longitudinal section of the Villalpando vein. Red lines are vein intersections.

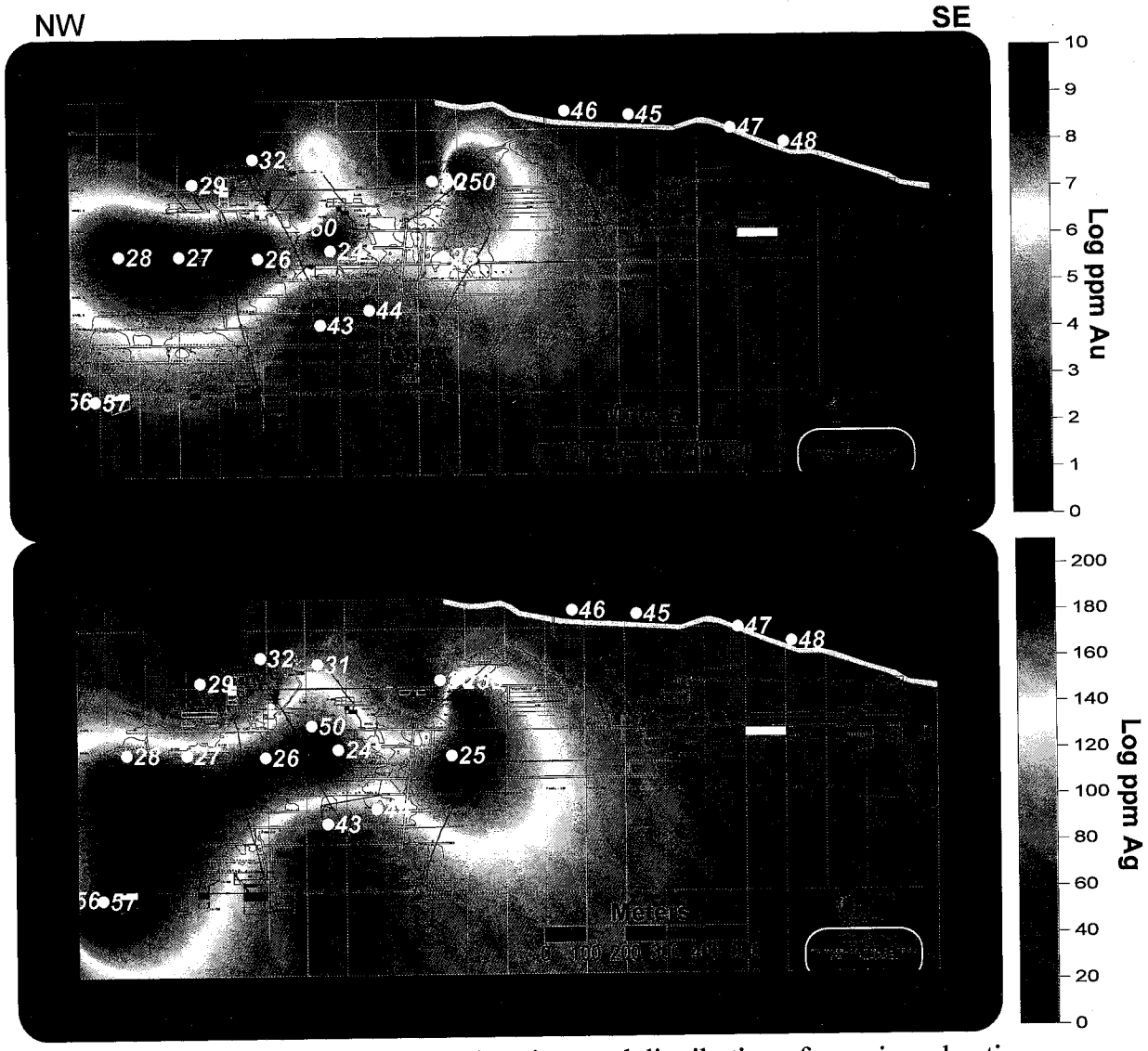

Appendix 2-2. Geochemical sample locations and distribution of arsenic and antimony on Villalpando vein longitudinal section. Red lines are vein intersections.

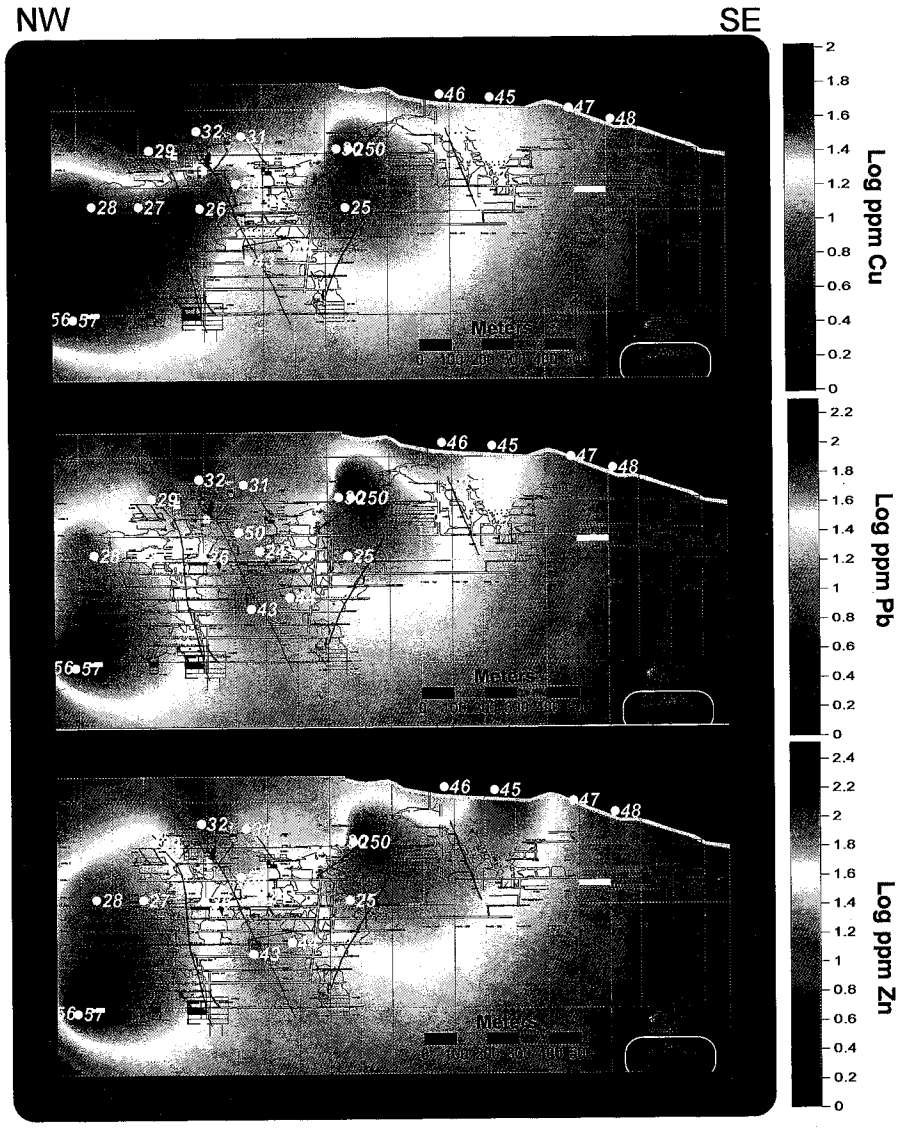

Appendix 2-3. Geochemical sample locations and distribution of copper, lead and zincon Villalpando vein longitudinal section. Red lines are vein intersections

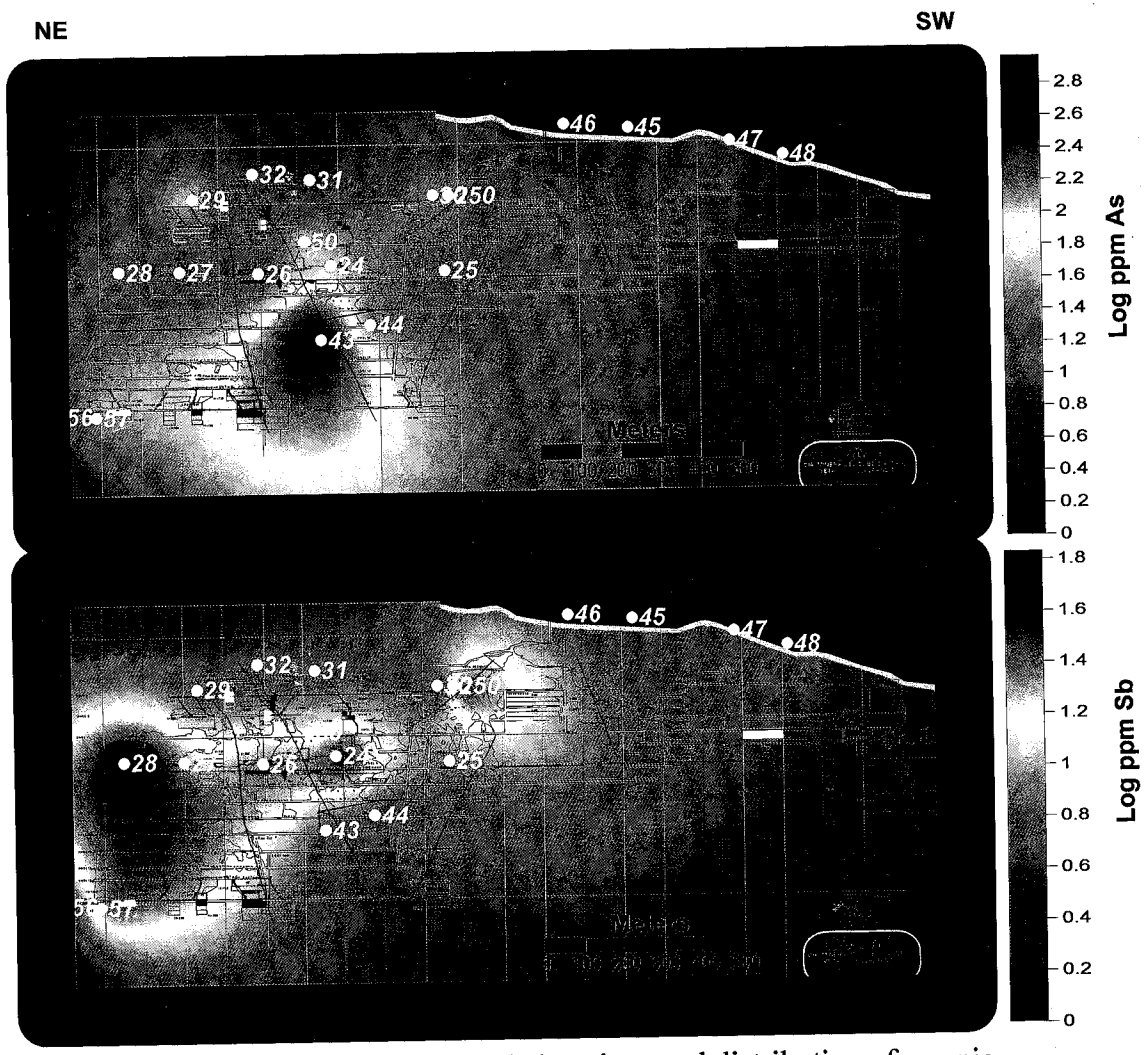

Appendix 2-4. Geochemical sample locations and distribution of arsenic and antimony on Villalpando vein longitudinal section. Red lines are vein intersections

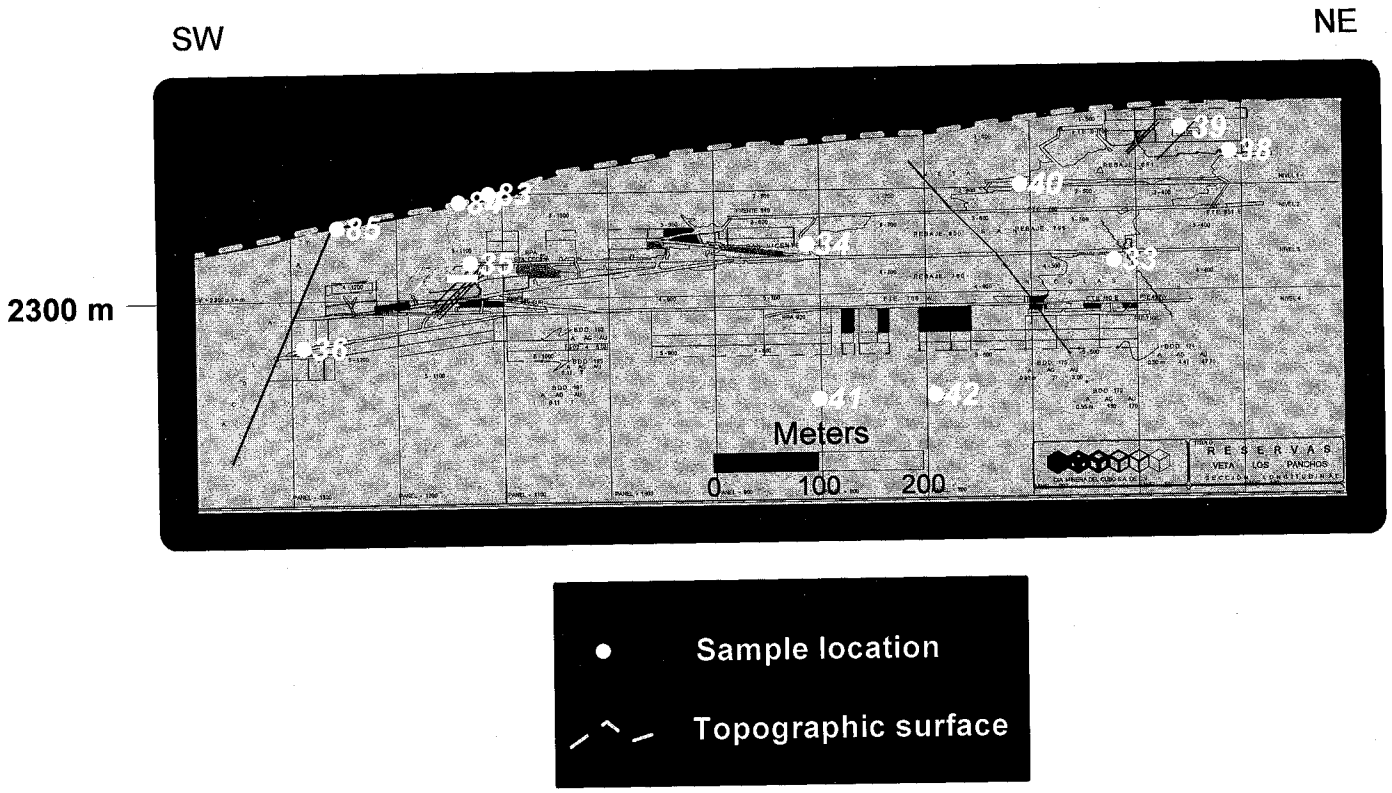

Appendix 2-5. Sample location map along longitudinal section of the Los Panchos vein.

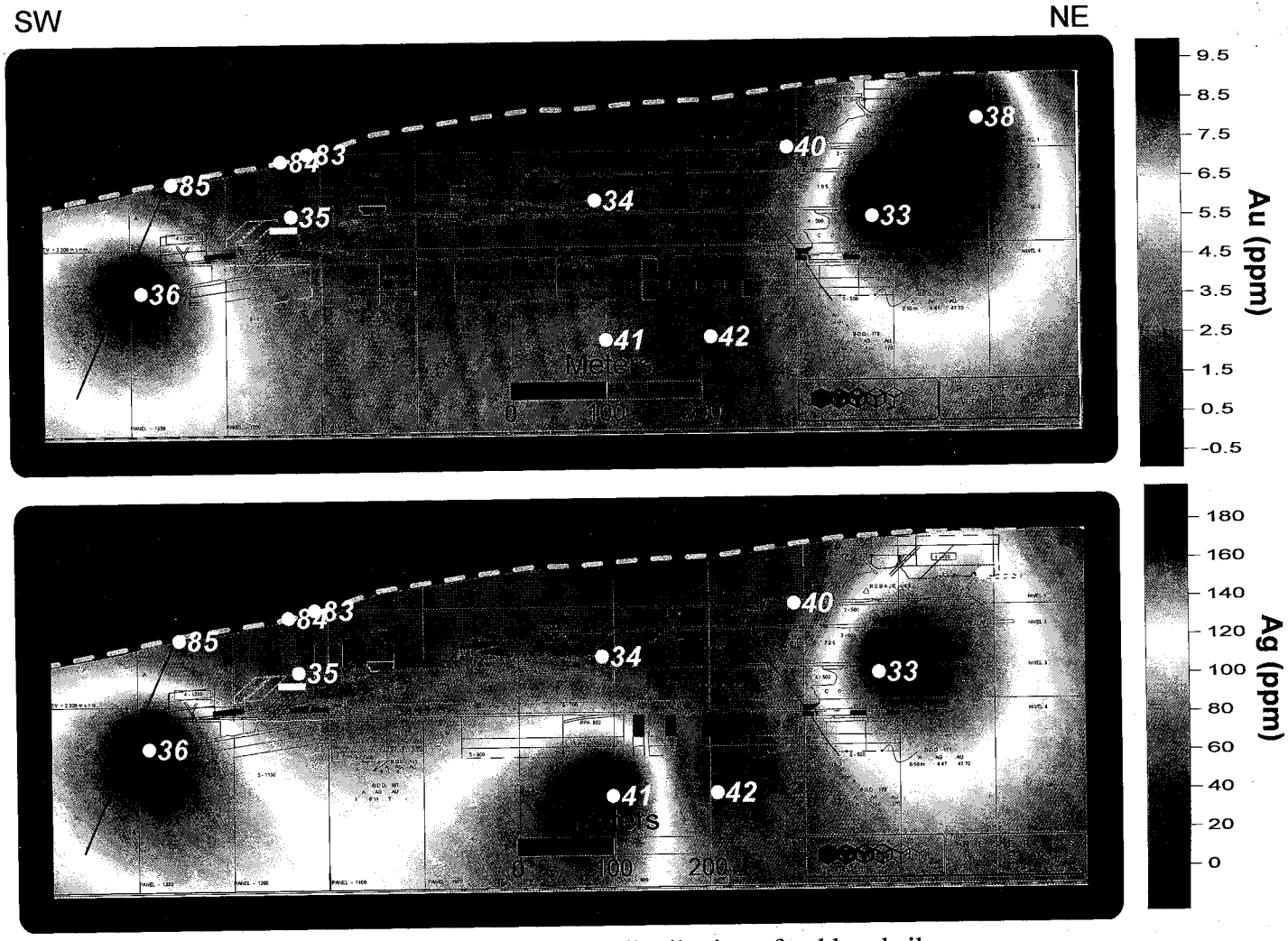

Appendix 2-6. Geochemical sample locations and distribution of gold and silver on San Juan de Dios vein longitudinal section.

Appendix 2 -7. Geochemical sample locations and distribution of copper, lead and zinc on San Juan de Dios vein longitudinal section.

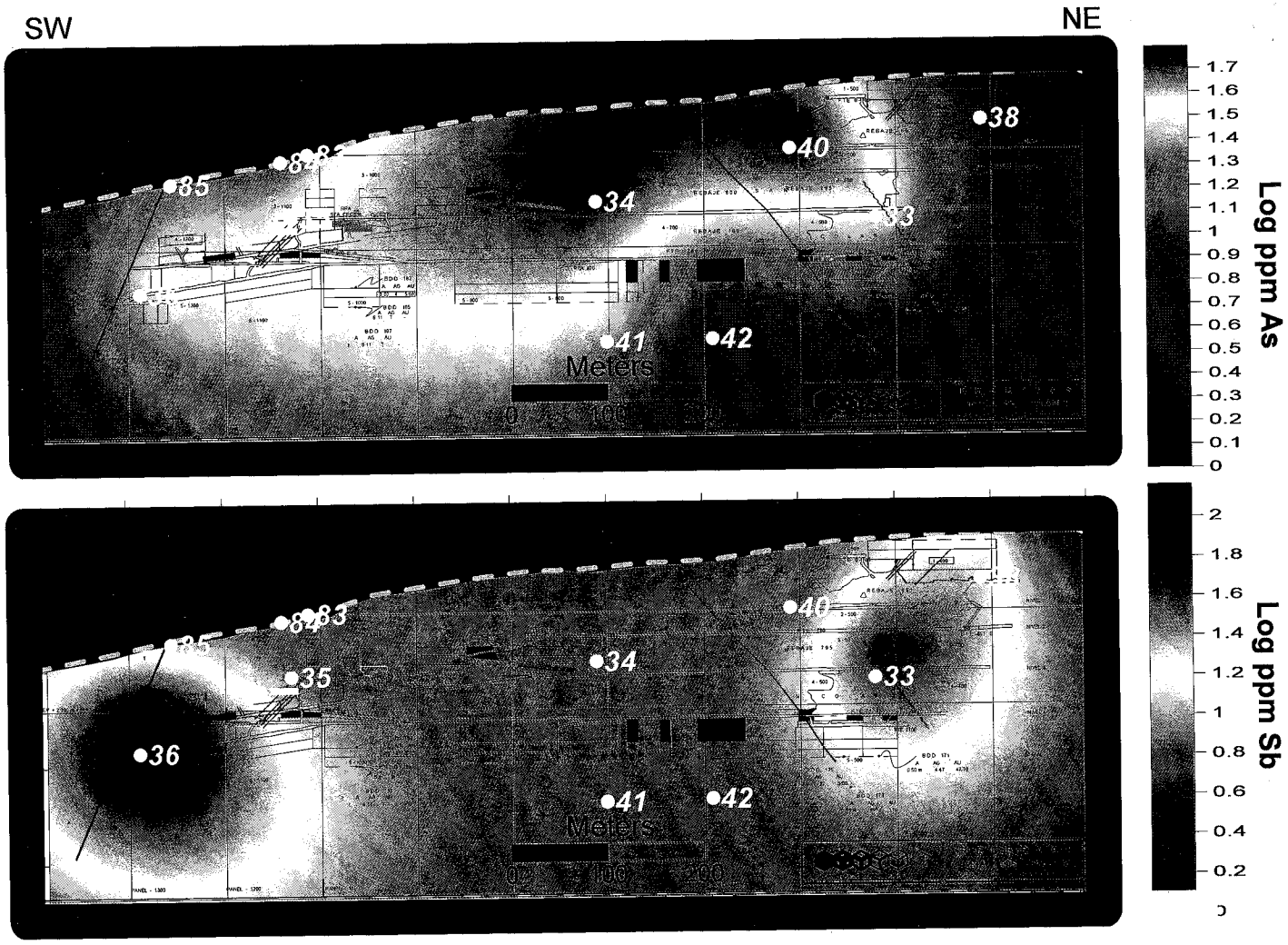

Appendix 2-8. Geochemical sample locations and distribution of arsenic and antimony on San Juan de Dios vein longitudinal section.

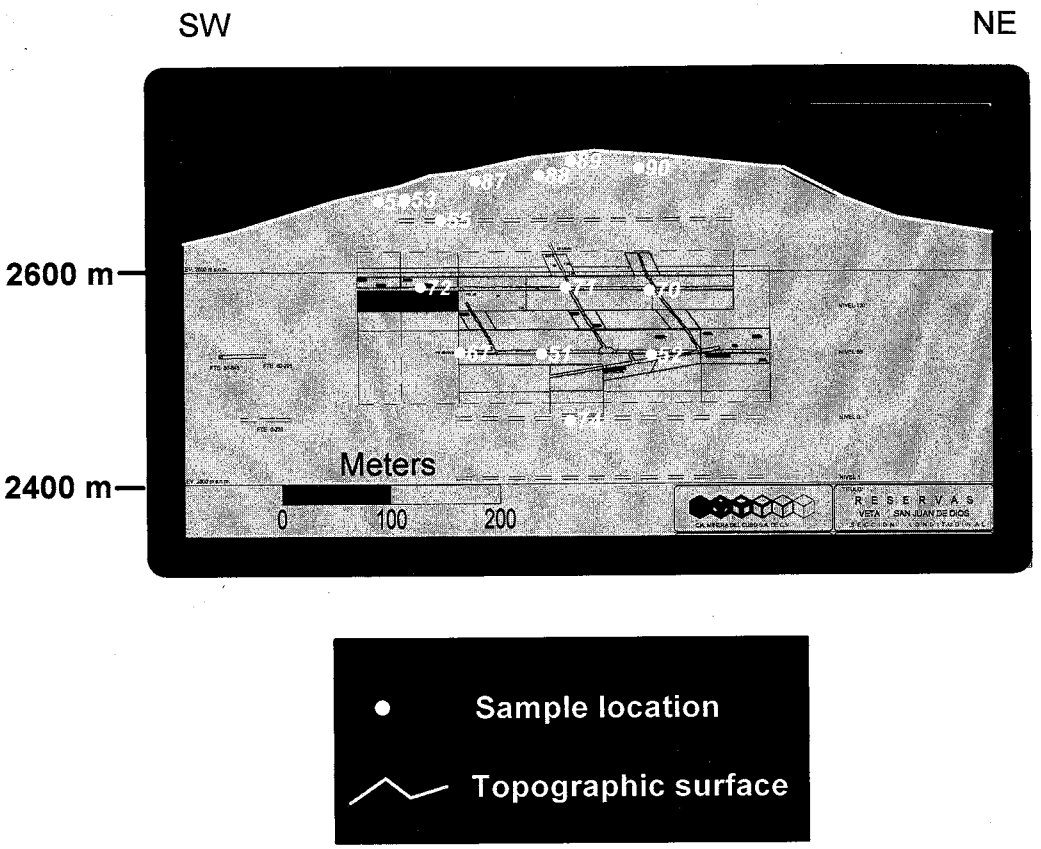

Appendix 2-9. Sample location map along longitudinal section of the of the San Juan de Dios vein.

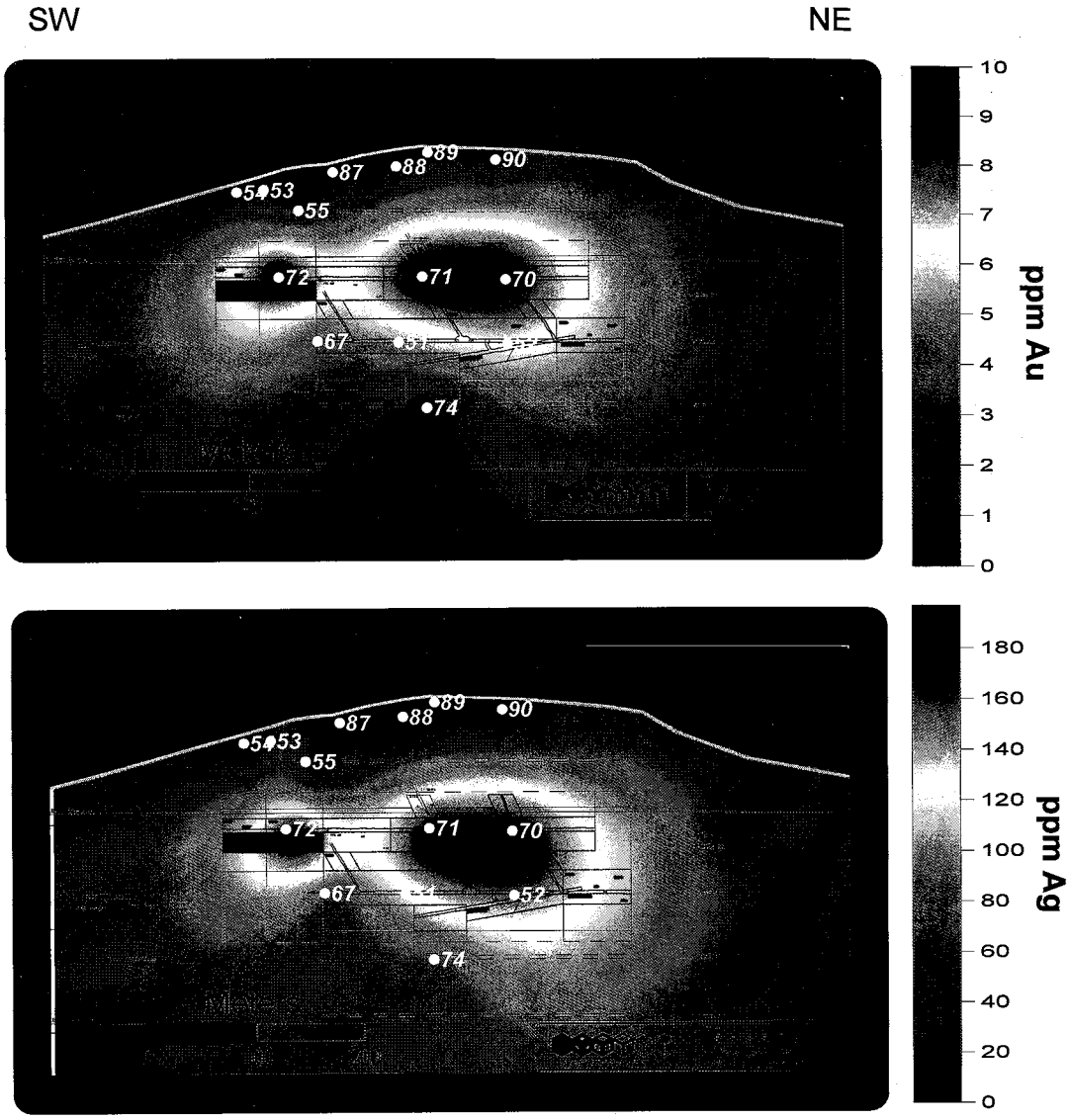

Appendix 2-10. Geochemical sample locations and distribution of gold and silver on San Juan de Dios vein longitudinal section.

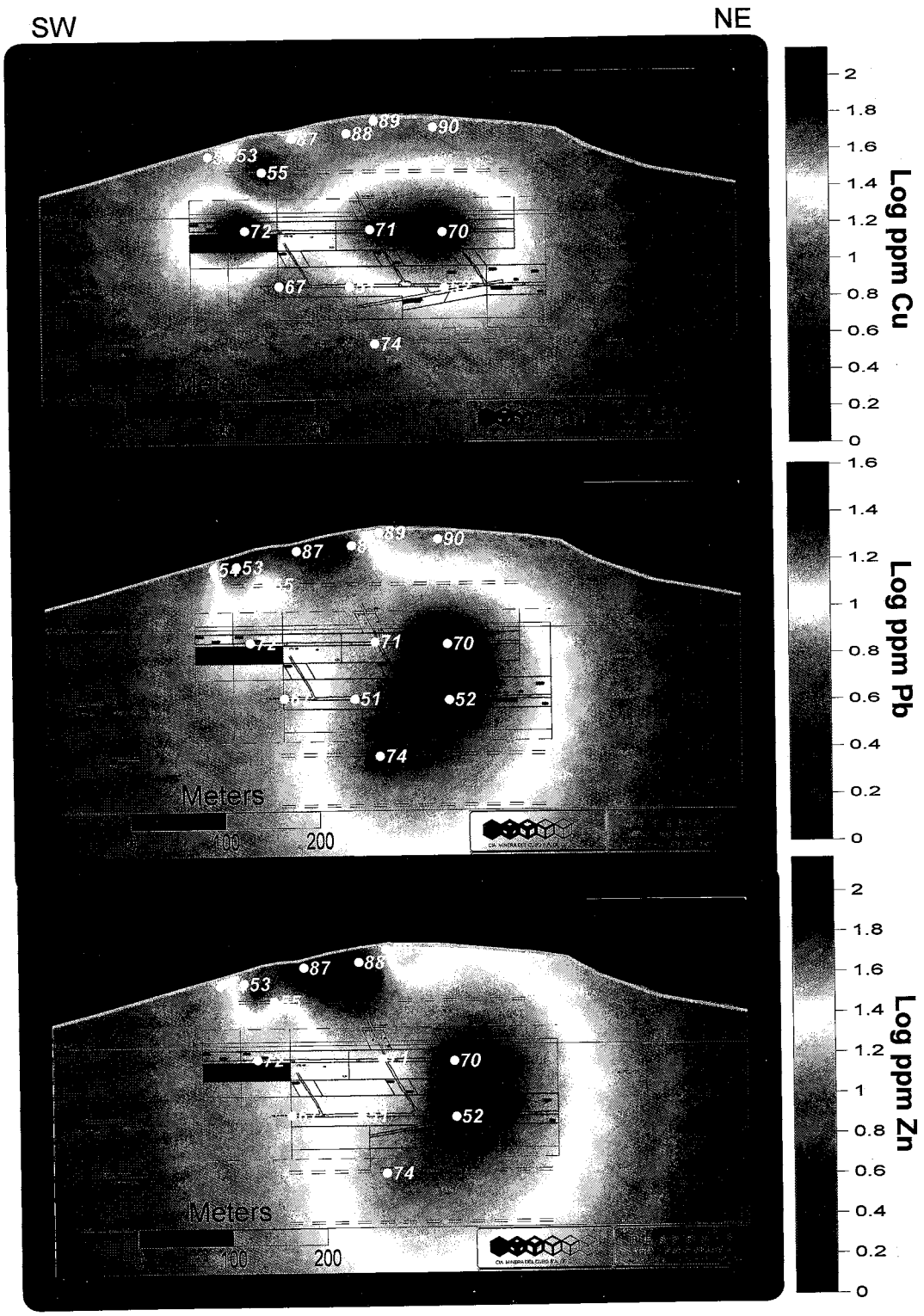

Appendix 2-11. Geochemical sample locations and distribution of gold and silver on San Juan de Dios vein longitudinal section.

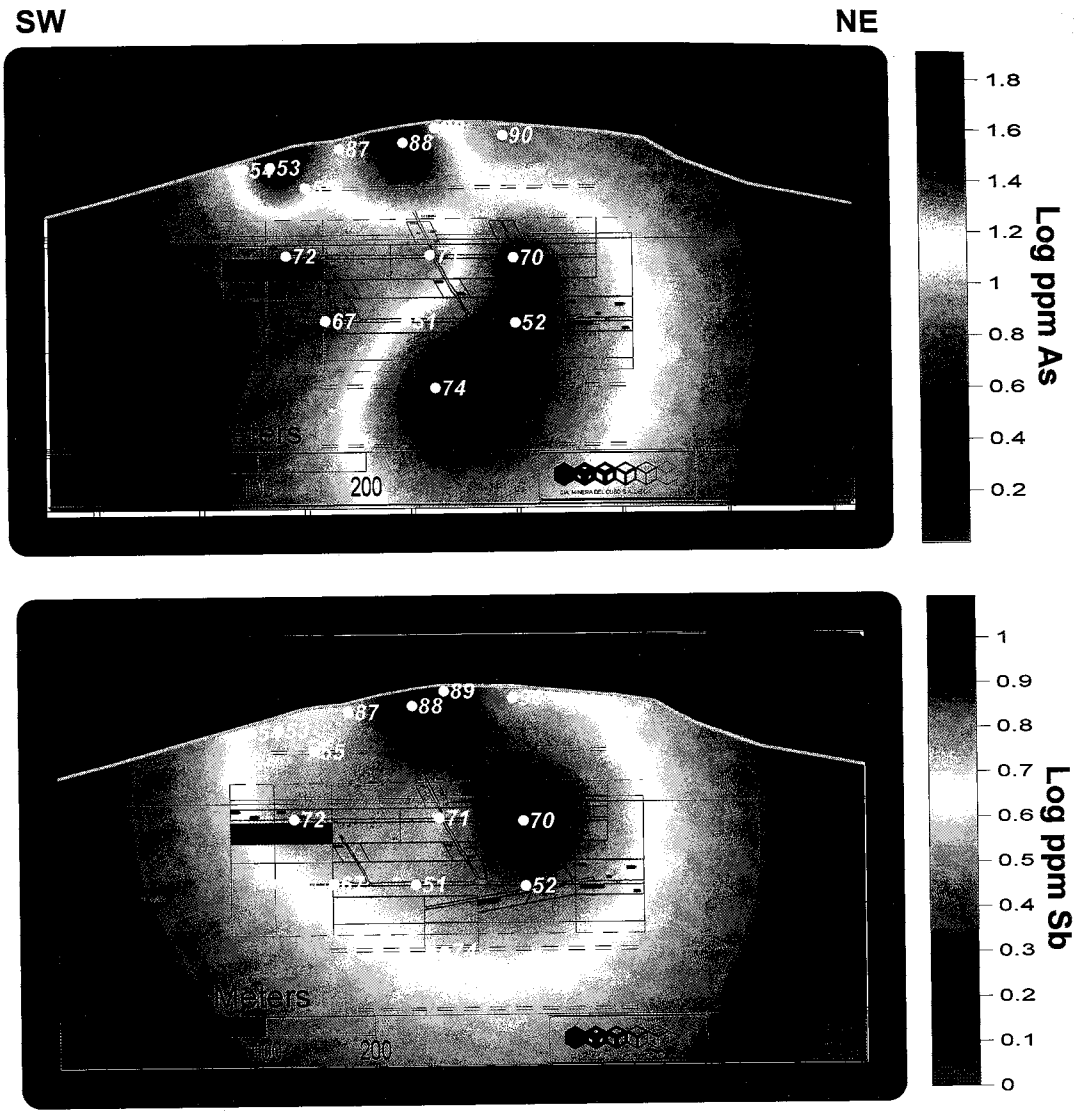

Appendix 2-12. Geocheimical sample locations and distribution of arsenic and antimony on San Juan de Dios vein longitudinal section.

Appendix 3
Fluid Inclusion Data

Sample #	Host Mineral	Type of inclusion	Paragenetic Stage	Th	Tm ice	Wt % NaCl eq.
1	mosaic quartz	secondary	Stage II	207.8	-0.6	1.0
1	mosaic quartz	secondary	Stage II	221.4	-0.5	0.8
1	mosaic quartz	secondary	Stage II	244.8	-0.5	0.8
1	mosaic quartz	secondary	Stage II	234.2	-0.5	0.8
1	mosaic quartz	secondary	Stage II	242.0	-0.5	0.8
2	quartz	Pseudosecondary	Stage II	279.9	-1.5	2.5
2	quartz	Pseudosecondary	Stage II	282.2	-1.4	2.3
2	quartz	Pseudosecondary	Stage II	271.6	-1.4	1.8
2	quartz	Pseudosecondary	Stage II	260.5	-1.2	2.0
2	quartz	Pseudosecondary	Stage II	260.5	-1.1	1.8
3	crystalline quartz	primary	Stage II	183.1	-1.4	2.3
3	crystalline quartz	primary	Stage II	201.4	-1.3	2.1
3	crystalline quartz	primary	Stage II	198.3	-1.3	2.1
3	crystalline quartz	primary	Stage II	194.7	-1.3	2.1
3	crystalline quartz	primary	Stage II	197.0	-1.3	2.1
3	crystalline quartz	primary	Stage II	203.2	-1.3	2.1
3	crystalline quartz	primary	Stage II	244.0	-0.3	0.5
3	crystalline quartz	primary	Stage II	236.0	-1.1	1.8
3	crystalline quartz	primary	Stage II	199.3	-0.3	0.5
3	crystalline quartz	primary	Stage II	230.0	-0.3	0.5
3	crystalline quartz	primary	Stage II	190.1	-0.3	0.5

Sample #	Host Mineral	Type of inclusion	Paragenetic Stage	Th	Tm ice	Wt % NaCl eq.
3	crystalline quartz	primary	Stage II	223.3	-0.4	0.7
4	crystalline quartz	secondary	Stage II	239.9	-0.4	0.7
4	crystalline quartz	secondary	Stage II	253.3	-0.4	0.7
4	crystalline quartz	secondary	Stage II	192.9	-1.2	2.0
4	crystalline quartz	secondary	Stage II	197.1	-1.2	2.0
4	crystalline quartz	secondary	Stage II	227.1	np	np
4	crystalline quartz	secondary	Stage II	214.2	-1.2	2.0
4	crystalline quartz	secondary	Stage II	240.7	-1.1	1.8
4	crystalline quartz	secondary	Stage II	185.4	-1.2	2.0
4	crystalline quartz	secondary	Stage II	229.5	-0.5	0.8
4	crystalline quartz	secondary	Stage II	243.1	np	np
4	crystalline quartz	secondary	Stage II	244.2	np	np
4	crystalline quartz	secondary	Stage II	239.3	-0.9	1.5
4	crystalline quartz	secondary	Stage II	234.6	-1.1	1.8
5	crystalline quartz	primary	Stage II	216.3	-0.4	0.7
5	crystalline quartz	primary	Stage II	212.0	-0.4	0.7
5	crystalline quartz	primary	Stage II	212.3	-0.4	0.7
5	crystalline quartz	primary	Stage II	211.3	-0.4	0.7
5	crystalline quartz	primary	Stage II	225.6	-0.4	0.7
5	crystalline quartz	primary	Stage II	229.9	-0.4	0.7
5	crystalline quartz	primary	Stage II	226.3	-0.5	0.8

Sample #	Host Mineral	Type of inclusion	Paragenetic Stage	Th	Tm ice	Wt % NaCl eq.
5	crystalline quartz	primary	Stage II	214.4	-0.4	0.7
5	crystalline quartz	primary	Stage II	209.0	-0.4	0.7
6	crystalline quartz	primary	Stage II	np	-0.2	0.3
6	crystalline quartz	primary	Stage II	np	-0.1	0.2
6	crystalline quartz	primary	Stage II	decrep	-0.3	0.5
6	crystalline quartz	primary	Stage II	decrep	np	np
6	crystalline quartz	primary	Stage II	decrep	-0.2	0.3
6	crystalline quartz	primary	Stage II	277.4	np	np
6	crystalline quartz	primary	Stage II	262.4	-0.2	0.3
6	crystalline quartz	primary	Stage II	270.7	np	np
6	crystalline quartz	primary	Stage II	247.8	-0.1	0.2
6	crystalline quartz	primary	Stage II	241.0	-0.1	0.2
6	crystalline quartz	primary	Stage II	260.7	-0.1	0.2
6	crystalline quartz	primary	Stage II	236.3	-0.1	0.2
6	crystalline quartz	primary	Stage II	np	-0.1	0.2
6	crystalline quartz	primary	Stage II	240.3	-0.2	0.3
6	calcite	primary	Stage II	240.5	-0.2	0.3
6	calcite	primary	Stage II	238.8	-0.2	0.3
8	mosaic quartz	secondary	Stage II	209.7	-1.2	2.0
8	mosaic quartz	secondary	Stage II	211.4	-1.3	2.1
8	mosaic quartz	secondary	Stage II	218.2	-1.4	2.3

Sample #	Host Mineral	Type of inclusion	Paragenetic Stage	Th	Tm ice	Wt % NaCl eq.
8	mosaic quartz	secondary	Stage II	207.3	np	np
8	mosaic quartz	secondary	Stage II	257.9	-0.9	1.5
8	mosaic quartz	secondary	Stage II	234.5	-0.1	0.2
8	mosaic quartz	secondary	Stage II	235.5	-0.1	0.2
8	mosaic quartz	secondary	Stage II	220.1	-0.1	0.2
8	mosaic quartz	secondary	Stage II	220.1	-0.1	0.2
8	mosaic quartz	secondary	Stage II	235.0	-0.1	0.2
9	crystalline quartz	primary	Stage III	193.5	-0.6	1.0
9	crystalline quartz	primary	Stage III	215.6	-0.6	1.0
9	crystalline quartz	primary	Stage III	219.9	-0.6	1.0
9	crystalline quartz	primary	Stage III	223.1	-0.7	1.2
9	crystalline quartz	primary	Stage III	223.9	-0.7	1.2
9	crystalline quartz	primary	Stage III	242.2	-0.7	1.2
9	crystalline quartz	primary	Stage III	245.3	-0.7	1.2
10	quartz	primary	Stage II	218.5	-0.5	0.8
10	quartz	primary	Stage II	239.8	-0.5	0.8
10	quartz	primary	Stage II	229.7	-0.6	1.0
13	crystalline quartz	pseudosecondary	Stage II	233.2	-0.7	1.2
13	crystalline quartz	pseudosecondary	Stage II	229.9	-0.8	1.3
13	crystalline quartz	pseudosecondary	Stage II	248.6	-0.8	1.3

Sample #	Host Mineral	Type of inclusion	Paragenetic Stage	Th	Tm ice	Wt % NaCl eq.
13	crystalline quartz	pseudosecondary	Stage III	254.1	-0.7	1.2
13	crystalline quartz	pseudosecondary	Stage II	231.4	-0.8	1.3
13	crystalline quartz	pseudosecondary	Stage II	250.5	-0.7	1.2
13	crystalline quartz	pseudosecondary	Stage II	250	-0.8	1.3
13	crystalline quartz	pseudosecondary	Stage II	250.2	-0.7	1.2
13	crystalline quartz	pseudosecondary	Stage II	202.3	-0.6	1.0
14	amethyst	pseudosecondary	Stage III	256.2	-0.5	0.8
14	amethyst	pseudosecondary	Stage III	248.6	-0.3	0.5
14	amethyst	pseudosecondary	Stage III	260.1	-0.4	0.7
14	amethyst	pseudosecondary	Stage III	258.4	-0.5	0.8
14	amethyst	pseudosecondary	Stage III	234.2	-0.4	0.7
14	amethyst	pseudosecondary	Stage III	242.3	-0.5	0.8
14	amethyst	pseudosecondary	Stage III	250.2	-0.5	0.8
14	amethyst	pseudosecondary	Stage III	231.0	-0.6	1.0
14	amethyst	pseudosecondary	Stage III	232.2	-0.6	1.0
14	amethyst	pseudosecondary	Stage III	250.6	-0.6	1.0
15	crystalline quartz	primary	Stage II	224.8	-0.2	0.3
15	crystalline quartz	primary	Stage II	248.8	-0.4	0.7
15	crystalline quartz	primary	Stage II	243.8	-0.3	0.5
15	crystalline quartz	primary	Stage II	248.2	-0.5	0.8
15	crystalline quartz	primary	Stage II	249.8	-0.4	0.7

Sample #	Host Mineral	Type of inclusion	Paragenetic Stage	Th	Tm ice	Wt % NaCl eq.
15	crystalline quartz	primary	Stage III	220.3	-0.2	0.3
15	calcite	pseudosecondary	Stage III	218.8	-0.1	0.2
15	bladed calcite	pseudosecondary	Stage III	205.4	-0.1	0.2
15	bladed calcite	pseudosecondary	Stage III	246.4	0.0	0.0
15	bladed calcite	pseudosecondary	Stage III	217.3	0.0	0.0
15	bladed calcite	pseudosecondary	Stage III	226.5	-0.7	0.0
15	bladed calcite	pseudosecondary	Stage III	227.1	-0.7	1.2
15	bladed calcite	pseudosecondary	Stage III	228.2	-0.9	1.5
15	bladed calcite	pseudosecondary	Stage III	228.0	-0.8	1.3
19	calcite	pseudosecondary	Stage III	216.5	-0.6	1.0
19	calcite	pseudosecondary	Stage III	217.6	-0.6	1.0
19	calcite	pseudosecondary	Stage III	218.6	-0.7	1.2
19	calcite	pseudosecondary	Stage III	221.0	-0.7	1.2
19	calcite	pseudosecondary	Stage III	220.6	-0.8	1.3
19	calcite	pseudosecondary	Stage III	214.4	-0.9	1.5
19	calcite	pseudosecondary	Stage III	214.3	-0.7	1.2
19	calcite	pseudosecondary	Stage III	218.3	-0.7	1.2
19	calcite	pseudosecondary	Stage III	208.9	-0.8	1.3
19	calcite	pseudosecondary	Stage III	213.2	-0.6	1.0
22	crystalline quartz	primary	Stage II	216.3	-0.3	0.5
22	crystalline quartz	primary	Stage II	226.3	-0.4	0.7

Sample #	Host Mineral	Type of inclusion	Paragenetic Stage	Th	Tm ice	Wt % NaCl eq.
22	crystalline quartz	primary	Stage III	225.0	-0.4	0.7
23	crystalline quartz	pseudosecondary	Stage III	230.0	-0.2	0.3
23	quartz	pseudosecondary	Stage III	242.4	-0.2	0.3
23	quartz	pseudosecondary	Stage III	232.2	-0.2	0.3
23	quartz	pseudosecondary	Stage III	255.5	-0.2	0.3
23	crystalline quartz	primary	Stage III	262.4	-0.4	0.7
23	crystalline quartz	primary	Stage III	266.1	-0.2	0.3
23	crystalline quartz	primary	Stage III	264.4	-0.3	0.5
23	crystalline quartz	primary	Stage III	256.2	-0.3	0.5
23	crystalline quartz	primary	Stage III	255.2	-0.4	0.7
23	calcite	primary	Stage III	242.2	0.0	0.0
23	calcite	secondary	Stage III	230.4	-0.9	1.5
23	calcite	secondary	Stage III	253.2	-1.3	2.1
23	calcite	primary	Stage III	254.1	-1.0	1.7
23	calcite	primary	Stage III	253.7	-0.8	1.3
49	crystalline quartz	primary	Stage III	229.9	-0.6	1.0
49	crystalline quartz	primary	Stage III	236.8	-0.8	1.3
49	crystalline quartz	primary	Stage III	226.5	-0.7	1.2
49	crystalline quartz	primary	Stage III	235.4	-0.5	0.8
49	crystalline quartz	primary	Stage III	228.1	-0.2	0.3
49	crystalline quartz	primary	Stage III	234.6	-0.3	0.5

Sample #	Host Mineral	Type of inclusion	Paragenetic Stage	Th	Tm ice	Wt % NaCl eq.
49	crystalline quartz	primary	Stage II	235.1	-0.2	0.3
58	calcite	primary	Stage III	248.0	-0.1	0.2
58	calcite	primary	Stage III	236.0	-0.1	0.2
60	crystalline quartz	pseudosecondary	Stage II	227.7	-1.8	3.0
60	crystalline quartz	pseudosecondary	Stage II	209.2	-1.7	2.8
60	crystalline quartz	pseudosecondary	Stage II	226.3	-1.8	3.0
60	crystalline quartz	pseudosecondary	Stage II	229.3	-1.7	2.8
60	crystalline quartz	pseudosecondary	Stage II	224.3	-1.7	2.8
60	crystalline quartz	pseudosecondary	Stage II	219.2	-1.7	2.8
61	mosaic quartz	secondary	Stage II	237.1	-0.4	0.7
61	mosaic quartz	secondary	Stage II	237.8	-0.5	0.8
61	mosaic quartz	secondary	Stage II	224.0	-0.4	0.7
66	quartz	pseudosecondary	Stage II	202.3	-1.0	1.7
66	quartz	pseudosecondary	Stage II	184.7	-1.0	1.7
66	quartz	pseudosecondary	Stage II	181.5	-1.1	1.8
66	quartz	pseudosecondary	Stage II	192.7	-1.1	1.8
66	quartz	pseudosecondary	Stage II	196.2	-0.9	1.5
66	quartz	pseudosecondary	Stage II	207.1	-0.9	1.5
66	quartz	pseudosecondary	Stage II	np	-0.9	1.5
66	quartz	pseudosecondary	Stage II	np	-0.9	1.5
66	quartz	pseudosecondary	Stage II	234.1	-0.2	0.3

Sample #	Host Mineral	Type of inclusion	Paragenetic Stage	Th	Tm ice	Wt % NaCl eq.
66	quartz	pseudosecondary	Stage II	237.1	-0.2	0.3
66	quartz	pseudosecondary	Stage II	243.9	-0.2	0.3
69	crystalline quartz	pseudosecondary	Stage II	224.2	-0.7	1.2
69	crystalline quartz	pseudosecondary	Stage II	251.2	-0.6	1.0
69	crystalline quartz	pseudosecondary	Stage II	250.9	-0.6	1.0
69	crystalline quartz	pseudosecondary	Stage II	290.4	-0.4	0.7
69	crystalline quartz	pseudosecondary	Stage II	212.2	-0.6	1.0
69	crystalline quartz	pseudosecondary	Stage II	257.5	-0.5	0.8
74	calcite	pseudosecondary	Stage I	139.9	-0.1	0.2
74	calcite	primary	Stage I	172.0	-0.1	0.2
74	calcite	primary	Stage I	193.9	-0.1	0.2
82	quartz veinlet	primary	Stage I	168.0	-0.7	1.2
82	quartz veinlet	primary	Stage I	197.9	-0.7	1.2
82	quartz veinlet	primary	Stage I	177.9	-0.6	1.0

Appendix 4:
Gas Data
Measurements are in mole %

Sample #	Counts	Run #	Paragenetic Stage	H_2	He	CH_4	H_2O	N_2	H_2S	Ar	CO_2	Total Gas
1	1787219	6878a	Stage II	0.0095	0.0000	0.1095	99.6	0.0756	0.0002	0.0008	0.2524	0.4478
1	2003022	6878b	Stage II	0.0006	0.0000	0.0520	99.8	0.0809	0.0003	0.0011	0.1080	0.2429
1	3678139	6878c	Stage II	0.0227	0.0000	0.0529	99.7	0.1127	0.0002	0.0026	0.1517	0.3428
1	13015920	6878d	Stage II	0.0655	0.0000	0.0211	99.8	0.0612	0.0006	0.0012	0.0814	0.2310
1	7851002	6878e	Stage II	0.0015	0.0000	0.0502	99.8	0.0775	0.0003	0.0012	0.0548	0.1856
1	13534280	6878f	Stage II	0.0028	0.0000	0.0504	99.7	0.1151	0.0008	0.0016	0.1316	0.3022
1	11596260	6878g	Stage II	0.0031	0.0000	0.0208	99.7	0.1108	0.0012	0.0019	0.1380	0.2758
1	12451630	6878h	Stage II	0.0039	0.0001	0.0238	99.5	0.2003	0.0020	0.0035	0.2342	0.4677
1	14213590	6878i	Stage II	0.0479	0.0000	0.0262	99.4	0.2399	0.0024	0.0037	0.2562	0.5762
1	11606420	6878j	Stage II	0.0087	0.0000	0.0216	99.7	0.0919	0.0013	0.0015	0.1595	0.2846
2	21379	6948c	Stage II	0.2210	0.0001	1.6319	91.5	0.7829	0.0070	0.0367	5.3876	8.5381
2	25565	6948d	Stage II	0.1623	0.0009	2.1290	89.4	2.3362	0.0044	0.0488	5.2540	10.5760
3	3287696	6874b	Stage II	0.0000	0.0001	0.0558	97.6	1.9408	0.0012	0.0222	0.3784	2.3984
3	9194563	6874c	Stage II	0.0173	0.0001	0.0492	98.1	1.4256	0.0013	0.0234	0.3582	1.8751
3	3586215	6874d	Stage II	0.0096	0.0001	0.0654	95.1	4.3462	0.0039	0.0582	0.4152	4.8985
3	3586215	6874d	Stage II	0.0096	0.0001	0.0654	95.1	4.3462	0.0039	0.0582	0.4152	4.8985
3	2043843	6874e	Stage II	0.0486	0.0000	0.1257	99.0	0.3653	0.0009	0.0091	0.4121	0.9618
3	5730924	6874f	Stage II	0.0034	0.0000	0.0453	96.6	3.0327	0.0043	0.0426	0.2978	3.4261
3	7049178	6874g	Stage II	0.0019	0.0001	0.0231	98.2	1.4908	0.0024	0.0254	0.2857	1.8293
3	10495200	6874h	Stage II	0.0007	0.0000	0.0338	95.1	4.5264	0.0064	0.0500	0.3239	4.9413
3	4147637	6874i	Stage II	0.0071	0.0001	0.0913	93.1	6.0114	0.0084	0.0899	0.6644	6.8727
3	12003850	6874j	Stage II	0.0193	0.0000	0.0519	94.8	4.6537	0.0068	0.0768	0.4154	5.2239
4	620805	6875a	Stage II	0.0000	0.0001	0.1194	98.3	0.6104	0.0028	0.0117	0.9526	1.6970
4	12147880	6875b	Stage II	0.0000	0.0000	0.0078	99.3	0.5882	0.0007	0.0118	0.1249	0.7335
4	5090601	6875c	Stage II	0.0041	0.0000	0.0071	99.9	0.0579	0.0001	0.0016	0.0525	0.1232
4	13601970	6875e	Stage II	0.0047	0.0000	0.0191	99.3	0.4692	0.0012	0.0077	0.2180	0.7199
4	12057650	6875f	Stage II	0.0064	0.0000	0.0304	98.8	0.8789	0.0025	0.0157	0.3018	1.2356
4	13172120	6875g	Stage II	0.0708	0.0000	0.0149	99.5	0.2807	0.0010	0.0035	0.0988	0.4697
4	10667450	6875h	Stage II	0.0167	0.0000	0.0097	99.8	0.0902	0.0004	0.0024	0.0575	0.1769
4	8363464	6875i	Stage II	0.0019	0.0000	0.0132	99.8	0.1144	0.0003	0.0022	0.0390	0.1709
5	201942	6949a	Stage II	0.0436	0.0001	0.0609	98.5	0.4729	0.0122	0.0172	0.7250	1.5431
5	426806	6949Bb	Stage II	0.0933	0.0001	0.0791	98.2	0.6554	0.0099	0.0150	0.5154	1.7732
5	364050	6949c	Stage II	0.0501	0.0001	0.0417	98.4	0.6070	0.0024	0.0136	0.4118	1.5684

Sample #	Counts	Run #	Paragenetic Stage	H_2	He	CH_4	H_2O	N_2	H_2S	Ar	CO_2	Total Gas
5	2438825	6949d	Stage II	0.6961	0.0001	0.0847	97.4	0.9250	0.0106	0.0165	0.5296	2.6228
5	215847	6949e	Stage II	0.0362	0.0001	0.0234	98.9	0.3095	0.0041	0.0105	0.4878	1.1280
5	293452	6949f	Stage II	0.0517	0.0001	0.0738	98.5	0.6135	0.0029	0.0120	0.3961	1.5094
5	513516	6949g	Stage II	0.0001	0.0000	0.0000	100.0	0.0000	0.0000	0.0000	0.0000	0.0001
5	536342	6949h	Stage II	0.1326	0.0002	0.1309	97.4	0.8346	0.0092	0.0160	0.8651	2.5747
5	334604	6949i	Stage II	0.0767	0.0001	0.0932	98.1	0.5436	0.0019	0.0137	0.5698	1.9310
5	730138	6949j	Stage II	0.2145	0.0003	0.0791	97.8	0.6485	0.0071	0.0125	0.5949	2.2291
6	11367940	6873b	Stage II	0.0000	0.0000	0.0104	99.7	0.0697	0.0003	0.0010	0.2380	0.3194
6	11353120	6873c	Stage II	0.0000	0.0000	0.0086	99.7	0.0413	0.0002	0.0006	0.2092	0.2598
6	13764810	6873d	Stage II	0.0074	0.0000	0.0249	99.3	0.3568	0.0016	0.0053	0.2762	0.6724
6	6776646	6873e	Stage II	0.0000	0.0000	0.0312	99.8	0.0654	0.0004	0.0010	0.1366	0.2346
6	8598605	6873f	Stage II	0.0000	0.0000	0.0019	100.0	0.0035	0.0001	0.0002	0.0263	0.0320
8a	2003022	6653a	Stage II		0.0006	0.0205	98.9	0.5703	0.0000	0.0076	0.4951	1.1074
8a	3678139	6653b	Stage II		0.0003	0.0063	99.9	0.0824	0.0000	0.0011	0.0589	0.1495
8a	13015920	6653c	Stage II		0.0005	0.0249	99.6	0.1969	0.0002	0.0022	0.1807	0.4173
8a	7851002	6653d	Stage II		0.0005	0.0103	99.9	0.0466	0.0000	0.0004	0.0296	0.0935
8a	13534280	6653e	Stage II		0.0007	0.0256	99.4	0.1052	0.0001	0.0009	0.4345	0.5887
8a	11596260	6653f	Stage II		0.0016	0.0400	98.9	0.2079	0.0002	0.0020	0.7969	1.0695
8a	12451630	6653g	Stage II		0.0009	0.0100	99.5	0.0901	0.0001	0.0012	0.4061	0.5120
8a	14213590	6653h	Stage II		0.0010	0.0341	99.7	0.0903	0.0001	0.0008	0.1770	0.3344
8b	11606420	6659a	Stage II		0.0000	0.0001	100.0	0.0003	0.0000	0.0000	0.0000	0.0005
8b	21379	6659b	Stage II		0.0006	0.0084	100.0	0.0095	0.0000	0.0002	0.0264	0.0451
8b	25565	6659c	Stage II		0.0000	0.0153	100.0	0.0117	0.0000	0.0002	0.0183	0.0455
8b	3287696	6659d	Stage II		0.0003	0.0113	100.0	0.0086	0.0000	0.0002	0.0199	0.0457
8c	9194563	6654a	Stage II		0.0004	0.0357	99.7	0.1179	0.0000	0.0007	0.0933	0.2689
8c	3586215	6654b	Stage II		0.0004	0.0281	99.8	0.1496	0.0000	0.0010	0.0495	0.2421
8c	3586215	6654c	Stage II		0.0007	0.0235	99.8	0.0825	0.0000	0.0005	0.0673	0.1999
8c	230601	6654d	Stage II		0.0006	0.0308	99.7	0.1043	0.0001	0.0006	0.0886	0.2574
8c	4350225	6654e	Stage II		0.0008	0.0112	99.9	0.0098	0.0001	0.0002	0.0275	0.0531
8c	392387	6654f	Stage II		0.0009	0.0253	99.8	0.0716	0.0001	0.0005	0.0757	0.1992
8c	392387	6654g	Stage II		0.0007	0.0098	100.0	0.0065	0.0000	0.0001	0.0157	0.0353
8d	395588	6660a	Stage III		0.0004	0.0327	99.7	0.2294	0.0000	0.0026	0.0210	0.2888
8d	257346	6660b	Stage III		0.0000	0.0386	99.8	0.1103	0.0000	0.0011	0.0078	0.1588

Sample #	Counts	Run #	Paragenetic Stage	H_2	He	CH_4	H_2O	N_2	H_2S	Ar	CO_2	Total Gas
8d	285116	6660c	Stage 3		0.0001	0.0074	99.9	0.0834	0.0000	0.0010	0.0213	0.1353
8d	276994	6660d	Stage 3		0.0005	0.0036	100.0	0.0077	0.0000	0.0001	0.0071	0.0191
8d	2096932	6660e	Stage 3		0.0003	0.0030	100.0	0.0057	0.0000	0.0002	0.0078	0.0172
8d	3590839	6660f	Stage 3		0.0005	0.0059	99.9	0.0410	0.0000	0.0005	0.0123	0.0634
8d	392387	6660g	Stage 3		0.0005	0.0043	99.9	0.0797	0.0001	0.0009	0.0116	0.0971
8e	513516	6661a	Stage 2		0.0024	0.1175	99.8	0.0467	0.0001	0.0003	0.0278	0.2006
8e	536342	6661b	Stage 2		0.0000	0.0115	100.0	0.0053	0.0001	0.0000	0.0107	0.0288
8e	334604	6661c	Stage 2		0.0006	0.0176	99.9	0.0137	0.0001	0.0001	0.0232	0.0769
8e	730138	6661d	Stage 2		0.0005	0.0160	100.0	0.0031	0.0001	0.0001	0.0109	0.0345
8e	11367940	6661e	Stage 2		0.0018	0.0096	99.9	0.0326	0.0000	0.0004	0.0311	0.0760
8f	386189	6655a	Stage 2		0.0005	0.0213	99.9	0.0549	0.0001	0.0003	0.0458	0.1433
8f	1270112	6655b	Stage 2		0.0005	0.0223	99.9	0.0164	0.0001	0.0001	0.0234	0.0704
8f	2665951	6655c	Stage 2		0.0007	0.0161	99.9	0.0101	0.0002	0.0001	0.0276	0.0592
8f	2665951	6655d	Stage 2		0.0005	0.0169	99.9	0.0219	0.0000	0.0002	0.0242	0.0714
8f	1167917	6655e	Stage 2		0.0006	0.0412	99.9	0.0268	0.0000	0.0004	0.0323	0.1079
8f	2558390	6655f	Stage 2		0.0008	0.0510	99.8	0.0706	0.0001	0.0007	0.0829	0.2441
10	5566321	6950b	Stage 2	0.0000	0.0001	0.0505	98.0	0.0000	0.0064	0.0093	1.3931	2.0382
10	4350225	6950c	Stage 2	0.4437	0.0001	0.0768	97.8	0.4781	0.0074	0.0103	0.9509	2.1860
10	392387	6950d	Stage 2	0.0712	0.0002	0.1320	97.9	0.4091	0.0018	0.0107	0.9777	2.0658
10	392387	6950e	Stage 2	0.0710	0.0002	0.1317	97.7	0.4082	0.0026	0.0107	0.9754	2.3011
10	395588	6950f	Stage 2	0.0695	0.0001	0.0374	98.7	0.2531	0.0023	0.0069	0.5740	1.2722
10	257346	6950g	Stage 2	0.0520	0.0001	0.0281	98.3	0.0982	0.0045	0.0088	1.0595	1.7134
10	4381372	6950h	Stage 2	0.4399	0.0001	0.0605	98.3	0.5454	0.0080	0.0063	0.4939	1.7049
10	987893	6950i	Stage 2	0.1850	0.0001	0.0485	98.6	0.4327	0.0062	0.0056	0.4718	1.3794
10	528969	6950j	Stage 2	0.0741	0.0001	0.0267	98.5	0.3748	0.0069	0.0074	0.6460	1.4664
13	11315490	6876a	Stage 2	0.0000	0.0000	0.0109	99.2	0.6695	0.0013	0.0077	0.1318	0.8213
13	9445306	6876b	Stage 2	0.0000	0.0000	0.0098	99.9	0.0587	0.0005	0.0008	0.0692	0.1390
13	11544670	6876c	Stage 2	0.0372	0.0000	0.0067	99.9	0.0829	0.0002	0.0011	0.0185	0.1466
13	12672850	6876d	Stage 2	0.1681	0.0000	0.0114	99.0	0.6506	0.0038	0.0079	0.1914	1.0332
13	13398380	6876e	Stage 2	0.0000	0.0000	0.0077	99.8	0.1057	0.0015	0.0015	0.1070	0.2234
13	13398380	6876e	Stage 2	0.0000	0.0000	0.0077	99.8	0.1057	0.0015	0.0015	0.1070	0.2234
14a	937204	6951a	Stage 3	0.0739	0.0001	0.0732	98.2	0.9609	0.0021	0.0109	0.3310	1.7536
14a	198968	6951b	Stage 3	0.0228	0.0002	0.0215	99.4	0.0920	0.0003	0.0038	0.2437	0.6184

14a	285116	6951c	Stage III	0.0563	0.0002	0.0100	99.1	0.2422	0.0011	0.0047	0.2773	0.9163
14a	276994	6951d	Stage III	0.0292	0.0001	0.0079	99.2	0.1879	0.0002	0.0046	0.2724	0.7959
14a	2096932	6951e	Stage III	0.4380	0.0001	0.0686	98.7	0.3410	0.0032	0.0032	0.2556	1.3068
14a	3590839	6951f	Stage III	0.5525	0.0001	0.0580	98.4	0.5215	0.0045	0.0048	0.3199	1.6153
14a	1239441	6951g	Stage III	0.4713	0.0003	0.1079	97.7	0.7575	0.0068	0.0184	0.4840	2.3161
14a	773392	6951h	Stage III	0.1675	0.0002	0.0440	98.2	0.5851	0.0044	0.0134	0.4188	1.7844
14a	278637	6951i	Stage III	0.0328	0.0002	0.0121	98.7	0.1176	0.0000	0.0044	0.3340	1.2925
14a	289643	6951j	Stage III	0.0819	0.0002	0.0163	98.4	0.1899	0.0000	0.0070	0.4155	1.5606
14a	187231	6951k	Stage III	0.0413	0.0001	0.0141	99.3	0.0803	0.0000	0.0031	0.2298	0.6997
14a	776972	6951l	Stage III	0.4542	0.0003	0.0529	97.8	0.4922	0.0031	0.0083	0.5312	2.2110
14a	386189	6951m	Stage III	0.0746	0.0002	0.0480	98.4	0.2689	0.0000	0.0056	0.4315	1.6169
14b	1270112	6952a	Stage III	0.0606	0.0001	0.0459	98.7	0.6153	0.0037	0.0080	0.2926	1.3078
14b	2665951	6952c	Stage III	0.0035	0.0000	0.0205	98.9	0.4430	0.0023	0.0056	0.3405	1.0861
14b	2665951	6952d	Stage III	0.2221	0.0002	0.0334	98.6	0.5428	0.0030	0.0061	0.3349	1.4065
14b	1167917	6952e	Stage III	0.0898	0.0002	0.0437	98.0	0.7283	0.0032	0.0090	0.5997	1.9540
14b	2558390	6952f	Stage III	0.2483	0.0002	0.0396	98.5	0.5606	0.0033	0.0067	0.3899	1.4882
14b	5566321	6952g	Stage III	0.2980	0.0001	0.0477	98.4	0.6627	0.0058	0.0074	0.4535	1.6397
15a	1156932	6945a	Stage II	0.0064	0.0001	0.0741	98.3	0.7006	0.0014	0.0104	0.4353	1.6613
15a	847631	6945b	Stage II	0.0729	0.0001	0.0425	98.7	0.5786	0.0016	0.0079	0.3120	1.3350
15a	2115228	6945d	Stage II	0.4361	0.0001	0.0354	98.6	0.3889	0.0016	0.0067	0.3199	1.4424
15a	378158	6945e	Stage II	0.0439	0.0002	0.0250	98.2	0.5320	0.0032	0.0124	0.6029	1.8315
15a	2247833	6945f	Stage II	0.4219	0.0002	0.0398	98.4	0.6353	0.0050	0.0087	0.3753	1.6483
15a	664398	6945g	Stage II	0.1163	0.0001	0.0244	98.2	0.6709	0.0030	0.0106	0.5017	1.8144
15a	256376	6945h	Stage II	0.0469	0.0000	0.0131	98.9	0.3161	0.0011	0.0076	0.4376	1.0958
15b	127260	6946a	Stage III	0.0187	0.0000	0.0107	99.6	0.0625	0.0007	0.0031	0.2051	0.4024
15b	343892	6946c	Stage III	0.0984	0.0001	0.0167	98.6	0.3575	0.0056	0.0080	0.4524	1.4027
15b	3349727	6946e	Stage III	0.5250	0.0001	0.0305	98.5	0.5401	0.0054	0.0055	0.2803	1.5097
15b	2170851	6946f	Stage III	0.0277	0.0002	0.0253	98.7	0.5469	0.0068	0.0072	0.4159	1.2985
15b	1779568	6946g	Stage III	0.3778	0.0003	0.0310	98.3	0.5416	0.0081	0.0063	0.4480	1.6534
15b	2495407	6946h	Stage III	0.5766	0.0002	0.0257	98.3	0.4920	0.0079	0.0050	0.3915	1.6820
15c	152689	6947c	Stage III	0.0325	0.0002	0.0291	96.4	0.1495	0.0000	0.0100	3.1781	3.6326
15c	410310	6947d	Stage III	0.0941	0.0002	0.0429	98.7	0.3755	0.0003	0.0051	0.4943	1.3491

Sample #	Counts	Run #	Paragenetic Stage	H_2	He	CH_4	H_2O	N_2	H_2S	Ar	CO_2	Total Gas
19	227645	6953a	Stage III	0.0238	0.0002	0.0148	98.6	0.1769	0.0000	0.0106	0.4218	1.4257
19	350583	6953b	Stage III	0.0001	0.0001	0.0349	98.8	0.3560	0.0000	0.0083	0.3924	1.2481
19	209803	6953c	Stage III	0.0028	0.0001	0.0083	99.3	0.2220	0.0000	0.0055	0.2288	0.6982
19	365782	6953d	Stage III	0.0343	0.0002	0.0106	98.9	0.1704	0.0004	0.0060	0.4418	1.1164
19	199854	6953e	Stage III	0.0264	0.0002	0.0177	99.2	0.2007	0.0000	0.0046	0.3283	0.8125
19	1110751	6953f	Stage III	0.1868	0.0002	0.0991	98.5	0.5607	0.0046	0.0091	0.4348	1.5219
19	165673	6953g	Stage III	0.0086	0.0001	0.0136	99.5	0.1667	0.0000	0.0020	0.1679	0.4854
19	2113073	6953h	Stage III	0.2739	0.0002	0.0529	98.6	0.4978	0.0049	0.0080	0.3720	1.3697
19	247396	6953i	Stage III	0.0099	0.0002	0.0115	99.4	0.0941	0.0000	0.0043	0.2566	0.6008
19	209196	6953j	Stage III	0.0341	0.0001	0.0161	99.3	0.1121	0.0000	0.0042	0.2567	0.6791
19	2592870	6953k	Stage III	0.4469	0.0001	0.0597	98.4	0.5360	0.0055	0.0061	0.3811	1.6172
19	430096	6953l	Stage III	0.0441	0.0002	0.0222	98.8	0.2454	0.0000	0.0074	0.4272	1.2162
19	175233	6953m	Stage III	0.0174	0.0002	0.0174	99.6	0.0665	0.0004	0.0020	0.2163	0.3885
19	300059	6953n	Stage III	0.0047	0.0002	0.0315	99.1	0.3072	0.0000	0.0055	0.3211	0.9446
22	435831	6954a	Stage II	0.0033	0.0001	0.0318	99.7	0.1510	0.0009	0.0057	0.1017	0.3285
49	1920059	6960a	Stage II	0.0030	0.0000	0.0016	100.0	0.0427	0.0000	0.0000	0.0000	0.0473
49	181441	6960b	Stage II	0.0375	0.0002	0.0424	97.5	0.9511	0.0000	0.0138	0.8364	2.5193
49	89494	6960c	Stage II	0.0226	0.0001	0.0219	99.2	0.1358	0.0000	0.0078	0.3712	0.8083
49	179774	6960d	Stage II	0.0402	0.0002	0.0513	97.3	1.4550	0.0000	0.0182	0.6320	2.7424
49	108009	6960e	Stage II	0.0291	0.0003	0.0459	99.1	0.1999	0.0000	0.0085	0.3497	0.9106
49	206838	6960f	Stage II	0.0415	0.0003	0.0750	97.1	1.0710	0.0000	0.0380	0.6767	2.9333
49	396798	6960g	Stage II	0.1297	0.0003	0.0979	97.3	0.8328	0.0000	0.0245	0.8344	2.7166
49	138878	6960h	Stage II	0.0420	0.0005	0.0570	99.1	0.1833	0.0000	0.0066	0.3170	0.8898
49	1206305	6960i	Stage II	0.2398	0.0003	0.2352	97.1	1.4670	0.0038	0.0193	0.5873	2.9206
49	524828	6960j	Stage II	0.1140	0.0001	0.1841	98.3	0.5925	0.0040	0.0125	0.5539	1.7368
49	2008856	6960k	Stage II	0.5310	0.0002	0.3815	97.7	0.5326	0.0034	0.0079	0.5062	2.2988
49	1922917	6960l	Stage II	0.0121	0.0000	0.1015	99.8	0.1227	0.0000	0.0000	0.0000	0.2363
58	1967684	6877a	Stage III	0.0000	0.0000	0.0437	96.0	3.5370	0.0042	0.0344	0.3511	3.9705
58	5183487	6877b	Stage III	0.0377	0.0000	0.0453	99.7	0.1359	0.0004	0.0019	0.0699	0.2910
58	1744496	6877c	Stage III	0.0189	0.0000	0.0841	99.1	0.5522	0.0012	0.0095	0.2761	0.9420
58	6038861	6877d	Stage III	0.0364	0.0000	0.0543	99.0	0.7648	0.0018	0.0106	0.1366	1.0045
58	14118240	6877e	Stage III	0.0126	0.0000	0.0285	99.3	0.4393	0.0036	0.0064	0.2286	0.7191
58	14118240	6877e	Stage III	0.0126	0.0000	0.0285	99.3	0.4393	0.0036	0.0064	0.2286	0.7191
58	12211720	6877f	Stage III	0.0375	0.0000	0.0103	99.5	0.3079	0.0017	0.0044	0.1297	0.4914
58	8827292	6877g	Stage III	0.0679	0.0000	0.0263	99.2	0.3064	0.0014	0.0040	0.3459	0.7518
58	9169045	6877h	Stage III	0.0592	0.0000	0.0160	99.6	0.2416	0.0010	0.0044	0.1016	0.4237
58	5011626	6877i	Stage III	0.0093	0.0000	0.0268	99.7	0.1499	0.0005	0.0029	0.1240	0.3132
58	14239900	6877j	Stage III	0.1376	0.0000	0.0232	98.9	0.6885	0.0039	0.0106	0.2149	1.0788

Sample #	Counts	Run #	Paragenetic Stage	H_2	He	CH_4	H_2O	N_2	H_2S	Ar	CO_2	Total Gas
58	14118240	6877e	Stage III	0.0126	0.0000	0.0285	99.3	0.4393	0.0036	0.0064	0.2286	0.7191
58	12211720	6877f	Stage III	0.0375	0.0000	0.0103	99.5	0.3079	0.0017	0.0044	0.1297	0.4914
58	8827292	6877g	Stage III	0.0679	0.0000	0.0263	99.2	0.3064	0.0014	0.0040	0.3459	0.7518
58	9169045	6877h	Stage III	0.0592	0.0000	0.0160	99.6	0.2416	0.0010	0.0044	0.1016	0.4237
58	5011626	6877i	Stage III	0.0093	0.0000	0.0268	99.7	0.1499	0.0005	0.0029	0.1240	0.3132
58	14239900	6877j	Stage III	0.1376	0.0000	0.0232	98.9	0.6885	0.0039	0.0106	0.2149	1.0788
60	571185	6957a	Stage II	0.0835	0.0001	0.2686	94.2	3.0875	0.0004	0.0565	2.0098	5.8422
60	186629	6957c	Stage II	0.0123	0.0001	0.0212	98.7	0.4317	0.0010	0.0064	0.7172	1.2747
60	501016	6957d	Stage II	0.0550	0.0002	0.0730	94.9	2.5158	0.0024	0.0459	2.1400	5.1215
60	553775	6957e	Stage II	0.0544	0.0002	0.1207	94.2	2.9033	0.0016	0.0468	2.1241	5.7520
60	433699	6957f	Stage II	0.0268	0.0001	0.0688	97.7	1.0421	0.0003	0.0206	0.8908	2.2983
60	5198994	6957g	Stage II	0.4424	0.0001	0.1548	97.6	0.9006	0.0041	0.0123	0.7038	2.4080
60	3979636	6957h	Stage II	0.3599	0.0001	0.1039	96.5	1.3653	0.0035	0.0192	1.1751	3.4695
66	11651580	6879a	Stage II	0.0018	0.0000	0.0213	97.8	1.7516	0.0052	0.0227	0.3617	2.1643
66	13291380	6879b	Stage II	0.0000	0.0000	0.0000	100.0	0.0001	0.0000	0.0000	0.0003	0.0005
66	13897660	6879c	Stage II	0.0326	0.0000	0.0120	99.4	0.4267	0.0020	0.0054	0.1085	0.5872
66	8402747	6879d	Stage II	0.0000	0.0000	0.0108	99.3	0.5392	0.0014	0.0082	0.0910	0.6505
66	9285268	6879e	Stage II	0.0129	0.0000	0.0157	99.1	0.6193	0.0014	0.0090	0.1930	0.8513
66	8694151	6879f	Stage II	0.0281	0.0000	0.0137	99.3	0.4791	0.0022	0.0073	0.1447	0.6751
66	14260530	6879g	Stage II	0.0000	0.0000	0.0211	99.0	0.7261	0.0028	0.0101	0.2056	0.9656
66	14165780	6879h	Stage II	0.0061	0.0000	0.0151	99.5	0.3407	0.0018	0.0047	0.1459	0.5143
66	14065320	6879i	Stage II	0.0320	0.0000	0.0189	99.1	0.6805	0.0023	0.0091	0.1975	0.9403
66	13965430	6879j	Stage II	0.0000	0.0000	0.0218	99.1	0.6880	0.0018	0.0091	0.1615	0.8821
69	914283	6958a	Stage II	0.0885	0.0002	0.0377	89.8	8.5202	0.0112	0.1306	0.7987	10.1672

Appendix 4
Gas Data
Organic Analyses

Sample #	Crush	C2H4	C2H6	C3H6	C3H8	C4H8	C4H10	C5H12	C6H6	C7H10
5	6949A	1.479	37.452	1.878	72.679	13.209	0.000	166.302	462.070	15.000
5	6949B	28.446	86.123	0.000	48.816	15.303	55.470	8.293	543.166	17.957
5	6949C	0.000	84.169	0.000	174.343	10.155	88.613	87.027	340.285	13.396
5	6949D	0.000	175.022	0.000	177.876	15.601	44.204	32.755	315.371	10.364
5	6949E	0.000	28.036	0.000	193.794	3.405	0.000	61.663	242.564	10.098
5	6949F	4.496	69.838	0.000	129.207	11.888	24.556	74.311	278.976	8.957
5	6949G	0.000	0.000	0.000	0.000	0.000	0.000	0.000	0.000	0.000
5	6949H	0.000	127.820	0.000	231.764	17.301	25.190	90.060	344.800	17.465
5	6949I	0.000	130.669	0.000	232.579	7.311	17.915	124.031	377.613	17.624
5	6949J	0.000	112.447	0.000	226.275	14.558	61.754	48.124	303.110	14.671
10	6950B	0.000	145.157	0.000	285.758	28.572	133.650	0.000	194.318	13.123
10	6950C	0.000	181.582	0.000	290.525	40.964	103.362	54.248	269.976	27.595
10	6950D	0.000	88.560	0.000	205.728	20.414	71.079	56.159	171.694	17.520
10	6950E	0.000	89.518	0.000	183.737	25.544	70.703	0.000	413.042	10.134
10	6950F	0.000	39.334	0.000	143.040	14.579	38.054	0.000	177.679	6.698
10	6950G	0.000	74.015	0.000	192.400	3.931	30.057	84.058	268.311	6.410
10	6950H	0.000	99.360	0.000	152.862	9.048	48.465	28.319	212.681	7.329
10	6950I	0.000	46.108	0.000	133.812	6.106	49.948	17.901	144.532	4.718
10	6950J	0.000	38.809	0.000	134.412	5.652	32.524	7.726	189.996	5.788
19	6953A	0.000	100.863	0.000	121.781	0.000	69.312	116.031	389.318	6.310
19	6953B	0.000	36.222	0.000	127.731	7.786	14.889	16.243	272.956	6.534
19	6953C	0.000	0.963	0.000	99.172	5.172	0.000	45.854	178.315	5.971
19	6953D	6.667	39.853	0.000	16.551	0.000	97.069	34.356	227.227	5.558
19	6953E	21.701	13.118	0.000	9.338	2.499	81.523	21.159	265.185	7.680
19	6953F	0.000	64.628	0.000	109.484	6.414	51.961	46.791	245.745	10.244
19	6953G	54.193	1.905	0.000	0.000	0.000	160.354	0.000	113.338	3.007
19	6953H	0.000	69.934	0.000	76.080	9.252	28.602	32.564	141.989	6.823
19	6953I	8.730	7.791	0.000	98.379	2.143	41.106	21.785	99.314	7.075
19	6953J	16.526	26.888	0.000	0.000	0.277	61.188	33.288	128.187	4.543
19	6953K	0.000	71.809	0.000	121.127	9.376	49.253	39.192	125.075	7.996
19	6953L	0.000	40.122	0.000	114.141	7.467	0.000	3.947	155.130	7.540

Sample #	Crush	C2H4	C2H6	C3H6	C3H8	C4H8	C4H10	C5H12	C6H6	C7H10
19	6953M	7.808	2.734	0.000	39.900	10.040	11.580	18.092	91.127	3.019
19	6953N	7.142	19.872	0.000	87.666	0.000	63.816	45.877	99.420	8.465
22	6954A	23.360	0.000	0.000	48.314	17.652	0.000	0.000	64.772	1.531
49	6960A	0.000	0.000	0.000	0.000	0.000	0.000	0.000	0.000	0.000
49	6960B	0.000	84.073	0.000	65.957	15.122	80.777	20.985	357.217	4.073
49	6960C	26.314	23.901	0.000	0.000	6.493	18.313	57.049	186.572	7.005
49	6960D	32.160	63.885	26.593	0.000	0.000	0.000	0.000	272.754	4.026
49	6960E	4.431	28.193	0.000	94.362	6.907	67.193	51.399	238.520	1.948
49	6960F	5.237	63.937	0.000	266.994	0.000	14.494	73.762	368.682	6.658
49	6960G	0.000	125.886	0.000	191.662	6.475	81.580	22.245	512.073	9.671
49	6960H	0.000	22.036	0.000	138.416	3.766	0.000	37.168	235.831	5.205
49	6960I	0.000	124.582	0.000	184.501	10.894	0.000	35.741	335.615	10.042
49	6960J	10.618	45.225	0.000	32.303	12.712	46.477	0.000	103.549	4.032
49	6960K	0.000	48.975	0.000	121.674	2.748	19.239	35.061	74.809	5.846
49	6960L	0.000	0.000	0.000	0.000	0.000	0.000	0.000	0.000	0.000
60	6957A	0.000	868.466	2.171	0.000	0.000	81.738	38.849	333.643	6.753
60	6957C	0.000	187.818	0.000	39.325	0.000	45.486	9.474	64.930	0.050
60	6957D	0.000	626.861	28.355	0.000	0.942	19.773	14.637	221.551	7.254
60	6957E	0.000	1310.544	104.656	0.000	9.686	0.000	64.850	232.932	2.422
60	6957F	0.000	314.574	0.000	68.041	5.291	0.000	41.984	211.017	5.603
60	6957G	0.000	320.678	0.000	128.639	9.340	39.168	40.913	291.941	8.411
60	6957H	0.000	802.378	0.000	229.983	18.519	130.232	75.498	538.401	19.941
69	6958A	49.458	158.949	0.000	132.806	3.746	43.539	10.216	107.862	3.570
14a	6951A	65.807	74.087	0.000	146.317	12.798	50.907	34.614	457.383	7.172
14a	6951B	20.467	77.085	40.514	0.000	23.620	0.000	13.064	121.900	0.000
14a	6951C	0.000	50.250	0.000	97.036	0.000	40.271	67.282	172.908	6.593
14a	6951D	12.799	34.822	0.000	58.427	2.983	0.000	112.202	142.122	10.521
14a	6951E	0.000	43.445	0.000	87.549	6.303	35.334	21.611	101.720	4.401
14a	6951F	0.000	60.347	0.000	145.718	6.309	48.287	35.836	134.681	6.987
14a	6951G	0.000	358.924	0.000	224.923	21.637	20.460	49.851	483.544	10.392

Sample #	Crush	C2H4	C2H6	C3H6	C3H8	C4H8	C4H10	C5H12	C6H6	C7H10
14a	6951H	0.000	259.805	0.000	137.122	18.221	56.743	12.559	372.299	7.978
14a	6951I	0.000	106.018	0.000	146.123	12.861	40.956	0.000	187.994	5.974
14a	6951J	0.000	92.795	0.000	69.717	7.118	0.000	80.434	216.934	6.831
14a	6951K	0.823	45.303	0.000	18.821	6.589	59.935	24.478	100.766	5.330
14a	6951L	0.000	113.701	0.000	235.546	14.529	48.646	70.479	237.692	12.075
14a	6951M	0.000	68.896	0.000	187.636	0.000	88.439	52.697	133.839	10.266
14b	6952A	25.792	68.043	0.000	49.434	7.475	20.950	15.544	484.756	8.212
14b	6952C	0.000	39.753	0.000	99.572	2.806	51.027	48.606	187.120	3.293
14b	6952D	0.000	56.277	0.000	124.944	8.355	37.999	24.101	222.177	5.053
14b	6952E	0.000	87.867	0.000	129.243	13.152	34.311	25.890	335.581	4.852
14b	6952F	0.000	71.593	0.000	124.187	6.796	29.496	33.652	224.500	5.151
14b	6952G	0.000	102.202	0.000	169.286	11.614	52.640	34.156	283.563	7.269
15a	6945A	16.250	119.093	0.000	138.930	26.806	57.701	112.641	471.185	9.142
15a	6945B	6.571	82.445	0.000	124.021	13.545	41.163	34.046	176.442	6.325
15a	6945d	0.000	71.640	0.000	142.970	5.775	31.008	30.804	132.742	5.036
15a	6945E	0.000	189.733	0.000	48.140	4.998	57.931	71.231	190.095	4.540
15a	6945f	0.000	151.619	0.000	90.637	9.334	33.007	24.026	185.669	4.087
15a	6945g	0.000	142.313	0.000	127.903	9.001	36.231	16.151	189.863	5.268
15a	6945H	0.000	112.369	0.000	18.800	16.148	0.000	24.004	96.658	4.753
15b	6946A	33.467	32.165	20.472	0.000	6.008	19.192	0.000	53.221	2.927
15b	6946C	7.256	59.782	0.000	123.288	0.000	110.277	41.316	96.461	7.985
15b	6946E	0.000	56.109	0.000	78.813	4.476	25.206	17.345	101.138	3.545
15b	6946F	0.000	75.966	0.000	115.820	6.659	19.961	23.625	134.367	4.579
15b	6946G	0.000	76.327	0.000	135.557	8.445	27.279	30.509	142.403	5.398
15b	6946H	0.000	70.465	0.000	123.571	7.755	29.824	20.025	121.085	5.238
15c	6947A	14.801	51.384	41.747	2.508	17.554	0.000	30.339	55.269	6.638
15c	6947B	34.190	35.084	170.615	0.000	0.223	0.000	0.000	52.067	2.905
15c	6947C	12.267	14.143	0.000	91.847	0.000	84.982	31.082	126.107	5.975
15c	6947D	5.091	36.972	0.000	63.653	7.118	81.378	15.540	133.993	5.368